OSMOREGULATED PERIPLASMIC GLUCAN METABOLISM IS REQUIRED FOR STRESS SURVIVAL AND MORPHOLOGY IN *CAULOBACTER CRESCENTUS*

by

Allison Katharine Daitch

A dissertation submitted to Johns Hopkins University in conformity with the requirements for the degree of Doctor of Philosophy

Baltimore, Maryland

May 2022

ABSTRACT

Bacterial growth and division requires precise regulation of enzymatic activity in order to remodel the cell envelope without compromising its integrity. Thus, it is essential to identify and characterize enzymes that maintain cell envelope homeostasis as they can be potential antibiotic targets. In this dissertation, we have identified the enzyme, EstG, that protects cells from a variety of lethal assaults in the α-proteobacterium *Caulobacter crescentus*. Despite homology to cell wall-acting enzymes, EstG does not have detectable activity on the cell wall. To explore the novel function of EstG, we identified and characterized genetic connections with OpgH and BglX, enzymes involved in the synthesis and hydrolysis of osmoregulated periplasmic glucans (OPGs). The crystal structure of EstG revealed similarities to esterases and transesterases and we consequently demonstrated *in vitro* esterase activity of EstG. We were ultimately able to identify the substrate of EstG through an unbiased mass spectrometry screen. The substrate, a cyclic hexamer of glucose, is the first OPG identified in *Caulobacter*, that we predict EstG modifies to contribute to cell envelope integrity during stress. Ultimately, this data places EstG in the undiscovered OPG pathway in *Caulobacter* and establishes a new class of enzymes required for resistance to stress through OPG metabolism. We further elucidated a connection between the OPG pathway and morphological homeostasis in *Caulobacter* through the enzyme, OpgH. Beyond a genetic interaction with EstG, OpgH is an essential factor required for maintaining cellular morphology during

growth and division. Cell lacking OpgH exhibit asymmetric bulging and lysis, as well as mislocalization of cell wall synthesis and the primary morphogenetic complexes. Lastly, we determined that the glycosyltransferase activity of OpgH, presumably synthesis of OPGs, that is responsible for preventing the observed morphological defects. Through this thesis work, we have characterized two enzymes in the OPG pathway that are required for stress response (EstG) and morphology (OpgH). Our findings have shed light on an unexplored pathway harboring numerous enzymes that can be investigated as potential targets for antibiotics.

Primary Reader and Advisor: Erin D. Goley

Secondary Reader: Joshua Modell

DEDICATION

Dedicated to my grandparents.

To Paula "Bubby" Daitch, for being one of my greatest supporters, and for reminding me that staying in the DC area is always the right decision.

To Alvin "Pappy" Daitch, for instilling in me the value of education and showing that not even distance (daily drives from Maryland to New Jersey) should keep you from finishing a degree.

To Jean "Grandma" Caswell, for being a pioneer in academia and creating a world where women, like myself, aren't scared to pursue a PhD.

To Randall "Grandpa" Caswell, for inspiring my love of science and for being a constant reminder that there is no greater strength a person can have than to always be kind and humble. And for teaching me that in a life filled with deferred gratification, always eat your Cinnabon first.

ACKNOWLEDGEMENTS

I would like to thank the following people for helping me through the numerous hurdles that come with pursuing a PhD.

First, thank you to Dr. Erin Goley. Without a doubt, the best decision I made in graduate school was the decision to join your lab. I joined your lab, not because I loved *Caulobacter* (I didn't at the time), but because I wanted you to mold me into a scientist. You were exactly the mentor I needed at every stage of this PhD. You were gentle and nurturing when I joined with minimal confidence. You were encouraging and optimistic when I felt discouraged and lost. You slowly released the reins as I gained confidence and took ownership over my project. I continued to learn and grow for years in your lab, until I finally realized that you had done it– you had trained me. You have taught me how to think critically, take pride in my research, and communicate effectively. I am so proud to have been taught by you and it has been an absolute pleasure being in your lab. Thank you for teaching me to ask hard questions, to not be afraid to follow the science where it takes me, and to lead with compassion. If I could stay on and pursue a second PhD in your lab, I would do it in a heartbeat. But I'm really excited to be your official friend now.

Thank you to the members of the Goley lab, past and present. Liz, you were the most encouraging and laidback mentor, thank you for starting off my journey as a biochemist and for pushing me to join the lab. Thank you to Kousik for initiating

the screen that started it all off and for your endless excitement about science and life. Thanks to PJ for always being down to do anything—whether it is a hallway chat or searching for hidden lights in the lab. Selam/Swarmy, thank you for your constant support and friendship—you helped dig me out of the tough times and reminded me to always celebrate the good times. Jordan, thank you for being you—for always being the first one to celebrate a positive result with me, for saying the exact right thing when I need a pick-me-up, for always being willing to drop what you are doing to chat about science (or more likely statistics)—you have been the most supportive bay-bae and I'll always thank you for that. Thank you to Erika, for being the most reliable constant in the lab, your work ethic continues to inspire me to this day. Wanda, thank you for always letting me vent to you and for sharing your journey through postdoc life with me which has prepared me for my next steps more than you probably realize. Thank you Trung and Dezmond for always being understanding of my chaotic experiments towards the end and for always offering to help, even though you don't work on *Caulobacter*. Thank you Isaac for being my one successful rotation student recruit; I am so glad you joined the lab even though you claim to have learned nothing from your rotation project.

Thank you to the members of my thesis committee, Carol Greider, Brendan Cormack, and Josh Modell. You all have molded me into a better scientist and my projects would not be what they are today without your guidance and input over the years.

reminded me of my potential. I truly would not be the scientist I am today without you.

An infinite thank you to my parents, William and Julia. Words cannot express my gratitude to you for your endless support during this journey. Thank you to Dad for constantly reminding me that you can accomplish anything in your 20's and that the best things in life are often the hardest, which is all the more reason to work for it. Thank you to Mom for keeping me grounded while also truly believing in your heart that I am singlehandedly going to change the world with my research. Thank you both for being my greatest support system and for hanging in there for all of the highs and the lows. These years would have been nearly impossible without our frequent dinners, unbelievable vacations, and endless concerts. Thank you for showing me the world, above and below the sea. Thank you for pushing me to follow my dreams wherever they take me, even though it is obvious you would do anything to make sure I stay close to home. Thank you to my sister, Caitlin, for everything. You have always been and will always be the greatest role model in my life. You are my biggest cheerleader, my forever scuba buddy, and my best friend. Your passion and excitement for work (and life) has always been an inspiration and I feel enormously lucky to have you as my sister.

Thank you to my lab partner and my life partner, Chris. Even though first-year Chris drove me crazy, to the point where I might've doubted joining the same lab as you, you weaseled your way into my life and I've never looked back. You bring

out the best in me, both scientifically and personally, and I can't thank you enough for your unwavering love and support. You are the person I immediately run to with every high and low life (or science) throws my way and I don't know how I would have made it through this journey without you. Thank you for loving me, for growing with me, and for being my person.

Thank you to all of the animals that have been in my life during this journey for their unequivocal love and support: Bonus Cat, Buddy, Monkey, Yoski, Watson, Cricket, Lucy, Ronin, Bmo, and Munchy.

Lastly, thank you to BlaB/EstG. Even though I hated you for keeping your function/substrate hidden from me for so long, thank you for being well behaved *in vitro* and for keeping me on my toes for five years.

Table of Contents

List of Tables

List of Figures

List of Supplementary Figures

List of Supplementary Tables

Chapter 1.   Uncovering unappreciated activities and niche functions of bacterial cell wall enzymes

1.1 Publication

This Chapter has been peer-reviewed and published in Current Biology:

1.2 Abstract

A peptidoglycan (PG) cell wall is an essential component of nearly all bacteria, providing protection against turgor pressure. Metabolism of this PG meshwork must be spatially and temporally regulated in order to support growth and division. Despite being an active area of research for decades, we have only recently identified the primary PG synthesis complexes that function during elongation (RodA-PBP2) and division (FtsW-FtsI), and we are still uncovering the importance of the other seemingly redundant cell wall enzymes. In this review, we highlight the discovery of the monofunctional glycosyltransferases, RodA and FtsW, and describe how these findings have prompted a reevaluation of the auxiliary role of the bifunctional class A penicillin binding proteins (aPBPs) as well as the L,D-transpeptidases (LDTs). Specifically, recent work indicates that the aPBPs and LDTs function independently of the primary morphogenetic complexes to support growth, provide protection from stresses, mediate

morphogenesis, and/or allow adaptation to different growth conditions. These paradigm-shifting studies have reframed our understanding of bacterial cell wall metabolism, which will only become more refined as emerging technology allows us to tackle the remaining questions surrounding PG biosynthesis.

1.3 Introduction

The cell wall is a critical structural component of almost all bacteria, and regulating cell wall metabolism is central to growth and division. Made of peptidoglycan (PG), the cell wall is a rigid structure that provides protection from lysis as the cell experiences high intracellular turgor pressure. PG is both necessary and sufficient to maintain bacterial cell shape, and spatially regulated PG synthesis and remodeling underlies morphogenesis. PG metabolism is mediated by a host of enzymes, many of which are direct targets of highly effective antibiotics. Despite being studied for over half a century, we continue to discover new essential PG enzymes and uncover the unique roles of others that were assumed to be functionally redundant.

PG comprises alternating N-acetylglucosamine (GlcNAc) and N-acetylmuramic acid (MurNAc) sugars polymerized into glycan strands that are covalently linked to each other through short peptide bridges to create a large mesh (Figure 1.1). PG synthesis and remodeling are mediated by cell wall enzymes and are especially important during two essential periods of dramatic cell shape change—growth and division. Two major biosynthetic functions are required to create the PG mesh: transglycosylation to polymerize the glycan strands and transpeptidation to crosslink them together (Figure 1.1). In the best-

studied transpeptidase reaction, D,D-transpeptidases (TPases) catalyze a 4-3

linkage between peptide stems, where the numbers correspond to the position of

the crosslinked amino acids in the peptide stem (Zhao, Patel, Helmann, & Dörr,

2017). Alternatively, L,D-TPases (LDTs) can form 3-3 linkages (Zhao et al.,

2017). D,D-TPase activity is carried out by two classes of penicillin binding

proteins (PBPs) with distinct roles. The aPBPs are bifunctional, containing a

TPase domain and a glycosyltransferase 51 (GT51) domain, whereas the

monofunctional bPBPs have only transpeptidase activity (Egan, Biboy, van't

Veer, Breukink, & Vollmer, 2015). In addition to the glycosyltransferase activity of

the aPBPs, some species also produce monofunctional GT51 domain-containing

proteins (Egan et al., 2015). Until recently, GT51 domain-containing proteins

were the only known GTases for PG synthesis. However, transformative studies

over the past five years revealed that the Shape, Elongation, Division, and

Sporulation (SEDS) family proteins RodA and FtsW are the primary

glycosyltransferases (GTases) associated with elongation and division,

respectively.

This review will focus on recent advances in our understanding of the

physiological functions and regulation of the major PG biosynthetic enzymes.

The field currently posits that protein complexes containing a GTase of the SEDS

family and a bPBP TPase are primarily responsible for cell wall synthesis during

growth and division. These complexes are supported by secondary PG enzymes,

including aPBPs and LDTs, that promote PG growth, maintenance, and

modification. The functions and importance of aPBPs and LDTs vary across

bacterial species and growth conditions (Cho et al., 2016; Emami et al., 2017; Meeske et al., 2016; Taguchi et al., 2019). Through the essential activities of these PG enzymes and their regulators, a bacterial cell is able to coordinate the tight spatio-temporal control of PG synthesis necessary for survival.

1.4 SEDS family proteins function as glycosyltransferases

PG synthesis begins with roughly a dozen cytoplasmic enzymes that catalyze the synthesis of lipid II, the cell wall precursor molecule (Zhao et al., 2017). Lipid II, consisting of a lipid-linked disaccharide pentapeptide, is flipped across the cytoplasmic membrane by MurJ, where it becomes available for incorporation into the nascent cell wall (Zhao et al., 2017) (Figure 1.1). The first step of incorporation links lipid II to a glycan strand via a GTase. Until recently, aPBPs and other GT51 domain-containing proteins like MtgA in *Escherichia coli* were thought to be the primary mediators of this function (Zhao et al., 2017). Surprisingly, however, some bacteria, notably *Bacillus subtilis,* are viable even when all known GT51-domain containing GTases are deleted (Emami et al., 2017; McPherson & Popham, 2003; Meeske et al., 2016). This observation suggested the existence of novel enzymes with GTase activity and ultimately led to the paradigm-shifting discovery of the GTase activity of the SEDS family proteins, RodA and FtsW.

Multiple groups sought to identify the unknown essential cell wall factor(s) that functions as the primary GTase during elongation and/or division (Emami et al., 2017; Meeske et al., 2016). When looking for potential candidates, the SEDS family proteins RodA and FtsW stood out due to the conspicuous fact that each

is a member of an essential morphogenetic complex—RodA being associated with the elongation machinery (elongasome/Rod complex) and FtsW with the division machinery (divisome). This was initially studied in a *B. subtilis* mutant lacking all four aPBPs (Δ4), which, though viable, has an increased propensity for lysis and decreased cell width (Emami et al., 2017; McPherson & Popham, 2003; Meeske et al., 2016). Consistent with a PG synthetic role for RodA, overproduction of RodA in the Δ4 mutant restored cells to wild type morphology and growth (Emami et al., 2017; Meeske et al., 2016). Additionally, in *E. coli,* on deletion or inhibition of all aPBPs, elongasome-dependent PG synthesis still occurred, implicating RodA as the GTase (Cho et al., 2016). *In vitro* assays of purified RodA in the presence of lipid II directly demonstrated its GTase activity and implicated two essential residues (W105 and D280) that are necessary for PG synthesis *in vivo* and *in vitro* (Meeske et al., 2016).

Like RodA, the division-associated SEDS protein FtsW was recently demonstrated to be a GTase (Taguchi et al., 2019). Previously, FtsW was proposed to function as a lipid II flippase, but *in vitro* assays established FtsW as the division-associated SEDS family GTase (Taguchi et al., 2019). The *in vitro* GTase activity of FtsW requires its partner TPase, in this case FtsI (Taguchi et al., 2019). However, FtsW's GTase activity is not reliant on the TPase activity of FtsI, as either a catalytically dead variant or simply the transmembrane helix of FtsI is sufficient to stimulate PG polymerization *in vitro* (Taguchi et al., 2019). These findings solidify the GTase activity of the SEDS protein FtsW and highlight the question of enzymatic regulation, which will be discussed in the following

section. Overall, discovering the GTase activity of the SEDS proteins was a seminal advance in our understanding of how bacterial PG is synthesized during growth and division (Meeske et al., 2016). As the essential functions of RodA and/or FtsW are required in nearly all bacteria, they present exciting new targets for antibiotic development; further work to fully characterize the catalytic mechanism and regulation of this group of enzymes is therefore crucial (Emami et al., 2017).

1.5 Regulation of the SEDS-bPBP cell wall synthetic complexes

Unlike the SEDS family GTases, the essential monofunctional bPBPs required for elongation and division are well-characterized TPases. These TPase enzymes are PBP2 for elongation and FtsI (PBP3) for division in *E. coli*. Since the bPBPs are known to interact directly with the SEDS family proteins (Fay, Meyer, & Dworkin, 2010; Fraipont et al., 2011; Sjodt et al., 2020; Taguchi et al., 2019) and crosslinking is required for PG mesh formation after strand polymerization, it is logical to hypothesize that their activities and regulation are linked. Disrupting the balance between GTase and TPase activities can be lethal, as during treatment with β-lactam antibiotics, suggesting that the SEDS-bPBP pairs require a high level of coordination (Cho, Uehara, & Bernhardt, 2014).

Regulation of SEDS-bPBP activity was first explored in *E. coli,* where RodA-PBP2 were already known to be spatially regulated by the components of the elongasome. The elongasome consists of the actin homolog MreB, regulatory proteins MreC, MreD, and RodZ, and the PG synthase complex RodA-PBP2. These proteins form a dynamic complex that moves around the cell's

circumference, driven by cell wall synthesis (Wagstaff & Löwe, 2018) (Figure

1.2). A PG synthesis activation pathway for the elongasome was first suggested

when a hyperactive variant of PBP2 was found to suppress mutations in or loss

of the elongasome proteins MreC, MreD, or RodZ, and to stimulate the *in vitro*

and *in vivo* cell wall synthesis activity of RodA-PBP2 (Rohs et al., 2018). Further

work implicated MreC and MreD in regulating RodA-PBP2 activity. MreD, which

directly interacts with PBP2, is proposed to hold the PG synthases in an inactive

state (X. Liu, Biboy, Vollmer, & den Blaauwen, 2019). Crystal structures of the

MreC-PBP2 complex from *Helicobacter pylori* revealed an MreC-dependent

conformational change of PBP2 (Contreras-Martel et al., 2017). Collectively,

these data led to a model wherein MreC binding to PBP2 displaces MreD and

activates the RodA-PBP2 PG synthases (X. Liu et al., 2019; Rohs et al., 2018).

Additionally, a recent structure of RodA in complex with its cognate bPBP

established the role of PBP2's pedestal domain as an allosteric activator of

RodA, providing molecular resolution of the coordinated activity of the SEDS-

bPBP pairs (Sjodt et al., 2020). Two lines of evidence also suggest positive

feedback from RodA-PBP2 to assembly of the elongasome in *E. coli*: (1)

activating mutations in PBP2 increase the number of moving MreB foci, while

decreasing MreB filament length (Rohs et al., 2018) and (2) single molecule

tracking indicated that PBP2 binding to a substrate (independent of its catalytic

activity) initiates elongasome recruitment to sites of new PG synthesis (Özbaykal

et al., 2020).

Though it has not yet been directly shown, a similar mechanism of regulation for the divisome complex seems likely. Like the elongasome, the divisome is a multi-protein complex made up of a cytoskeletal protein (the tubulin homolog FtsZ), regulators (including FtsA, FtsK, the FtsQ-FtsL-FtsB complex, and FtsN), and a SEDS-bPBP pair (FtsW-FtsI). Also like the elongasome, the divisome moves dynamically, but its movement is driven by treadmilling of FtsZ filaments rather than by PG synthesis in *E. coli* and *B. subtilis* (Wagstaff & Löwe, 2018) (Figure 1.2). A large body of genetic evidence suggests that the divisome requires activation to drive constriction. The current model in *E. coli* proposes that FtsA acts through FtsN to initiate constriction (Pichoff, Du, & Lutkenhaus, 2015). Genetic evidence implicates other division proteins in this activation pathway, as suppressors of an inactive FtsN variant were found in the division proteins FtsB and FtsL (B. Liu, Persons, Lee, & de Boer, 2015; Tsang & Bernhardt, 2015).

The constriction activation pathway in *E. coli* is presumed to culminate in PG synthesis by FtsW and FtsI. The most direct evidence in support of this model comes from hyperactive mutants of FtsW and FtsI (called FtsW-FtsI*) that were identified in *Caulobacter crescentus*. The FtsW-FtsI* mutant enzymes are proposed to be biased towards an active state, as FtsW-FtsI*-producing cells constrict faster and are shorter than wild type (Lambert et al., 2018; Modell, Hopkins, & Laub, 2011; Modell, Kambara, Perchuk, & Laub, 2014). These hyperactive division mutants appear to function comparably to their elongasome counterparts, as one of the mutations in FtsW (A246T) is directly analogous to an

E. coli RodA(A234T) variant with increased PG synthesis activity *in vivo* (Rohs et al., 2018). In *Caulobacter,* the FtsW-FtsI* mutant is able to render the normally essential division protein FzlA nonessential, suggesting that FzlA participates in the activation of FtsW-FtsI (Lariviere et al., 2019). Hyperactivity of FtsW-FtsI* both impacts the rate of constriction and increases sensitivity to cell wall antibiotics that primarily target PBP2 or FtsI, reflecting the importance of FtsW-FtsI regulation in building a robust cell wall (Lambert et al., 2018; Lariviere et al., 2019; Modell et al., 2014). The evolving model for divisome regulation requires biochemical exploration and confirmation, but it highlights the complex regulation of the PG synthetic machinery required to maintain cell envelope integrity during growth and division. Moreover, as divisome regulation is explored in more bacteria, we are likely to uncover variations on the themes described here, as some of the characterized components of the *E. coli* or *C. crescentus* activation pathways are not broadly conserved.

1.6 Bifunctional PBPs fulfill a PG repair role and are required under stress conditions

With the discovery of the SEDS proteins as the primary GTases for growth and division, the physiological function of the aPBPs must now be re-examined. Emerging research is revealing that the aPBPs fulfill a unique maintenance role during growth and stress conditions. Recent evidence establishes a division of labor where the SEDS-bPBP complexes build a PG foundation at the site of elongation or division, while the aPBPs can expand and repair the PG mesh for growth and support as needed (Cho et al., 2016) (Figure 1.2). In *E. coli,* the two

major aPBPs - PBP1a and PBP1b - are individually dispensable, yet it is clear

that they collectively fulfill an essential role, as loss of both is lethal (Yousif,

Broome-Smith, & Spratt, 1985). PBP1a and PBP1b are also regulated, requiring

interaction with their respective activators, LpoA and LpoB (Paradis-Bleau et al.,

2010; Typas et al., 2010). In *E. coli*, the aPBPs were thought to be coordinated

with the primary PG synthetic machinery since there is *in vitro* and *in vivo*

evidence of an interaction between the aPBPs and bPBPs (Banzhaf et al., 2012;

Bertsche et al., 2006). The aPBPs also have a direct interaction with divisome

proteins that stimulate the aPBP's GTase activity. In *E. coli,* the divisome

proteins ZipA and FtsN increase the GTase activity *in vitro* of PBP1a and PBP1b,

respectively (Pazos et al., 2018). However, *in vivo* single molecule studies

revealed that the movements of the aPBPs are not linked to the cytoskeletally-

associated SEDS-bPBP pairs, implying spatial separation of aPBP activity from

the dynamic morphogenetic complexes (Cho et al., 2016; Lee, Meng, Shi, &

Huang, 2016; Vigouroux et al., 2020) (Figure 1.2).

      Despite their apparent redundancy, there are morphological

consequences of loss of aPBP activity. Loss of the aPBPs in *E. coli* or *B. subtilis*

decreases cell width, reduces the rate of cell wall incorporation, and impacts

overall cell wall integrity (Banzhaf et al., 2012; Cho et al., 2016; McPherson &

Popham, 2003; Vigouroux et al., 2020). In *E. coli,* deletion of PBP1b results in

reduced cell wall stiffness, suggesting an ability of aPBPs to find and repair cell

wall defects (Vigouroux et al., 2020). Other work in *B. subtilis* discovered a

balance between the two PG synthesis systems to achieve optimize cell size: the

elongasome decreases cell width, and the aPBPs increase cell width (Dion et al.,

2019). This supportive role of the aPBPs has been corroborated in other species

including *Streptococcus pneumoniae,* where the aPBPs modify and strengthen

the newly synthesized PG made by the SEDS-bPBP complexes (Straume et al.,

2020). These findings imply a conserved role of the aPBPs in normal growth as

maintenance enzymes that fill in the gaps in the cell wall as they arise (Figure

1.2).

Though the aPBPs do not appear to function as the primary PG synthases

in normal growth, recent studies reveal a major responsibility of these enzymes

during fluctuating environmental conditions. For instance, growth of *E. coli* in

acidic or alkaline environments was found to be dependent on the presence of

PBP1b and PBP1a, respectively (Mueller, Egan, Breukink, Vollmer, & Levin,

2019). This impact on viability likely does not involve a novel enzymatic activity -

the global cell wall composition is unchanged in altered pH (Peters et al., 2016) -

but rather reflects the ability of specific synthases to retain enzymatic activity and

act as repair enzymes under conditions when others are inactive (Mueller et al.,

2019). Interestingly, PBP1b also appears critical in the context of β-lactam

sensitivity, as loss of PBP1b or its regulator LpoB results in hypersensitivity to

cell wall-targeting antibiotics (Garcia Del Portillo & De Pedro, 1990). The aPBPs

also appear to be important for adapting to osmotic changes and mechanical

stresses, as well as for initiating *de novo* PG synthesis (Auer et al., 2016; Ranjit,

Jorgenson, & Young, 2017). These findings are likely the beginning of a

complete understanding of the PG enzymes and their distinct roles in cell wall homeostasis and repair.

1.7 LDT activity can protect against cell envelope stress

Among the cell wall enzymes, the less-well studied LDTs occupy a unique category within the TPases. Though the LDTs crosslink peptide stems, they are not members of the PBP family. Rather, they have minimal amino acid similarity and a distinct active site from the PBPs, explaining their insensitivity to inhibition by penicillin (Tolufashe et al., 2018). In *E. coli*, the predominant 4-3 crosslink is between a meso-diaminopimelic acid (mDAP) in the third position of a tetra-peptide to a terminal D-alanine (D-ala) in the fourth position of a neighboring tetra-peptide stem. However, roughly 3-10% of the crosslinks in *E. coli* consist of a 3-3 linkage, mDAP-mDAP, which is synthesized by the LDTs from already processed tetrapeptides (Glauner, Holtje, & Schwarz, 1988) (Figure 1.1). Similar to the SEDS-bPBP pairs, PG remodeling by the LDTs functions in concert with a GTase, specifically an aPBP (Hugonnet et al., 2016; Morè et al., 2019). Though nonessential in *E. coli,* LDTs appear to be important under stress conditions: inhibiting the LDTs with copper ions results in cell envelope defects (Peters et al., 2018), increased LDT activity provides resistance to cell lysis during OM stress (Morè et al., 2019), and LDT-mediated crosslinking can confer resistance to broad spectrum β-lactam antibiotics in *E. coli* and *Enterococcus faecium* (Hugonnet et al., 2016; Mainardi et al., 2000).

In contrast to *E. coli*, LDTs appear to play a major role in organisms that exhibit polar growth, notably *Mycobacterium tuberculosis* and *Agrobacterium*

tumefaciens (Figure 1.2). LDT-generated 3-3 linkages comprise about 80% of the total crosslinks in *M. tuberculosis* and more than 50% of the crosslinks in *A. tumefaciens* (Cameron, Anderson-Furgeson, Zupan, Zik, & Zambryski, 2014; Lavollay et al., 2008). In these organisms, the abundance of 3-3 crosslinks appears to be important for resistance to certain cell wall-targeting agents. For instance, loss of LDT activity in *M. tuberculosis* results in growth defects, loss of virulence, and increased sensitivity to the β-lactam antibiotics that target PBPs (Schoonmaker, Bishai, & Lamichhane, 2014). Similarly, the PG of *A. tumefaciens* is highly resistant to lysozyme-mediated degradation (Stankeviciute et al., 2019). The distinct chemistry of the cell wall resulting from LDT activity likely underlies these protective effects.

LDTs are also important for generating spatially discrete areas within the cell wall of uniquely crosslinked PG and for formation of polar structures, as was found in *C. crescentus* (Billini, Biboy, Kühn, Vollmer, & Thanbichler, 2019; Stankeviciute et al., 2019)*. C. crescentus* forms a unipolar appendage called the stalk, which contains all elements of the cell envelope and requires PG synthesis for its formation (Figure 1.2). Interestingly, stalk morphology is unaffected by treatment with β-lactams and cell wall digesting enzymes like lysozyme, which can be attributed to increased LDT activity in the stalk (Schmidt & Stanier, 1966; Stankeviciute et al., 2019). Though the physiological significance of high LDT activity in the stalk is unknown, it highlights a spatially-regulated PG metabolic activity that provides protection against PG assaults. As with the aPBPs, we are only now learning the importance of these previously overlooked enzymes as we

push the limits of stress and culture conditions and explore PG metabolism in diverse bacteria.

1.8 Conclusions and future perspectives

Only a decade ago, our understanding of the bacterial cell wall synthesis machinery was profoundly different than it is today. Previously, the primary biosynthetic PG machinery was thought to consist of the monofunctional TPases and the GTase activity of aPBPs. The SEDS family proteins had an unknown essential function and we knew very little about the activation of cell wall synthesis during growth and division. The SEDS-bPBP complexes are now characterized as the primary morphogenetic PG enzymes, and we are beginning to understand their activity and regulation. In retrospect, it seems the SEDS GTases were hidden in plain sight - some bacteria lack aPBPs, but encode at least one bPBP and a SEDS protein (Meeske et al., 2016) – making it somewhat surprising their activity was not discovered earlier. Despite the progress made in recent years, there are still many unknowns. For one, the activation pathway and regulatory machinery for SEDS-bPBP pairs is undoubtedly complex. In addition to identifying the activating factors, the link between these enzymes and the dynamic cytoskeletal complexes with which they associate is poorly understood. Through single molecule studies we are now able to observe the directed movement of the cytoskeletal components and associated enzymes, which will begin to reveal more about the distribution of morphogenetic proteins and corresponding PG synthesis (Wagstaff & Löwe, 2018). A more in depth

understanding of these highly conserved PG synthetic enzymes is also pivotal as they can be exploited as antimicrobial targets.

As the genomes of a growing number of bacteria have been sequenced, we can identify most of the cell wall family enzymes of either known or unknown physiological function. With this knowledge, we can continue to dissect the importance of apparently "redundant" PG enzymes, which are likely not redundant at all. The recent work on the aPBPs and LDTs has scratched the surface of identifying conditions when apparently nonessential PG enzymes become essential for viability. Future work will expand this paradigm to other cell wall enzymes, potential activators, and novel cell wall chemistries. One avenue that will inform this work is the study of PG biochemistry and regulation in a diversity of bacterial systems. Many of the discoveries discussed above were only possible as a result of studying different bacterial systems, each offering unique technical strengths and/or occupying distinct biological niches. This could immediately be applied to one outstanding question in this realm which is the apparent lack of aPBP activators, e.g. the LpoA/B proteins, outside of the γ-proteobacteria. It is unlikely that the aPBPs do not require activators and/or regulators in other species; rather we simply have not yet discovered them. Ultimately, we marvel at the rapid advancement of the field of PG biogenesis in recent years and anticipate an increasing rate of discovery as tool development continues to push the limits of what is discoverable.

1.9 Figures and Legends
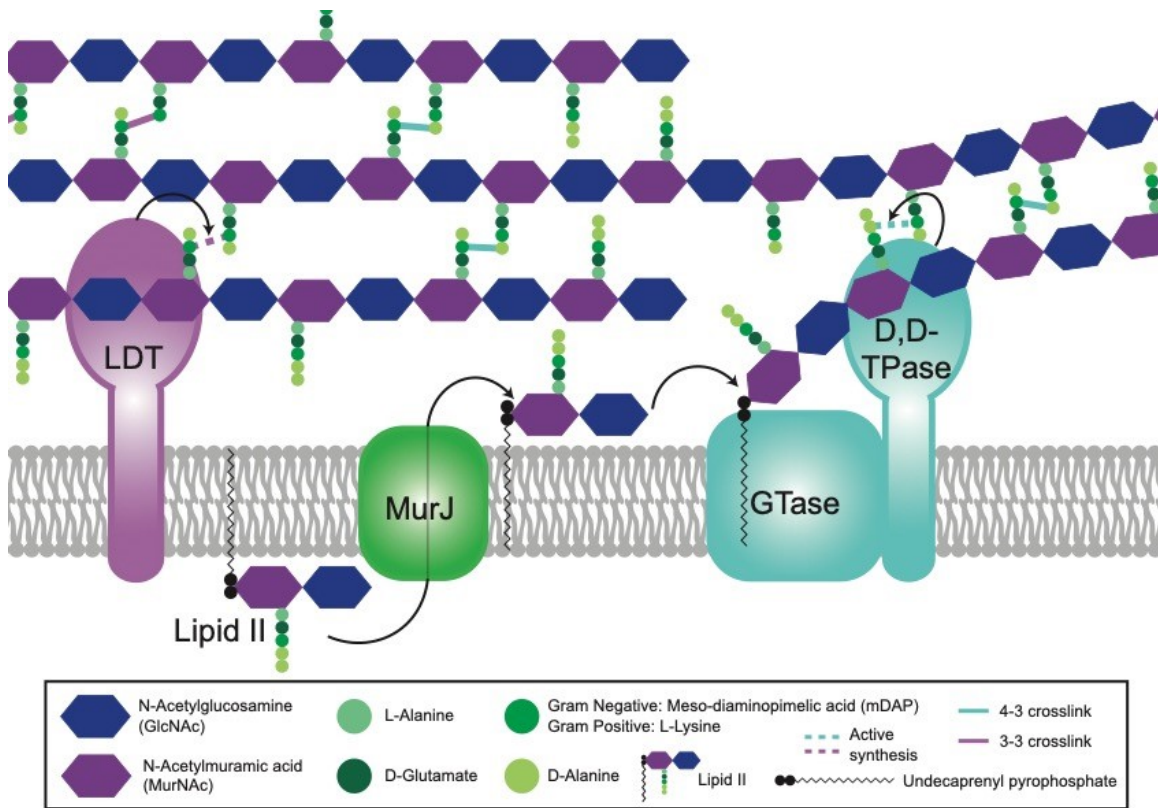
Figure 1.1: The basics of peptidoglycan (PG) synthesis.

The PG precursor is synthesized in the cytoplasm to create the lipid-linked disaccharide-pentapeptide moiety, lipid II. Lipid II is then flipped across the cytoplasmic membrane by MurJ. Once in the periplasm, a glycosyltransferase (GTase) polymerizes the lipid II moiety onto the growing glycan strand, through the action of either a SEDS protein (RodA or FtsW), a bifunctional class A penicillin binding protein (aPBP), or a GT51 containing enzyme. Once polymerized, the peptide stem can then be crosslinked to a neighboring strand through the action of a transpeptidase (TPase). A monofunctional bPBP (PBP2 or FtsI) or a bifunctional aPBP acts as a D,D-TPase, creating a 4-3 linkage, shown in teal. For simplicity, only the SEDS/bPBP synthases are shown to depict transglycosylation and transpeptidation steps. The peptide stem can alternatively be

crosslinked in a 3-3 linkage (shown in purple) through the action of an L,D-

transpeptidase (LDT).
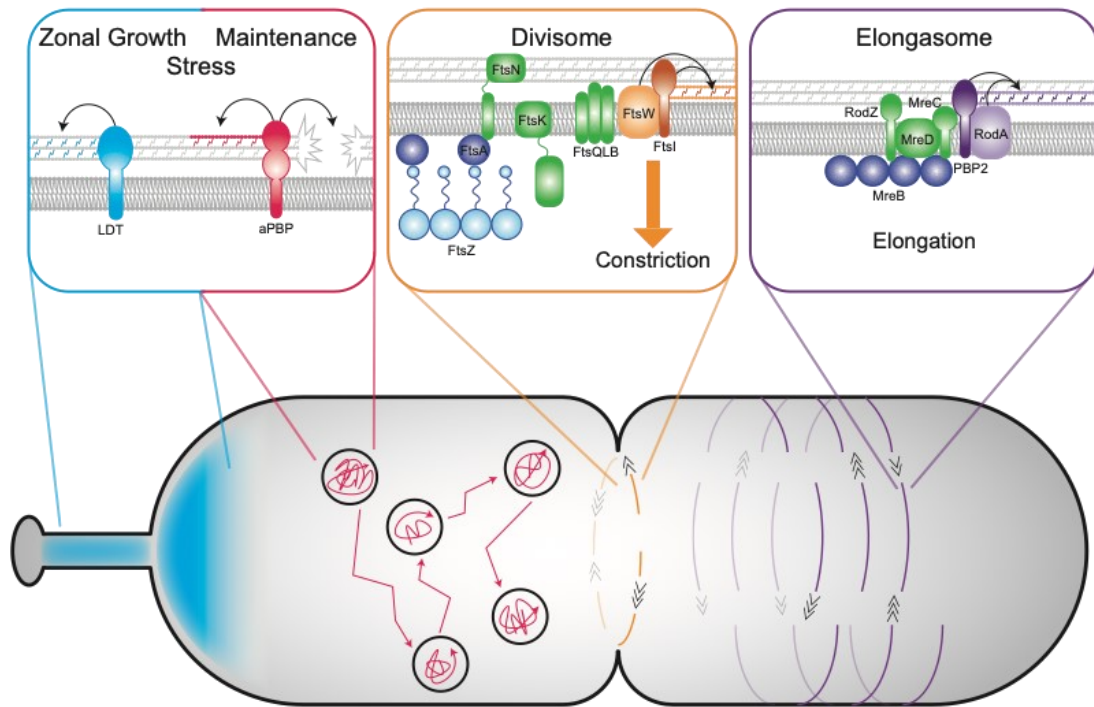
Figure 1.2: Dynamics and functions of distinct PG synthetic enzymes.

SEDS-bPBP pairs are associated with morphogenetic complexes to direct spatially-regulated PG synthesis, while movement of the aPBPs and LDTs are independent of the division/elongation machinery. Left panel: The importance of LDT activity varies among species. In some organisms, LDT-mediated crosslinking is important in specific regions in a cell, such as during stalk formation or unipolar growth. LDT activity also appears important for resistance to antibiotic treatment. Movement of the aPBPs is diffusive followed by periods of confinement. The bifunctional aPBPs likely act as repair machinery necessary for efficient growth and/or PG synthesis during stress conditions. Middle panel: In almost all bacteria with a cell wall, PG synthesis associated with the divisome is carried out by the FtsW-FtsI enzyme pair. The movement of FtsW-FtsI is bidirectional around the short axis of the division plane, directed by treadmilling of FtsZ filaments. The conserved activation pathway for FtsW-FtsI likely requires the divisome

proteins FtsA, FtsK, FtsN, and FtsQLB. Right panel: In many rod-shaped organisms,

RodA-PBP2 synthesize PG for elongation and are regulated by elongasome proteins,

notably MreC. The elongation machinery moves bidirectionally about the circumference

of the short axis of the cell but, unlike the divisome, movement is directed by PG

synthesis rather than MreB dynamics.

1.10 References

Auer, G. K., Lee, T. K., Rajendram, M., Cesar, S., Miguel, A., Huang, K. C., & Weibel, D. B. (2016). Mechanical genomics identifies diverse modulators of bacterial cell stiffness. *Cell Systems*, *2*(6), 402–411. https://doi.org/10.1016/j.cels.2016.05.006

Banzhaf, M., van den Berg van Saparoea, B., Terrak, M., Fraipont, C., Egan, A., Philippe, J., … Vollmer, W. (2012). Cooperativity of peptidoglycan synthases active in bacterial cell elongation. *Molecular Microbiology*, *85*(1), 179–194. https://doi.org/10.1111/j.1365-2958.2012.08103.x

Bertsche, U., Kast, T., Wolf, B., Fraipont, C., Aarsman, M. E. G., Kannenberg, K., … Vollmer, W. (2006). Interaction between two murein (peptidoglycan) synthases, PBP3 and PBP1B, in *Escherichia coli*. *Molecular Microbiology*, *61*(3), 675–690. https://doi.org/10.1111/j.1365-2958.2006.05280.x

Billini, M., Biboy, J., Kühn, J., Vollmer, W., & Thanbichler, M. (2019). *A specialized MreB-dependent cell wall biosynthetic complex mediates the formation of stalk-specific peptidoglycan in* Caulobacter crescentus. *PLoS Genetics* (Vol. 15). https://doi.org/10.1371/journal.pgen.1007897

Cameron, T. A., Anderson-Furgeson, J., Zupan, J. R., Zik, J. J., & Zambryski, P. C. (2014). Peptidoglycan synthesis machinery in *Agrobacterium tumefaciens* during unipolar growth and cell division. *MBio*, *5*(3), 1–10. https://doi.org/10.1128/mBio.01219-14

Cho, H., Uehara, T., & Bernhardt, T. G. (2014). Beta-lactam antibiotics induce a lethal malfunctioning of the bacterial cell wall synthesis machinery. *Cell*,

159(6), 1300–1311. https://doi.org/10.1016/j.cell.2014.11.017

Cho, H., Wivagg, C. N., Kapoor, M., Barry, Z., Rohs, P. D. A., Suh, H., …
Bernhardt, T. G. (2016). Bacterial cell wall biogenesis is mediated by SEDS
and PBP polymerase families functioning semi-autonomously. *Nature
Microbiology*, *1*(October), 1–8. https://doi.org/10.1038/nmicrobiol.2016.172

Contreras-Martel, C., Martins, A., Ecobichon, C., Trindade, D. M., Matteï, P. J.,
Hicham, S., … Dessen, A. (2017). Molecular architecture of the PBP2-MreC
core bacterial cell wall synthesis complex. *Nature Communications*, *8*(1), 1–
10. https://doi.org/10.1038/s41467-017-00783-2

Dion, M. F., Kapoor, M., Sun, Y., Wilson, S., Ryan, J., Vigouroux, A., … Garner,
E. C. (2019). Bacillus subtilis cell diameter is determined by the opposing
actions of two distinct cell wall synthetic systems. *Nature Microbiology*, *4*(8),
1294–1305. https://doi.org/10.1038/s41564-019-0439-0

Egan, A. J. F., Biboy, J., van't Veer, I., Breukink, E., & Vollmer, W. (2015).
Activities and regulation of peptidoglycan synthases. *Philosophical
Transactions of the Royal Society B: Biological Sciences*, *370*, 1–20.
https://doi.org/10.1098/rstb.2015.0031

Emami, K., Guyet, A., Kawai, Y., Devi, J., Wu, L. J., Allenby, N., … Errington, J.
(2017). RodA as the missing glycosyltransferase in Bacillus subtilis and
antibiotic discovery for the peptidoglycan polymerase pathway. *Nature
Microbiology*, *2*(January), 1–8. https://doi.org/10.1038/nmicrobiol.2016.253

Fay, A., Meyer, P., & Dworkin, J. (2010). Interactions between late-acting
proteins required for peptidoglycan synthesis during sporulation. *Journal of*

Molecular Biology, *399*(4), 547–561.

https://doi.org/10.1016/j.jmb.2010.04.036

Fraipont, C., Alexeeva, S., Wolf, B., Der Ploeg, R., Schloesser, M., Den

Blaauwen, T., & Nguyen-Distèche, M. (2011). The integral membrane FtsW

protein and peptidoglycan synthase PBP3 form a subcomplex in *Escherichia*

coli. *Microbiology*, *157*(1), 251–259. https://doi.org/10.1099/mic.0.040071-0

Garcia Del Portillo, F., & De Pedro, M. A. (1990). Differential effect of mutational

impairment of penicillin-binding proteins 1A and 1B on *Escherichia coli*

strains harboring thermosensitive mutations in the cell division genes ftsA,

ftsQ, ftsZ, and pbpB. *Journal of Bacteriology*, *172*(10), 5863–5870.

https://doi.org/10.1128/jb.172.10.5863-5870.1990

Glauner, B., Holtje, J. V., & Schwarz, U. (1988). The composition of the murein of

Escherichia coli. *Journal of Biological Chemistry*, *263*(21), 10088–10095.

Hugonnet, J. E., Mengin-Lecreulx, D., Monton, A., den Blaauwen, T.,

Carbonnelle, E., Veckerlé, C., … Arthur, M. (2016). Factors essential for

L,D-transpeptidase-mediated peptidoglycan cross-linking and β-lactam

resistance in *Escherichia coli*. *ELife*, *5*(OCTOBER2016), 1–22.

https://doi.org/10.7554/eLife.19469

Lambert, A., Vanhecke, A., Archetti, A., Holden, S., Schaber, F., Pincus, Z., …

Manley, S. (2018). Constriction rate modulation can drive cell size control

and homeostasis in C. crescentus. *IScience*, *4*, 180–189.

https://doi.org/10.1016/j.isci.2018.05.020

Lariviere, P. J., Mahone, C. R., Santiago-Collazo, G., Howell, M., Daitch, A. K.,

Zeinert, R., … Goley, E. D. (2019). An Essential Regulator of Bacterial

Division Links FtsZ to Cell Wall Synthase Activation. *Current Biology*, *29*(9),

1460-1470.e4. https://doi.org/10.1016/j.cub.2019.03.066

Lavollay, M., Arthur, M., Fourgeaud, M., Dubost, L., Marie, A., Veziris, N., …

Mainardi, J. L. (2008). The peptidoglycan of stationary-phase

Mycobacterium tuberculosis predominantly contains cross-links generated

by L,D-transpeptidation. *Journal of Bacteriology*, *190*(12), 4360–4366.

https://doi.org/10.1128/JB.00239-08

Lee, T. K., Meng, K., Shi, H., & Huang, K. C. (2016). Single-molecule imaging

reveals modulation of cell wall synthesis dynamics in live bacterial cells.

Nature Communications, *7*, 1–9. https://doi.org/10.1038/ncomms13170

Liu, B., Persons, L., Lee, L., & de Boer, P. A. J. (2015). Roles for both FtsA and

the FtsBLQ subcomplex in FtsN-stimulated cell constriction in *Escherichia

coli*. *Molecular Microbiology*, *95*(6), 945–970.

https://doi.org/10.1111/mmi.12906

Liu, X., Biboy, J., Vollmer, W., & den Blaauwen, T. (2019). MreC and MreD

balance the interaction between the elongasome proteins PBP2 and RodA.

BioRxiv. https://doi.org/https://doi.org/10.1101/769984.

Mainardi, J. L., Legrand, R., Arthur, M., Schoot, B., Van Heijenoort, J., &

Gutmann, L. (2000). Novel mechanism of β-lactam resistance due to bypass

of DD- transpeptidation in *Enterococcus faecium*. *Journal of Biological

Chemistry*, *275*(22), 16490–16496. https://doi.org/10.1074/jbc.M909877199

McPherson, D. C., & Popham, D. L. (2003). Peptidoglycan synthesis in the

absence of class A penicillin-binding proteins in *Bacillus subtilis*. *Journal of Bacteriology*, *185*(4), 1423–1431. https://doi.org/10.1128/JB.185.4.1423-1431.2003

Meeske, A. J., Riley, E. P., Robins, W. P., Uehara, T., Mekalanos, J. J., Kahne, D., … Rudner, D. Z. (2016). SEDS proteins are a widespread family of bacterial cell wall polymerases. *Nature*, *537*(7622), 634–638. https://doi.org/10.1038/nature19331

Modell, J. W., Hopkins, A. C., & Laub, M. T. (2011). A DNA damage checkpoint in *Caulobacter crescentus* inhibits cell division through a direct interaction with FtsW. *Genes and Development*, *25*(12), 1328–1343. https://doi.org/10.1101/gad.2038911

Modell, J. W., Kambara, T. K., Perchuk, B. S., & Laub, M. T. (2014). A DNA damage-Induced, SOS-independent checkpoint regulates cell division in Caulobacter crescentus. *PLoS Biology*, *12*(10), 1–15. https://doi.org/10.1371/journal.pbio.1001977

Morè, N., Martorana, A. M., Biboy, J., Otten, C., Winkle, M., Serrano, C. K. G., … Polissi, A. (2019). Peptidoglycan remodeling enables Escherichia coli to survive severe outer membrane assembly defect. *MBio*, *10*(1), 1–18. https://doi.org/10.1128/mBio.02729-18

Mueller, E. A., Egan, A. J., Breukink, E., Vollmer, W., & Levin, P. A. (2019). Plasticity of *Escherichia coli* cell wall metabolism promotes fitness and antibiotic resistance across environmental conditions. *ELife*, *8*, 1–24. https://doi.org/10.7554/eLife.40754

Özbaykal, G., Wollrab, E., Simon, F., Vigouroux, A., Cordier, B., Aristov, A., …

    van Teeffelen, S. (2020). The transpeptidase PBP2 governs initial

    localization and activity of the major cell-wall synthesis machinery in E. coli.

    ELife, *9*, 1–74. https://doi.org/10.7554/eLife.50629

Paradis-Bleau, C., Markovski, M., Uehara, T., Lupoli, T. J., Walker, S., Kahne, D.

    E., & Bernhardt, T. G. (2010). Lipoprotein cofactors located in the outer

    membrane activate bacterial cell wall polymerases. *Cell*, *143*(7), 1110–1120.

    https://doi.org/10.1016/j.cell.2010.11.037

Pazos, M., Peters, K., Casanova, M., Palacios, P., VanNieuwenhze, M.,

    Breukink, E., … Vollmer, W. (2018). Z-ring membrane anchors associate

    with cell wall synthases to initiate bacterial cell division. *Nature*

    Communications, *9*(1), 1–12. https://doi.org/10.1038/s41467-018-07559-2

Peters, K., Kannan, S., Rao, V. A., Biboy, J., Vollmer, D., Erickson, S. W., …

    Vollmer, W. (2016). The redundancy of peptidoglycan carboxypeptidases

    ensures robust cell shape maintenance in Escherichia coli. *MBio*, *7*(3), 1–14.

    https://doi.org/10.1128/mBio.00819-16

Peters, K., Pazos, M., Edoo, Z., Hugonnet, J. E., Martorana, A. M., Polissi, A., …

    Vollmer, W. (2018). Copper inhibits peptidoglycan LD-transpeptidases

    suppressing β-lactam resistance due to bypass of penicillin-binding proteins.

    Proceedings of the National Academy of Sciences of the United States of

    America, *115*(42), 10786–10791. https://doi.org/10.1073/pnas.1809285115

Pichoff, S., Du, S., & Lutkenhaus, J. (2015). The bypass of ZipA by

    overexpression of FtsN requires a previously unknown conserved FtsN motif

essential for FtsA-FtsN interaction supporting a model in which FtsA monomers recruit late cell division proteins to the Z ring. *Molecular Microbiology*, *95*(6), 971–987. https://doi.org/10.1111/mmi.12907

Ranjit, D. K., Jorgenson, M. A., & Young, K. D. (2017). PBP1B glycosyltransferase and transpeptidase activities play different essential roles during the *de novo* regeneration of rod morphology in Escherichia coli. *Journal of Bacteriology*, *199*(7), 1–17.

Rohs, P. D. A., Buss, J., Sim, S. I., Squyres, G. R., Srisuknimit, V., Smith, M., … Bernhardt, T. G. (2018). A central role for PBP2 in the activation of peptidoglycan polymerization by the bacterial cell elongation machinery. *PLoS Genetics*, *14*(10), 1–25. https://doi.org/10.1371/journal.pgen.1007726

Schmidt, J., & Stanier, R. Y. (1966). The development of cellular stalks in bacteria. *Journal of Cell Biology*, *28*, 423–436.

Schoonmaker, M. K., Bishai, W. R., & Lamichhane, G. (2014). Nonclassical transpeptidases of *Mycobacterium tuberculosis* alter cell size, morphology, the cytosolic matrix, protein localization, virulence, and resistance to β-lactams. *Journal of Bacteriology*, *196*(7), 1394–1402. https://doi.org/10.1128/JB.01396-13

Sjodt, M., Rohs, P. D. A., Gilman, M. S. A., Erlandson, S. C., Zheng, S., Green, A. G., … Kruse, A. C. (2020). Structural coordination of polymerization and crosslinking by a SEDS–bPBP peptidoglycan synthase complex. *Nature Microbiology*, *5*, 813–820. https://doi.org/10.1038/s41564-020-0687-z

Stankeviciute, G., Miguel, A. V., Radkov, A., Chou, S., Huang, K. C., & Klein, E.

A. (2019). Differential modes of crosslinking establish spatially distinct

regions of peptidoglycan in *Caulobacter crescentus*. *Molecular Microbiology*,

111(4), 995–1008. https://doi.org/10.1111/mmi.14199

Straume, D., Piechowiak, K. W., Olsen, S., Stamsås, G. A., Berg, K. H., Kjos, M.,

… Håvarstein, L. S. (2020). Class A PBPs have a distinct and unique role in

the construction of the pneumococcal cell wall. *PNAS*, *117*, 1–10.

https://doi.org/10.1101/665463

Taguchi, A., Welsh, M. A., Marmont, L. S., Lee, W., Sjodt, M., Kruse, A. C., …

Walker, S. (2019). FtsW is a peptidoglycan polymerase that is functional

only in complex with its cognate penicillin-binding protein. *Nature

Microbiology*, *4*(4), 587–594. https://doi.org/10.1038/s41564-018-0345-x

Tolufashe, G. F., Sabe, V. T., Ibeji, C. U., Ntombel, T., Govender, T., Maguire, G.

E. M., … Honarparvar, B. (2018). Structure and function of L,D- and D,D-

transpeptidase family enzymes from *Mycobacterium tuberculosis*. *Current

Medicinal Chemistry*, *26*, 1–17.

https://doi.org/10.2174/0929867326666181203150231

Tsang, M. J., & Bernhardt, T. G. (2015). A role for the FtsQLB complex in

cytokinetic ring activation revealed by an ftsL allele that accelerates division.

Molecular Microbiology, *95*(6), 925–944. https://doi.org/10.1111/mmi.12905

Typas, A., Banzhaf, M., Van Den Berg Van Saparoea, B., Verheul, J., Biboy, J.,

Nichols, R. J., … Vollmer, W. (2010). Regulation of peptidoglycan synthesis

by outer-membrane proteins. *Cell*, *143*(7), 1097–1109.

https://doi.org/10.1016/j.cell.2010.11.038

Vigouroux, A., Cordier, B., Aristov, A., Alvarez, L., Özbaykal, G., Chaze, T., …
van Teeffelen, S. (2020). Class-A penicillin binding proteins do not contribute
to cell shape but repair cell-wall defects. *ELife*, *9*, 1–26.
https://doi.org/10.7554/elife.51998

Wagstaff, J., & Löwe, J. (2018). Prokaryotic cytoskeletons: Protein filaments
organizing small cells. *Nature Reviews Microbiology*, *16*(4), 187–201.
https://doi.org/10.1038/nrmicro.2017.153

Yousif, S. Y., Broome-Smith, J. K., & Spratt, B. G. (1985). Lysis of *Escherichia
coli* by β-lactam antibiotics: Deletion analysis of the role of penicillin-binding
proteins 1A and 1B. *Journal of General Microbiology*, *131*(10), 2839–2847.
https://doi.org/10.1099/00221287-131-10-2839

Zhao, H., Patel, V., Helmann, J. D., & Dörr, T. (2017). Don't let sleeping dogmas
lie: new views of peptidoglycan synthesis and its regulation. *Molecular
Microbiology*, *106*(6), 847–860. https://doi.org/10.1111/mmi.13853

Chapter 2. EstG is a novel esterase required for cell envelope integrity

2.1 Publication

This Chapter has been posted on *bioRxiv*:

2.2 Abstract

Proper regulation of the bacterial cell envelope is critical for cell survival. Identification and characterization of enzymes that maintain cell envelope homeostasis is crucial, as they can be targets for effective antibiotics. In this study, we have identified a novel enzyme, called EstG, whose activity protects cells from a variety of lethal assaults in the α-proteobacterium *Caulobacter crescentus*. Despite homology to transpeptidase family cell wall enzymes and an ability to protect against cell wall-targeting antibiotics, EstG does not demonstrate biochemical activity towards cell wall substrates. Instead, EstG is genetically connected to the periplasmic enzymes OpgH and BglX, responsible for synthesis and hydrolysis of osmoregulated periplasmic glucans (OPGs), respectively. The crystal structure of EstG revealed similarities to esterases and transesterases, and we demonstrated esterase activity of EstG *in vitro*. Using biochemical fractionation, we identified a cyclic hexamer of glucose as a likely substrate of EstG. This molecule is the first OPG described in *Caulobacter* and establishes a novel class of OPGs, the regulation and modification of which is important for stress survival

and adaptation to fluctuating environments. Our data indicate that EstG, BglX, and OpgH comprise a previously unknown OPG pathway in *Caulobacter*. Ultimately, we propose that EstG is a novel enzyme that, instead of acting on the cell wall, acts on cyclic OPGs to provide resistance to a variety of cellular stresses.

2.3 Introduction

The bacterial cell envelope is a multi-component structure that protects bacteria from the external environment. The envelope is an essential physical barrier to the surroundings, and the factors responsible for building and maintaining the envelope are therefore ideal targets for antibiotics. The Gram-negative cell envelope consists of the inner and outer membranes, with the periplasmic space (or periplasm) between them (Silhavy, Kahne, & Walker, 2010). The bacterial cell wall, made of peptidoglycan (PG), forms a protective meshwork in the periplasm that prevents cell lysis due to turgor pressure (Huang et al., 2008). During growth and division, essential PG metabolic enzymes synthesize, modify, and hydrolyze the PG. Two major classes of PG synthetic enzymes include the glycosyltransferases and transpeptidases (TPases), which catalyze polymerization of the glycan strands and crosslinking of strands via the peptide stems, respectively (Daitch & Goley, 2020). For almost all bacteria, PG is an essential structural component, and the primary biosynthetic PG enzymes are essential during normal growth and division (Daitch & Goley, 2020). Because of this function, these enzymes are the targets of bactericidal antibiotics, such as β-lactams, which inhibit the TPase activity of penicillin-binding proteins (PBPs) (Fisher & Mobashery, 2020). Though some of the most effective antibiotic targets

are PG enzymes, disruption of other components of the envelope can also sensitize cells to stress or antibiotics (May & Grabowicz, 2018; Sutterlin et al., 2016). Thus, understanding the elements of the cell envelope and their relationships to each other is crucial for identifying new drug targets.

In addition to PG, the periplasm of proteobacteria may contain glycopolymers important for maintaining cell envelope integrity called osmoregulated periplasmic glucans (OPGs, also called membrane-derived oligosaccharides). OPGs are glucose polymers that are made in the periplasm and are thought to function as osmoprotectants in response to changes in the environment (Bontemps-Gallo, Bohin, & Lacroix, 2017). Across Gram-negative species, OPGs vary in size, ranging from 5 to 24 glucose units, and geometry, exhibiting linear, branched, and/or cyclic structures depending on which OPG metabolic enzymes are encoded in a given organism (Bohin, 2000; Bontemps-Gallo et al., 2017). OPGs may also be modified with, for example, phospholipid moieties (e.g. phosphoglycerol) or products of intermediary metabolism (e.g. succinyl), which can influence the polymer's overall charge (Bohin, 2000; Bontemps-Gallo et al., 2017). Previously characterized OPGs in α-proteobacteria are large (10-25 glucose units), cyclic, and highly modified (Bohin, 2000). In some bacteria, OPGs are implicated in stress tolerance, as disruption of OPG genes results in increased sensitivity to antibiotics and cell envelope stresses (Bontemps-Gallo et al., 2017; Bontemps-Gallo & Lacroix, 2015). Despite decades of research on OPGs, we have limited knowledge about the diversity of OPG structures, modifications, and metabolic enzymes

across bacteria, suggesting the possibility of undiscovered OPG molecules, pathways, and functions.

In this study, we sought to identify factors required to survive cell wall stress in the α-proteobacterium *Caulobacter crescentus*, which is a well-studied model for morphogenesis and PG metabolism (S. A. Woldemeskel & Goley, 2017). We used a genetic screen to identify an uncharacterized protein required for survival during cell wall stress that we called EstG (*E*sterase for *S*tress *T*olerance acting on *G*lucans, described below). Although EstG is annotated as a member of the TPase superfamily, which consists primarily of PG-acting enzymes, it has no detectable activity towards PG. Our data indicate that EstG instead acts in the OPG metabolic pathway in *Caulobacter,* as it has genetic interactions with the putative OPG enzymes BglX, a periplasmic glucohydrolase, and OpgH, the OPG synthase. The crystal structure of EstG revealed similarity to esterases and transesterases and we confirmed esterase activity *in vitro.* An unbiased mass spectrometry approach identified a native substrate of EstG as a periplasmic, cyclic hexamer of glucose. This is the first OPG identified in *Caulobacter* and establishes a new class of OPGs in α-proteobacteria. We propose that EstG is a novel enzyme that, instead of acting on the PG like most other well-characterized members of the TPase superfamily, acts on cyclic OPGs to fortify the cell envelope and provide resistance to a variety of cellular stresses.

2.4 Results

2.4.1 EstG is essential for suppression of toxic cell wall misregulation

This study initiated with our interest in understanding *Caulobacter* PG metabolism during cell division, which is orchestrated by the polymerizing tubulin homolog FtsZ. We previously demonstrated that expression of a mutant of *ftsZ* lacking the C-terminal linker domain (called ΔCTL) results in misregulation of PG enzymes and cell death, similar to the effects of β-lactam antibiotic treatment (Figure 2.1A) (Sundararajan et al., 2015). We leveraged ΔCTL toxicity to understand mechanisms of stress survival. To this end, we conducted a screen to identify spontaneous suppressors of ΔCTL-induced lethality (Figure 2.1A) (Woldemeskel et al., 2020). Whole genome sequencing of suppressors revealed mutations in genes largely involved in nutrient stress responses (i.e., *spoT* (Boutte & Crosson, 2011), *cdnL* (Woldemeskel et al., 2020; Gallego-Garcia et al., 2017)*,* and *phoB* (Lubin, Henry, Fiebig, Crosson, & Laub, 2016)) (Figure 2.1A, Supplemental Table 2.1). Although each of the ΔCTL suppressors reduce growth rate on their own, slow growth was not sufficient to suppress ΔCTL-induced lethality as tested by growth at low temperature, or in the presence of sub-lethal doses of chloramphenicol or fosfomycin to reduce translation or PG synthesis respectively (Supplemental Figure 2.1A-F). This indicated that these mutations suppressed ΔCTL through other mechanisms. We were especially intrigued by the identification of suppressing mutations in *spoT*, since SpoT is the primary mediator of the stringent response in *Caulobacter* and the stringent response has been implicated in antibiotic resistance (Boutte & Crosson, 2011).

We determined that SpoT-mediated suppression of ΔCTL was a result of high levels of the signaling alarmone (p)ppGpp using an inducible and constitutively activated form of the *Escherichia coli* (*E. coli*) (p)ppGpp synthase, RelA (hereafter called RelA') (Supplemental Figure 2.1G) (Gonzalez & Collier, 2014). To better understand how high levels of (p)ppGpp suppress ΔCTL-induced lethality, we conducted comparative transposon sequencing (Tn-Seq) to identify genes that were synthetically lethal with ΔCTL expression, using the following strains: wild type (WT), RelA'-producing, and RelA'-producing with ΔCTL. Notably, we identified a gene, *CCNA_01638* (hereafter named *estG* for *E*sterase for *S*tress *T*olerance acting on *G*lucans, for reasons described below), that appeared to be essential only in the presence of ΔCTL stress (Figure 2.1B). *estG* acquired abundant transposon insertions in WT and RelA' backgrounds, suggesting that it is non-essential in those strains. However, there were almost no transposon insertions in *estG* in RelA'-producing cells that also produced ΔCTL, indicating an essential function of EstG in the presence of ΔCTL (Figure 2.1B). EstG is an uncharacterized protein that is annotated as a β-lactamase family protein in the transpeptidase superfamily, which primarily consists of PG enzymes. We were therefore interested in studying EstG and its relationship to surviving PG stress.

To validate our Tn-Seq findings, we deleted *estG* in a strain with xylose-inducible production of ΔCTL (Figure 2.1C-D). This strain grew comparably to a ΔCTL uninduced strain in the absence of xylose (Figure 2.1C, solid lines). Production of ΔCTL in an otherwise WT background resulted in cell filamentation and lysis over time, as expected (Figure 2.1C-D, black). Notably, producing ΔCTL

in a Δ*estG* background resulted in faster cell lysis compared to ΔCTL in a WT background (Figure 2.1C-D, grey). We were struck by the importance of *estG* in the presence of ΔCTL-induced stress and sought to further understand the function of EstG.

2.4.2 *estG* is non-essential in unstressed conditions, but required for survival during cell wall stress

Our Tn-Seq results, as well as prior Tn-Seq data, indicated that *estG* would be non-essential in an otherwise WT background (Figure 2.1B) (Christen et al., 2011). We confirmed this by generating a deletion of *estG* (Δ*estG*) and comparing its growth and morphology to WT. We confirmed deletion of *estG* via western blotting with an affinity-purified EstG antibody (Supplemental Figure 2.2A). Δ*estG* cells grew comparably to WT by optical density (Figure 2.2A) and spot dilution (Figure 2.2B), though the colony size of the Δ*estG* strain is slightly smaller than WT. Additionally, by phase contrast microscopy, Δ*estG* cells look morphologically identical to WT (Figure 2.2C). Therefore, *estG* is non-essential under normal growth conditions, but becomes essential during the cell wall stress induced by ΔCTL.

After observing the essentiality of *estG* during ΔCTL production, we hypothesized that EstG may also be required to survive other cell wall stresses, such as cell wall-targeting antibiotics. To test this, we measured the minimum inhibitory concentrations (MIC) of a variety of antibiotics against WT and Δ*estG* cells (Figure 2.2D). Δ*estG* was hypersensitive to every cell wall antibiotic tested (mecillinam, vancomycin, ampicillin, fosfomycin, and cephalexin) compared to WT,

represented by a decreased MIC value. To confirm that hypersensitivity was specifically attributable to loss of EstG, we complemented with a vanillate-inducible copy of *estG* and showed that resistance to ampicillin was restored (Supplemental Figure 2.2B). This indicates a broadly important role of EstG during cell wall stress.

While exploring the possible role of EstG, we noticed the gene immediately downstream from *estG*, *CCNA_01639*, is also annotated as a β-lactamase family protein and we wondered if the two might be functionally related. CCNA_01639 has high sequence identity to EstG (52%), and both are predicted to reside in the periplasm (Juan et al., 2019). Despite similarity to EstG, however, deletion of *CCNA_01639* did not result in hypersensitivity to the β-lactam antibiotics ampicillin or cephalexin (Supplemental Figure 2.2C). Moreover, the double deletion, Δ*estG*Δ*CCNA_01639*, phenocopied the single Δ*estG* mutant (Supplemental Figure 2.2C). Since Δ*CCNA_01639* had no detectable phenotype or genetic relationship to *estG*, we focused the remainder of our study on characterizing EstG.

2.4.3 EstG is periplasmic with no detectable cell wall activity

EstG is 462 amino acids and has an N-terminal putative signal sequence, with cleavage predicted between residues 30 and 31 (Juan et al., 2019). To study the periplasmic localization of EstG, we expressed an inducible EstG-β-lactamase (EstG-BlaM) fusion protein in an otherwise β-lactamase deficient strain (Δ*blaA*; BlaA is the primary β-lactamase that confers β-lactam resistance to *Caulobacter* (West, Yang, & Stephens, 2002)). These cells will only be resistant to ampicillin if EstG contains a periplasmic signal sequence to transport the fused β-lactamase

to the periplasm (Möll, Schlimpert, Briegel, Jensen, & Thanbichler, 2010). The EstG-BlaM strain, when plated in the presence of inducer, displayed resistance to ampicillin, thus validating the predicted periplasmic localization of EstG (Supplemental Figure 2.2D).

The classification of EstG as a β-lactamase family protein as well as the hypersensitivity of ΔestG to ΔCTL and PG-targeting antibiotics suggested that EstG might act as a β-lactamase. However, purified EstG displayed negligible activity against nitrocefin, a substrate used to detect β-lactamase activity *in vitro* (Supplemental Figure 2.2E), compared to a *Caulobacter* enzyme with moderate β-lactamase activity, EstA (Ryu et al., 2016). This, however, does not rule out an activity against the cell wall, so we next tested for ability to bind to the cell wall. *In vitro,* purified EstG pelleted with PG isolated from WT *Caulobacter*, whereas a non-cell wall binding protein (glutathione S-transferase, GST) remained soluble (Supplemental Figure 2.2F). This demonstrates the ability of EstG to bind to some component of the PG. Despite this, EstG did not have detectable activity against any of the most abundant muropeptide species (M4, M5, D44, and D45) or purified PG sacculi *in vitro* (Supplemental Figure 2.3A-G). Finally, we asked if we could identify EstG-dependent chemical changes in PG via muropeptide analysis of sacculi isolated from ΔestG cells as compared to WT. Again, there were no significant differences between ΔestG and WT PG (Supplemental Figure 2.3H-I, Table 2.1). This was surprising given the classification of EstG as a transpeptidase superfamily enzyme, consisting of TPases and carboxypeptidases, which often have detectable activity on cell wall substrates. Considering EstG's lack of activity

against cell wall substrates *in vitro*, we hypothesized that EstG's substrate is novel and not directly related to PG metabolism.

2.4.4 *estG* interacts genetically with *opgH*, which encodes a putative OPG synthase

To search for the molecular function of EstG in an unbiased fashion, we isolated and characterized spontaneous suppressors of the ampicillin sensitivity of Δ*estG*. We sequenced four suppressors total (Supplemental Table 2.2), but were most intrigued by a suppressing mutation in the essential gene, *opgH*, a periplasmic glucan glucosyltransferase (OpgH$_{L480P}$) (Figure 2.3A). OpgH has been characterized in other organisms as the synthase of osmoregulated periplasmic glucans (OPGs) (Bontemps-Gallo et al., 2017). By BLAST searching, OpgH is the only homolog of known OPG-biosynthetic enzymes encoded in the *Caulobacter* genome, but the presence of OpgH indicates the existence of an undiscovered OPG pathway. Isolation of a suppressing mutation in OpgH led us to hypothesize that the sensitivities of Δ*estG* could be related to OPG production or modification.

To characterize the suppressing mutation in *opgH*, we generated the suppressing mutation (*opgH$_{L480P}$*) in a clean genetic background, in the presence or absence of *estG*. In the absence of stress, *opgH$_{L480P}$* did not impact growth, but did restore Δ*estG* cells to a WT colony size (Figure 2.3A). In the presence of ampicillin, *opgH$_{L480P}$* completely restored growth in a Δ*estG* background (Figure 2.3A). We also note that the *opgH$_{L480P}$* mutation in a WT background exhibited moderate growth defects in the presence of ampicillin.

We hypothesized that the *opgH~L480P~* mutation might result in a loss of function variant, as the proline substitution is located within a predicted transmembrane domain (Figure 2.3B) (Krogh, Larsson, Von Heijne, & Sonnhammer, 2001; Sonnhammer & Krogh, 2008). To ensure that the L480P mutation was not destabilizing the protein, we assessed the steady state levels of a 3x-Flag tagged version of the L480P mutant expressed from the native *opgH* locus and saw no difference in protein levels compared to WT (Supplemental Figure 2.4A). We then tested if OpgH~L480P~ could suppress Δ*estG* sensitivity to stress in the presence of WT OpgH by expressing vanillate-inducible *opgH~L480P~*. Indeed, expression of *opgH~L480P~* suppressed Δ*estG* sensitivity to ampicillin in a dominant fashion (Supplemental Figure 2.4B). These data led us to conclude that the OpgH~L480P~ mutant suppresses Δ*estG* by altering OpgH activity or function and is not a loss of function variant.

Interestingly, in revisiting our original ΔCTL suppressors, we discovered an independent suppressing mutation in *opgH* that restored growth in the presence of ΔCTL (Supplemental Table 2.1). This mutant, OpgH~L434P~ (Figure 2.1A), is also a leucine to proline mutation and is located at the edge of a different predicted transmembrane domain (Figure 2.3B). We tested if, like L480P, the L434P mutant could suppress Δ*estG* sensitivity in a dominant fashion. Strikingly, the OpgH~L434P~ mutant completely restored growth of Δ*estG* in the presence of ampicillin (Figure 2.3C). Collectively, our suppressor analyses solidify a genetic link between *estG* and *opgH*.

2.4.5 *estG* and *bglX* are synthetically sick

To gain further insight into which pathway(s) EstG may impact, we examined *estG* on the Fitness Browser database (Wetmore et al., 2015). This database includes sensitivities of a genome-wide library of transposon mutants in *Caulobacter* to numerous stress and environmental conditions and reports on each gene's mutant fitness profile. This resource reflected Δ*estG*'s sensitivities to cell wall antibiotics and also revealed genes that share a similar sensitivity profile to Δ*estG* when disrupted (i.e., genes that are "co-fit"). The top hit for co-fitness with *estG* was an uncharacterized gene, *bglX (CCNA_01162)*, predicted to encode a β-D-glucoside glucohydrolase. The BglX homolog in *Pseudomonas aeruginosa* (*P. aeruginosa*) cleaves glucose polymers (including OPGs) *in vitro*, but BglX homologs are otherwise uncharacterized, with little known about their physiological functions (Mahasenan et al., 2020).

We tested for activity of purified *Caulobacter* BglX as a glucohydrolase *in vitro* against the reporter substrate 4-nitrophenyl-β-D-glucopyranoside (pNPG), where hydrolysis of pNPG results in a color change that can be measured as absorbance over time (Mahasenan et al., 2020). BglX was able to hydrolyze pNPG in a concentration dependent manner, confirming its activity as a glucohydrolase (Figure 2.4A), while EstG displayed no activity against pNPG (Supplemental Figure 2.5A). *In vivo,* we determined that *bglX* is non-essential and that its loss does not appreciably affect growth or morphology (Figure 2.4B-C). As predicted, however, we found that Δ*bglX* shares all of the antibiotic sensitivities we observed for Δ*estG* (Figure 2.2D). We also confirmed periplasmic localization of BglX

(Supplemental Figure 2.5B). Their similar sensitivity profiles indicated a possible genetic interaction between *estG* and *bglX*. Indeed, when both *estG* and *bglX* were deleted (Δ*estG*Δ*bglX*), cells had a growth defect and exhibited slight cell filamentation in unstressed conditions when compared to WT or either single deletion mutant (Figure 2.4B-C). The double deletion also had a lower MIC for all tested antibiotics compared to either of the single deletions, confirming a synthetic sickness between *estG* and *bglX* (Figure 2.2D).

From this synthetic interaction, we hypothesized that EstG and BglX fulfill a similar function. If so, overexpression of one of the enzymes may compensate for loss of the other. To test this, we generated overexpression constructs of *estG* and *bglX,* placed them in a genetic background lacking the other gene, induced overexpression, and subjected the strains to ampicillin treatment. Overproduction of BglX in a Δ*estG* background completely rescued the β-lactam sensitivity of Δ*estG* (Figure 2.4D). Surprisingly, the reverse was not true—overproduction of EstG did not compensate for loss of Δ*bglX*, which was still sensitive to ampicillin (Figure 2.4D). Therefore, though there is a genetic interaction between *estG* and *bglX*, these results suggest that EstG and BglX are not functionally redundant.

2.4.6 Δ*estG* and Δ*bglX* sensitivities are similar to OPG deficient mutants

Inspired by the genetic links to *bglX* and *opgH* that implicated *estG* in the OPG pathway, we wondered whether other aspects of the Δ*estG* phenotype align with the behavior of OPG mutants in other bacteria. In *P. aeruginosa*, OPG production is important for resistance to the ribosome-targeting aminoglycoside antibiotics (Bontemps-Gallo & Lacroix, 2015). Indeed, we found that Δ*estG*, Δ*bglX*, and

$\Delta estG\Delta bglX$ all have decreased MIC values when treated with the ribosome-targeting antibiotics spectinomycin or tetracycline (Figure 2.2D). We hypothesized that, like OPG mutants, deletion of *estG* or *bglX* creates a general disruption of the cell envelope, allowing antibiotics to more easily enter the cell, resulting in lower MIC values.

In *E. coli,* OPG synthesis mutants demonstrate increased sensitivity to outer membrane detergents (Rajagopal, Eis, Bhattacharya, & Nickerson, 2003). We therefore assessed *estG* and *bglX* mutants for sensitivity to the detergent sodium deoxycholate (NaDOC). At 0.6 mg/mL, NaDOC impaired growth of $\Delta estG$ and $\Delta bglX$ mutants, and almost entirely inhibited growth of the double mutant (Supplemental Figure 2.5C). The sensitivities of $\Delta estG$ and/or $\Delta bglX$ strains to ribosome-targeting antibiotics and detergents are consistent with a putative role for both EstG and BglX in maintaining cell envelope integrity via the OPG pathway.

2.4.7 Δ*estG* sensitivities are rescued by increasing osmolarity

In some organisms, increased OPG production is thought to compensate for a decrease in environmental osmolarity. In low osmolarity media, OPGs in *E. coli* comprise up to 5% of the dry weight, while in high osmolarity media, OPGs account for as low as 0.5% of the dry weight (Bontemps-Gallo et al., 2017). With our hypothesis that $\Delta estG$ and $\Delta bglX$ are defective at some point in the OPG pathway, we altered media osmolarity to assess reliance on OPGs in our mutants. We tested this by adding solutes to the media to increase the osmolarity, which we predicted would alleviate the sensitivities of $\Delta estG$ and $\Delta bglX$. When grown in complex media (peptone yeast extract (PYE)), $\Delta estG,$ $\Delta bglX,$ and $\Delta estG\Delta bglX$ are all

hypersensitive to 50 μg/mL ampicillin (Figure 2.4E). However, these sensitivities are almost completely alleviated when PYE + ampicillin is supplemented with 50 mM Tris-HCl to increase the osmolarity (Figure 2.4E). The change in osmolarity does not rescue all mutants with ampicillin sensitivity, as we do not see rescue for a strain bearing deletion of the primary β-lactamase, *blaA* (West et al., 2002). We see a similar result when sodium chloride is provided as an osmolyte instead of Tris-HCl (Supplemental Figure 2.5D). This osmolarity-dependent rescue is further evidence supporting a link between EstG, BglX, and OPGs, and led us hypothesize that EstG acts on OPGs.

2.4.8 EstG structurally resembles and functions as an esterase *in vitro*

To obtain more insight into a putative substrate for EstG, we determined its structure to 2.1 Å resolution using X-ray crystallography (Figure 2.5A, PDB ID 7UIC). The EstG final map shows well-defined density for amino acids 30 to 352 and 367 to 444 with excellent geometry (Figure 2.5A, Table 2.2). EstG is annotated as a member of the transpeptidase superfamily, and within this family are the well-studied PG enzymes with an α/β hydrolase fold, such as penicillin binding proteins (PBPs) and carboxypeptidases. EstG displays a seven stranded, antiparallel β-sheet sandwiched by the N- and the C-terminal helices in the front and other helices in the back (Figure 2.5A). The hydrolase domain in EstG is formed by amino acids 30 to 121 and 218 to 444 and displays two motifs that are highly conserved (Ryu et al., 2016). Motif I consists of the Ser-X-X-Lys sequence, residues 101-104, in EstG (Figure 2.5B) located at the beginning of helix α2, similar to the structure of EstB, a cytoplasmic esterase from *Burkholderia gladioli*

(PDB ID 1CI8, Supplemental Figure 2.6). Motif II contains a highly conserved Tyr, which acts as a base to activate the serine nucleophile. In EstG, this is Tyr218 (Figure 2.5B, Supplemental Figure 2.6) and is also conserved in the other proteins that share this same fold (Supplemental Figure 2.6). Motif I and II are both located in the active site at about 2.7 Å from each other (Figure 2.5A and B).

In total, we determined three structures of EstG: EstG bound to tris (EstG+TRS), EstG bound to tris and sulfate (EstG+TRS+SO$_4$), and EstG bound to tris, sulfate, and tantalum bromide (EstG+TRS+SO$_4$+(Ta$_6$Br$_{12}$)^2). The structures are very similar with a pairwise root-mean-square deviation ranging 0.24 to 0.26 Å for amino acids 398-401 as calculated with SSM Coot (Emsley & Cowtan, 2004). The binding of a SO$_4$ molecule close to Motif I and Motif II correlates with the presence of clear electron density for the loop 346-357 (PDB ID 7UIC, 7UIB, Figure 2.5B, Supplemental Figure 2.7). Structural alignment of EstG+TRS+SO$_4$ with EstB bound to diisopropyl fluorophosphate (DFP, PDB ID 1CI9) highlights the partial overlap between the SO$_4$ in EstG and the DFP bound to catalytic serine residue in EstB (Figure 2.5C).

In EstG, residues 122 to 217 are on top of the hydrolase fold (Figure 2.5A). Within it, residues 138 through 151 define an insertion of a hairpin formed by strand β4-β5 (Supplemental Figure 2.6, 2.8) which is also present in the transesterase enzyme, simvastatin synthase (*Aspergillus terreus* LovD, PDB ID 4LCM). Notably, this hairpin is absent in EstB.

The structural alignment over those deposited in the PDB highlights a structural conservation among enzymes in this large family of proteins. The most

44

similar structures to EstG by structure/sequence are esterases (EstB, PDB ID 1CI8), transesterases (LovD, PDB ID 3HLB), carboxylesterases (PDB ID 4IVK), PBP homologs (PDB ID 2QMI), and D-amino acid amidases (PDB ID 2DNS). All these enzyme classes are referenced in the literature as having homology to β-lactamase folding esterases (Ryu et al., 2016). Interestingly, D-amino acid amidases and aminohydrolases also lack the hairpin insertion described for EstG (Supplemental Figure 2.8).

Based on the structural similarity of EstG to EstB, a cytoplasmic esterase with an unknown native substrate, we sought to compare the two enzymatically. Despite the β-lactamase fold, EstB has no β-lactamase or peptidase activity (Wagner, Petersen, Schwab, & Kratky, 2009), similar to our observations with EstG (Supplemental Figure 2.2E, Supplemental Figure 2.3). EstB does, however, demonstrate esterase hydrolytic activity (Wagner et al., 2009). *In vitro* esterase activity can be detected using p-nitrophenyl esters, such as p-nitrophenyl butyrate (pNB), as hydrolysis of the substrate creates a visible color change that can be measured as absorbance over time (similar to pNPG hydrolysis). Using this assay, EstG significantly hydrolyzed pNB as compared to the negative control, GST (Figure 2.5D). We sought to create a catalytically dead mutant of EstG by mutating the predicted active site serine, Ser101, within motif I. Consistent with our prediction, the S101A mutant cannot hydrolyze pNB *in vitro*, confirming that it is a catalytically dead variant (Figure 2.5D). Additionally, when Ser101 is mutated to alanine (S101A) in the chromosomal copy of *estG*, this mutant phenocopies the β-lactam sensitivity of Δ*estG in vivo* (Figure 2.5E). These data establish the

essentiality of EstG's enzymatic activity in protecting the cell against stress and confirms activity of EstG as an esterase.

2.4.9 EstG enzymatically modifies a cyclic hexasaccharide periplasmic glucan

EstG can act as an esterase *in vitro* and our genetic and osmolarity data implicate OPGs as a substrate. However, *Caulobacter* OPGs have never been characterized, and the absence of homologs of most characterized OPG-metabolizing enzymes in this organism precludes a simple prediction of which OPG species may be present. To identify the native substrate of EstG, we fractionated WT cells into periplast and spheroplast fractions followed by isolation of putative periplasmic sugars (Figure 2.6A). Given that *E. coli* OPGs are between 1 to 10 kDa, we hypothesized that *Caulobacter* OPGs might be of similar size. Therefore, we further fractionated to isolate only components within our desired size range. The remaining sample was boiled to remove contaminating proteins, leaving sugars or other heat-resistant metabolites intact. *In vitro,* we combined this 1-10 kDa periplast isolate with purified EstG or the catalytically dead mutant, EstG$_{S101A}$. We then separated molecules in the treated periplast by high-performance liquid chromatography (HPLC) and selected for peaks that decreased in abundance when mixed with EstG, but not when mixed with EstG$_{S101A}$. Peaks of interest were then identified by mass spectrometry. Using this approach, we identified a molecule that decreased in abundance ~40% when incubated with EstG (Figure 2.6B), indicating that EstG enzymatically modified this substrate in some way. The mass of the parental ion led us to hypothesize that the molecule

resembled α-cyclodextrin (α-CD), a cyclic, hexameric glucose polymer. Notably, the MS/MS spectra for this molecule in the periplast + EstG$_{S101A}$ (top half of Figure 2.6C), most closely matches the library spectra for α-CD (bottom half of Figure 2.6C). Greater than 80% of the fragmentation signal generated from our experiments match the ion profile for α-CD. We next attempted to detect chemical modification of α-CD by EstG using our periplast and mass spectrometry workflow. However, due to the complexity of the periplast fraction and the small expected amount of modified α-CD, we were not able to identify a modified α-CD molecule or determine a specific activity of EstG on α-CD. Though this small, cyclic sugar is a novel structure for an OPG, it is consistent with the existence of cyclic OPGs in other bacteria, notably Family IV cyclic OPGs synthesized by OpgH in *Rhodobacter sphaeroides* and related α-proteobacteria (Bontemps-Gallo et al., 2017).

We next sought to validate α-CD as an EstG substrate *in vitro*. If α-CD is a substrate for EstG, we reasoned we could add α-CD to the pNB hydrolysis assay and inhibit pNB hydrolysis through competition for the active site. Indeed, increasing amounts of α-CD reduced EstG's hydrolysis of pNB in a concentration-dependent manner, while EstG$_{S101A}$ remained unchanged with added α-CD (Figure 2.6D). Though the inhibition is clearly concentration-dependent, we wanted to confirm that α-CD was competitively inhibiting EstG's active site, consistent with it being a substrate. To achieve this, we measured the rate of pNB hydrolysis with increasing concentrations of pNB and a consistent amount of α-CD. For a competitive inhibitor, we expect to see a constant V_{max} and an increased K_m value

with added α-CD. By plotting the rate of hydrolysis +/- α-CD, the V_{max} values of the two curves are close at 0.92 molecules/min without α-CD and 1.15 molecules/minute with α-CD (Figure 2.6E, Supplemental Figure 2.9). However, the K_m values differ, at 11.2 mM without α-CD and 53.7 mM with α-CD (Figure 2.6E, Supplemental Figure 2.9). These values produce the expected pattern for a competitive inhibitor and gave us confidence that α-CD interacts directly with the active site of EstG and is thus structurally similar to the native substrate. Collectively, these data suggest that EstG modifies a previously uncharacterized cyclic, hexameric OPG in a novel manner, thereby contributing to cell envelope homeostasis during stress (Figure 2.7).

2.5 Discussion

It is clear from our work that proteins and pathways that play critical roles in maintaining cell envelope homeostasis remain undiscovered. Our identification of EstG and its novel role in the *Caulobacter* OPG pathway suggests there might be unexplored substrates of other TPase family enzymes. We identified EstG through a Tn-Seq screen as an essential factor for surviving ΔCTL-induced cell wall stress (Figure 2.1). Though *estG* is non-essential in unstressed conditions (Figure 2.2), Δ*estG* is hypersensitive to cell envelope stresses (Figure 2.2D, Supplemental Figure 2.5C). Despite its homology to TPase family proteins, EstG does not detectably modify the PG (Supplemental Figure 2.3, Table 2.1). Instead, genetic interactions with *opgH* (Figure 2.3), encoding the predicted OPG synthase, and *bglX* (Figure 2.4), encoding a putative OPG hydrolase, implicate EstG in the OPG pathway. *In vitro* biochemistry revealed a periplasmic substrate of EstG as a cyclic hexamer of glucose, which is the first reported OPG in *Caulobacter* (Figure 2.6).

In this study, we originally set out to identify mechanisms of ΔCTL suppression. We were surprised to primarily recover suppressing mutations in stress response pathways, instead of cell envelope- or cell wall-related genes. Activation of stress response pathways typically leads to sweeping changes in cellular physiology, suggesting that the stress imposed by ΔCTL is multifaceted and cannot easily be suppressed by mutation of a single factor. We leveraged (p)ppGpp-mediated suppression of ΔCTL to identify more direct factors involved in surviving ΔCTL-induced stress and, through this approach, found *estG*. While following up on the role of EstG in (p)ppGpp-dependent suppression of ΔCTL, we

found that *estG* is unrelated to (p)ppGpp. Instead, it was the additional antibiotic stress (e.g., introduction of gentamycin marked *relA'* to produce high (p)ppGpp) in the presence of ∆CTL stress that made *estG* essential (data not shown). We further confirmed this by deleting *estG* in a ∆CTL background suppressed by high (p)ppGpp through a hyperactive *spoT* mutant, which was not lethal (data not shown). In retrospect, this finding is not entirely surprising given the critical role we established for EstG in surviving a variety of antibiotic stresses.

Both our own characterization of the ∆*estG* strain and information in the Fitness Browser database (Price et al., 2018; Wetmore et al., 2015) indicated a wide range of antibiotic sensitivities. Those we tested (Figure 2.2D) include many classes of PG- and ribosome-targeting antibiotics such as β-lactam (ampicillin, mecillinam, cefaphlexin), glycopeptide (vancomycin), phosphonic (fosfomycin), aminoglycoside (spectinomycin), and tetracycline antibiotics (Figure 2.2D). The Fitness Browser additionally indicated sensitivities to a DNA-gyrase-targeting antibiotic (nalidixic acid) and an inhibitor of lipid A biosynthesis (CHIR-090). Collectively, this establishes ∆*estG* hypersensitivity to antibiotics that target at least four different cellular processes (PG metabolism, protein synthesis, DNA topology, and outer membrane biosynthesis/homeostasis). We looked for similarities among these drug classes but found no obvious biochemical similarities. For instance, nalidixic acid and ampicillin are relatively small, while vancomycin is a large glycopeptide, and though most molecules tested were polar and uncharged, others, such as chloramphenicol (data not shown) and sodium deoxycholate are charged. Ultimately, these broad antibiotic sensitivities support the idea of a global

cell envelope defect resulting from loss of EstG's enzymatic activity, and not a sensitivity specific to a particular molecular feature.

EstG is classified as a β-lactamase family protein within the TPase superfamily, which is why it stood out as an attractive candidate from a cell wall stress screen. Of characterized proteins, EstG shares the most structural and biochemical similarities to EstB from *B. gladioli*, another enzyme in the β-lactamase family that adopts an α/β hydrolase fold. They both contain an active site serine, but EstG lacks the common esterase motif, G-X-S-X-G, present in EstB. This esterase motif is not required for EstB's hydrolase activity, however (Wagner et al., 2009). Our data provide evidence of EstG acting as an esterase and not a β-lactamase, and we have also identified a novel EstG substrate. Within *Caulobacter*, EstG is one of eight enzymes that are classified as putative β-lactamases (West et al., 2002) that potentially do not function as β-lactamases at all. EstG is just one example of the numerous enzymes across bacteria that fall into the TPase superfamily but have novel activities or substrates.

Though not required under normal growth, our data demonstrate the importance of EstG acting on its sugar substrate and implicates an essential role for OPGs in stress survival. OPGs have not been previously identified in *Caulobacter*, though the presence of an *opgH/mdoH* homolog in the genome was reported (Bohin, 2000). OPGs in several α-proteobacterial species of the orders Rhizobiales and Rhodobacterales are characterized and have a wide variety of sizes and structures, consisting of family II, III, and IV OPGs (Bohin, 2000). These OPGs can range from 10-25 glucose monomers, but all three classes are cyclic

polymers, as opposed to the linear family I OPGs commonly found in γ-proteobacteria. We were surprised to find that the only *opg* gene in *Caulobacter* is *opgH*. As we report a cyclic OPG-like molecule, we would expect other OPG genes responsible for cyclizing and modifying OPGs to be present in *Caulobacter*. Uniquely, other α-proteobacteria encode OPG metabolic enzymes that are not homologs of the *opg* genes in *E. coli* including *chvA* and *chvB* in *Agrobacterium tumefaciens*, *ndvA* and *ndvB* in *Sinorhizobium meliloti,* and *cgs* and *cgt* in *Brucella abortus* (Bontemps-Gallo et al., 2017)*.* Distinct from the well-described *opg*/*mdo* genes, these genes imply the existence of a wide variety of OPG enzymes and OPG structures across bacteria. Additionally, among these OPG metabolic genes, there are proteins whose precise enzymatic functions remain elusive, such as NdvD in *S. meliloti* (Bontemps-Gallo et al., 2017). We propose that EstG and BglX are additional examples of enzymes with unique roles in OPG synthesis, modification, and/or hydrolysis.

Mutants of OPG enzymes in diverse bacteria typically have pleiotropic phenotypes, including those discussed for *estG* and *bglX* mutants (e.g. antibiotic sensitivity) as well as defects in motility, biofilm formation, and/or virulence (Bontemps-Gallo et al., 2017)*.* Despite the impact of OPGs on important cellular behaviors and properties, we do not know the mechanism(s) behind OPG-mediated effects. One model suggests OPGs function as osmoprotectants by establishing a Donnan equilibrium across the outer membrane. The idea is that production of negatively charged OPGs in the periplasm (as occurs in *E. coli*) creates a high concentration of fixed, charged molecules that cannot cross the

outer membrane. The accumulation of charged OPGs attracts counterions to the periplasm, and maintains a Donnan membrane potential across the outer membrane, allowing for isosmolarity of the periplasm and cytoplasm even in low osmolarity environments (Kennedy et al., 1982; Stock, Rauch, & Roseman, 1977). The Donnan potential has also been suggested to play a role in permeability of the envelope to antibiotics (Alegun, Pandeya, Cui, Ojo, & Wei, 2021). These mechanisms, however, presume that OPGs are always highly charged, which is not the case in all bacteria, and may or may not be the case in *Caulobacter* (Bontemps-Gallo et al., 2017). Though we were not able to determine the exact EstG-mediated modification on *Caulobacter* OPGs, it is possible that EstG adds a charged moiety in order to mediate the Donnan potential and protect the cell envelope.

Beyond the Donnan potential, OPGs are postulated to have other functions in cell envelope homeostasis, such as a role in envelope organization, cell signaling, and protein folding (Bontemps-Gallo et al., 2017)*.* For instance, loss of OPGs in *E. coli* was reported to cause an increase in the periplasmic space of plasmolyzed cells, perhaps reflecting a structural role in maintaining envelope geometry (Holtje, Fiedler, Rotering, Walderich, & Van Duin, 1988). Deletion of *estG*, however, did not result in a notable increase in periplasmic space (data not shown) and suggests that *Caulobacter opg* mutants may not directly impact the structure of the periplasm.

Despite the unclear mechanism of OPG-mediated envelope protection, our data suggest that the modification and/or hydrolysis activity of EstG and BglX on

53

Caulobacter OPGs contributes to osmoprotective properties, most notably supported by the osmolarity-dependent rescue of antibiotic sensitivity (Figure 2.4E). It is possible that more mechanistic insight can be revealed with further study of OPG pathways and enzymes in other organisms. For instance, the *E. coli* OpgH enzyme links nutrient availability with cell size by inhibiting FtsZ when UDP-glucose levels are high (Hill, Buske, Shi, & Levin, 2013). This is likely not a conserved function of *Caulobacter* OpgH, as it lacks most of the N-terminal FtsZ-interacting region. Suppressor mutations within *opgH* have also been identified in *E. coli* that further implicate OpgH with envelope homeostasis. A nonsense mutation in *opgH* was isolated in a lipopolysaccharide (LPS) mutant that together conferred resistance to a polypeptide antibiotic (bacitracin), a polyketide antibiotic (rifampin), and sodium dodecyl sulfate (Falchi et al., 2018). Due to the integral role of LPS in outer membrane integrity, it was proposed that either the lack of OPGs or loss of OpgH reduces membrane permeability to antibiotics, thus conferring resistance. However, unlike the *opgH* suppressing mutations identified in this study (L480P and L434), the *E. coli opgH* nonsense mutation was recessive to WT. Though this suggests a different mechanism of suppression, it does not rule out the possibility of deficient OPG production in the *Caulobacter opgH* mutants, resulting in a less permeable membrane and our observed resistance to stress. Two spontaneous *opgH* mutants were also isolated in *Vibrio cholerae* that suppressed the hyperosmotic lethality of a lytic transglycosylase (LTG) mutant (Weaver et al., 2022). This model suggested that LTG mutants inadequately recycle PG products, resulting in excessive periplasmic crowding (Weaver et al.,

2022). Additional production of OPGs exacerbated this periplasmic crowding, which was lethal in low osmolarity environments (Weaver et al., 2022). Though the hyperosmotic growth defect of LTG mutants and periplasmic crowding could indicate a similar role for EstG, the identification of an OPG substrate indicates a direct link to OPG metabolism, rather than an indirect consequence of molecular crowding. An important avenue for future work includes functional studies of OpgH and these mutants as well as determination of the exact structure and potential modifications on *Caulobacter* OPGs. These insights can ultimately bridge our gap in understanding of the mechanistic role of OPGs in the *Caulobacter* envelope.

2.6 Materials and Methods

***Caulobacter crescentus* and *Escherichia coli* growth media and conditions**

C. crescentus NA1000 cells were grown at 30˚C in peptone-yeast extract (PYE) medium. *E. coli* Rosetta(DE3)/pLysS cells were grown at 30˚C in Luria-Bertani (LB) medium. Xylose or glucose were used at concentrations of 0.3% (w/v) for induction experiments. Antibiotics were used in liquid (solid) medium at the following concentrations for *Caulobacter* growth: gentamycin, 1 (5) μg/mL; kanamycin, 5 (25) μg/mL; spectinomycin, 25 (100) μg/mL. Streptomycin was used at 5 μg/mL in solid medium. *E. coli* antibiotics were used in liquid (solid) medium as follows: ampicillin, 50 (100) μg/mL; gentamicin, 15 (20) μg/mL; kanamycin, 30 (50) μg/mL; and spectinomycin, 50 (50) μg/mL. For growth curves, a Tecan Infinite M200 Pro plate reader measured absorbance every 30 minutes at OD_{600} of a 100 μL culture volume in a 96 well plate in biological triplicate with intermittent shaking. For spot dilution assays, mid-log cells were diluted to an OD_{600} of 0.05 and serially diluted up to 10^{-6} before spotting 5 μL of each dilution onto a PYE plate with indicated inducer and/or antibiotic. Plates were incubated at 30˚C for 48 hours, or until the appearance of colonies at the lowest dilution in the control strain. To determine the minimum inhibitory concentration (MIC), mid-log phase cells were diluted to OD_{600} of 0.5 and 200 μL were spread out onto a PYE plate. Antibiotic strips with increasing concentration of antibiotic were placed on the dried plate, inverted, and grown at 30˚C for 48 hours. Some MIC values were estimated by loss of growth

on plates with a range of antibiotic added to the media. A summary of all strains, plasmids, and primers used in this study can be found in Supplement Table 3.

Atypical strain construction

We were unable to generate the following strains in low osmolarity PYE media, so they were constructed in M2G minimal media: EG3116 (ΔCTL+$\Delta estG$), EG3369 ($opgH_{L480P}$), EG3371 ($\Delta estG$+OpgH$_{L480P}$), and EG3377 (P_{van}-$opgH$). For a 500 mL batch of M2G plates, 465 mL of water and 7.5 g agar (1.5%) were autoclaved. Once cooled, 25 mL of 5x M2 salts, 500 µL of 500 mM MgSO$_4$, 500 µL of 10 mM FeSO$_4$ 10 mM EDTA (Sigma F-0518), and 0.3% glucose were added. Additional antibiotics or media supplements needed for selection were also added at this time.

Phase-contrast microscopy

Exponential phase cells were spotted on 1% agarose pads and imaged using a Nikon Eclipse Ti inverted microscope equipped with a Nikon Plan Fluor 100X (NA1.30) oil Ph3 objective and Photometrics CoolSNAP HQ^2 cooled CCD camera. Images were processed using Adobe Photoshop.

Suppressor screening and whole genome sequencing

For the ΔCTL suppressor screen, *Caulobacter* strains EG937 or EG1214 strains were inoculated from individual colonies and grown overnight in PYE media (with no inducer) until stationary phase. Cells were plated on PYE agar plates containing

0.3% (w/v) xylose to induce ΔCTL expression and incubated at 30˚C until the appearance of colonies (suppressors). Suppressors were tested for growth in PYE media with 0.3% xylose overnight. Immunoblotting with FtsZ-antiserum was used to confirm xylose-induced ΔCTL expression. Genomic DNA was extracted from suppressors using Qiagen DNeasy Blood and Tissue Kit. Mutations were identified from MiSeq analysis of genomic DNA from suppressor strains. Spontaneous suppressors of Δ*estG* were isolated by plating Δ*estG* (EG2658) on PYE+100 µg/mL ampicillin and isolating resistant colonies. Resistance was confirmed by spot dilution on plates containing 50 µg/mL ampicillin. Genomic DNA was extracted from suppressors using Qiagen DNeasy Blood and Tissue Kit and sent to Microbial Genome Sequencing Center (MiGS) for whole genome sequencing and BreSeq analysis.

Cell fractionation

Cells were fractionated into periplasm and spheroplast using the previously described methods in Judd et al, except that 2 µg/mL lysozyme was used (Judd et al., 2005). Briefly, cells were grown at 30˚ to an OD_{600} of 0.5 in 10 mL of PYE. Cells were pelleted at 3,500 x g for 10 minutes and the supernatant removed. The pellet was resuspended in 1 mL of periplasting buffer (50 mM Tris-HCl pH 8.0, 18% sucrose, and 1 mM $CaCl_2$) and then 2 µg/mL of lysozyme and 1 mM EDTA was added. Contents were left on ice for 30 minutes and then spun at 3,140 x g for 5 minutes. The supernatant (periplast fraction) was carefully removed to a fresh tube, and the pellet (spheroplast fraction) was saved.

Transposon library preparation, sequencing, and analysis

Transposon libraries were prepared, sequenced, and analyzed using the same methods as previously described in Woldemeskel et al. and Lariviere et al. (Woldemeskel et al., 2020; Lariviere et al., 2019). Tn-Seq libraries were generated for WT (EG865), RelA' (EG1799) and ∆CTL+RelA' (EG1616). 1L PYE cultures were harvested at OD_{600} of 0.4–0.6, washed 5 times with 10% glycerol, and electroporated with the Ez-Tn5 <Kan-2> transposome (Epicentre, Charlotte, North Carolina). Cells recovered at 30˚C shaking for 90 minutes, and plated on PYE-Kan plates. The RelA' library was plated on PYE-Kan with gentamycin and 0.003% xylose to induce RelA' expression. ∆CTL+RelA' library was plated on PYE-Kan plates with spectinomycin, streptomycin, gentamycin, and 0.003% xylose to induce RelA' and ∆CTL. Colonies were scraped off plates, combined, resuspended to form a homogeneous solution in PYE, and flash frozen in 20% glycerol. The DNeasy Blood and Tissue Kit (Qiagen, Hilden, Germany) was used to extract genomic DNA from each pooled library. Libraries were prepared for Illumina Next-Generation sequencing through sequential PCR reactions. The initial PCR round used arbitrary hexamer primers with a Tn5 specific primer going outward. The second round used indexing primers with unique identifiers to filter artifacts arising from PCR duplicates. Indexed libraries were pooled and sequenced at the University of Massachusetts Amherst Genomics Core Facility on the NextSeq 550 (Illumina, San Diego, California).

Sequencing reads were first demultiplexed by index, each library was concatenated and clipped of the molecular modifier added in the second PCR using Je (Girardot, Scholtalbers, Sauer, Su, & Furlong, 2016):

java -jar /je_1.2/je_1.2_bundle.jar clip F1 = compiled.gz LEN = 6

Reads were then mapped back to the Caulobacter crescentus NA1000 genome (NCBI Reference Sequence: NC_011916.1) using BWA (Li & Durbin, 2010) and sorted using Samtools (Li et al., 2009):

bwa mem -t2 clipped.gz | samtools sort -@2 - > sorted.bam

Duplicates were removed using Je (Girardot et al., 2016) and indexed with Samtools (Li et al., 2009) using the following command:

java -jar /je_1.2/je_1.2_bundle.jar markdupes I = sorted.bam O = marked.bam M = METRICS.txt MM = 0 REMOVE_DUPLICATES = TRUE

samtools index marked.bam

The 5' insertion site of each transposon were converted into .wig files comprising counts per position and visualized using Integrative Genomics Viewer (IGV) (J. T. Robinson et al., 2011; Thorvaldsdottir, Robinson, & Mesirov, 2012). Specific hits

for each library were determined with coverage and insertion frequency using a bedfile containing all open reading frames from NC_011916.1 and the outer 20% of each removed to yield a clean and thorough insertion profile. This was determined using BEDTools (Mccarthy, Chen, & Smyth, 2012; M. D. Robinson, Mccarthy, & Smyth, 2010) and the following commands:

```
bedtools genomecov -5 -bg marked.bam > marked.bed
```

```
bedtools map -a NA1000.txt -b marked.bed -c 4 > output.txt
```

Tn-Seq data have been deposited in the Sequence Read Archive (SRA) under accession numbers:

Protein purification

All purified proteins were overproduced in Rosetta (DE3) pLysS *E. coli* from the following plasmids: His_6-EstG-His_6, pEG1622; His_6-EstG$_{S101A}$-His_6, pEG1706; His_6-EstA, pEG1950; His_6-BglX-His_6, pEG1779. Cells were induced with 1mM IPTG for 4 hours at 30˚C. Cell pellets were resuspended in Column Buffer A (50 mM Tris-HCl pH 8.0, 300 mM NaCl, 10% glycerol, 20 mM imidazole, 1 mM β-mercaptoethanol) flash frozen in liquid nitrogen and stored at -80˚C. To purify the His-tagged proteins, pellets were thawed at 37˚C, and 10 U/mL DNAse 1, 1 μg/mL lysozyme, and 2.5 mM $MgCl_2$ were added. Cell slurries were left on ice and

occasionally inverted for 45 minutes, then sonicated and centrifuged for 30 minutes at 15,000 x g at 4°C. The protein supernatant was then filtered and loaded onto a pre-equilibrated HisTrap FF 1mL column (Cytiva, Marlborough, Massachusetts). The His-tagged proteins were eluted in 30% Column Buffer B (same as Column Buffer A but with 1M imidazole). Peak fractions were concentrated and applied to a Superdex 200 10/300 GL (Cytiva) column equilibrated with EstG storage buffer (50 mM HEPES-NaOH pH 7.2, 150 mM NaCl, 10% glycerol, 1 mM β-mercaptoethanol). Peak fractions were combined, concentrated, and snap-frozen in liquid nitrogen and stored at -80°C.

Immunoblotting

Purified His$_6$-EstG-His$_6$ was dialyzed into PBS and used to immunize a rabbit for antibody production (Pocono Rabbit Farm & Laboratory, Canadensis, Pennsylvania). To affinity purify the EstG antisera, His$_6$-EstG-His$_6$ in EstG storage buffer was coupled to Affigel 10 resin (Bio-Rad, Hercules, California). After washing the resin 3 times with cold water, add approximately 10 mg of protein to 1 mL of Affigel 10 resin to rotate at 4°C for 4 hours. 75 mM Tris pH 8.0 was added to terminate the reaction and left to rotate at 4°C for 30 minutes. EstG-resin was washed in a column with the following cold reagents: 10 mL EstG storage buffer, 15 mL Tris-buffered saline (TBS), 15 mL 0.2 M glycine-HCl pH 2.5 with 150 mM NaCl, 15 mL TBS, 15 mL guanidine-HCl in TBS, and 20 mL TBS. EstG antisera was combined with EstG-resin, and incubated, rotating, overnight at 4°C. Unbound sera flowed through the column and was washed with 25 mL TBS, 25 mL TBS with

500 mM NaCl and 0.2% Triton X-100, and a final wash of 25 mL TBS. Bound Anti-EstG was eluted with 0.2 M glycine pH 2.5 and 150 mM NaCl, dialyzed into TBS, and diluted 1:1 with glycerol. Anti-EstG antibody specificity was validated by western blot to recognize a band in wild type lysate that is absent in a Δ*estG* mutant.

Western blotting was performed using standard lab procedures. Cells in log phase were isolated and lysed in SDS-PAGE loading buffer and boiled for 10 minutes. For a given experiment, equivalent OD units of cell lysate were loaded. SDS-PAGE and transfer of protein to nitrocellulose membrane were performed using standard procedures. Antibodies were used at the following concentrations: EstG-1:1000; SpmX-1:10,000 (Radhakrishnan, Thanbichler, & Viollier, 2008); Flag-1:1,000 (Sigma, St. Louis, Missouri); CdnL-1:2,500 (Woldemeskel et al., 2020).

In vitro pNB hydrolysis or pNPG assay

To test for serine hydrolase activity using p-nitrophenyl butyrate (pNB, Sigma), indicated proteins were used at 10 µM in a 50 µL reaction containing 50 mM Tris-HCl pH 8. pNB was added last to the samples at a concentration of 4 µM. Absorbance was measured every minute at 405 nm for 10 minutes. To test for glucosidase activity using 4-Nitrophenyl-β-D-glucopyranoside (pNPG, Sigma), indicated proteins were used at listed concentrations in a 50 µL reaction containing 50 mM Tris-HCl pH 8. pNPG was added last at a final concentration of 4 µM. Absorbance was measured every minute at 405 nm for 10 minutes.

Nitrocefin hydrolysis assay

To assess β-lactamase activity through hydrolysis of nitrocefin, 10 µM of indicated proteins were mixed with 100 µM nitrocefin (Calbiochem, Sigma) in a reaction buffer containing EstG storage buffer (50 mM HEPES-NaOH pH 7.2, 150 mM NaCl, 10% glycerol, 1 mM BME) to a final volume of 100 µL. Absorbance was measured at 492 nm every 10 minutes for 4 hours.

Sacculi purification and PG binding assay

Sacculi for PG binding assay were prepared as previously described in Meier et al (Meier et al., 2017). Wild type (EG865) *Caulobacter* cells were grown in 1L of PYE at 30˚C to an OD_{600} of 0.5. Cells were pelleted by centrifugation at 6,000 x *g* for 10 minutes and resuspended in 10 mL of 1X PBS. The cells were added dropwise to a boiling solution of 4% SDS where they were continuously mixed and boiled for 30 minutes, then incubated overnight at room temperature. Sacculi were pelleted by ultracentrifugation at 42,000 x g in an MLA-80 rotor for 1 hour at 25˚C and remaining pellet was washed four times with ultra-pure water with a final resuspension in 1 mL PBS with 20 µL of 10 mg/mL amylase, left at room temperature overnight. Then the sacculi were pelleted at 90,000 x g in an MLA-130 rotor for 15 minutes at 25˚C and washed three times with ultra-pure water, with a final resuspension in 1 mL of PG binding buffer (20 mM Tris-HCl pH 6.8, 1 mM $MgCl_2$, 30 mM NaCl, 0.05% Triton X-100). To each reaction, 6 µg of each protein was added to either PG or buffer. Reactions were left on ice for 30 minutes

and then centrifuged for 30 minutes at 90,000 x g in the MLA-130 rotor at 4˚C. Supernatant was saved and the pellet was resuspended in PG binding buffer and saved as the PG bound isolate. SDS-PAGE loading dye was added to a final concentration of 1X to each sample and run on an SDS-PAGE gel, Coomassie stained, and imaged.

PG purification and analysis

PG samples were analyzed as described previously (Alvarez, Hernandez, de Pedro, & Cava, 2016; Desmarais, De Pedro, Cava, & Huang, 2013). In brief, samples were boiled in SDS 5% for 2 h and sacculi were repeatedly washed with MilliQ water by ultracentrifugation (110,000 x g, 10 min, 20˚C). The samples were treated with muramidase (100 µg/mL) for 16 hours at 37ºC. Muramidase digestion was stopped by boiling and coagulated proteins were removed by centrifugation (10 min, 22,000 x g). The supernatants were first adjusted to pH 8.5-9.0 with sodium borate buffer and then sodium borohydride was added to a final concentration of 10 mg/mL. After reduction during 30 min at room temperature, the samples pH was adjusted to pH 3.5 with orthophosphoric acid. UPLC analyses of muropeptides were performed on a Waters UPLC system (Waters Corporation, USA) equipped with an ACQUITY UPLC BEH C18 Column, 130 Å, 1.7 µm, 2.1 mm X 150 mm (Waters, USA) and a dual wavelength absorbance detector. Elution of muropeptides was detected at 204 nm. Muropeptides were separated at 45°C using a linear gradient from buffer A (formic acid 0.1% in water) to buffer B (formic acid 0.1% in acetonitrile) in an 18-minute run, with a 0.25 mL/min flow.

To test the activity of EstG against cell wall substrates, sacculus or purified muropeptides were used as substrate. Reactions were performed in triplicates and contained 10 µg of purified enzyme, 50 mM Tris-HCl pH 7.5, 100 mM NaCl, and 10 µg of purified *Caulobacter* sacculus or 5 µg of purified M4, M5, D44 or D45, in a final 50 µL reaction volume. Reactions were incubated at 37°C for 24 h, then heat inactivated (100°C, 10 min) and centrifuged (22,000 x g, 15 min), for separation of soluble and pellet fractions. Soluble fractions were adjusted to pH 3.5. Pellet fractions were resuspended in water and further digested with muramidase for 16 h at 37˚C. Muramidase reactions were reduced and adjusted to pH 3.5 as explained before. Both soluble and muramidase digested samples were run in the UPLC using the same PG analysis method described above.

Relative total PG amounts were calculated by comparison of the total intensities of the chromatograms (total area) from three biological replicas normalized to the same OD600 and extracted with the same volumes. Muropeptide identity was confirmed by MS/MS analysis, using a Xevo G2-XS QTof system (Waters Corporation, USA). Quantification of muropeptides was based on their relative abundances (relative area of the corresponding peak) normalized to their molar ratio. The program GraphPad PRISM® Software (Inc., San Diego, California, www.graphpad.com) was used for all statistical analyses. To determine the significance of the data, the t-test (unpaired) was performed.

Crystallography, Data Collection, Structure Determination and Refinement

EstG protein purified for crystallography was prepared the same way as described above, with the exception of the storage buffer changed to 50 mM HEPES-NaOH pH 7.2, 150 mM NaCl, 1 mM DTT. Crystals of wild type EstG were grown by vapor diffusion in hanging drops set up with a Mosquito LCP robot (SPT Labtech, Melbourn, United Kingdom). Crystal growth was monitored using a crystallization imager ROCKIMAGER (Formulatrix, Bedford, Massachusetts). High quality crystals grew with a reservoir solution containing 20% PEG500 MME, 10% PEG20000, 0.1 M Tris/Bicine pH 8.5 and 90 mM mixture of sodium nitrate, sodium phosphate dibasic and ammonium sulfate (called EstG+SO_4+TRS) or 20% PEG500 MME, 10% PEG20000, 0.1 M Tris/Bicine pH 8.5 and 100 mM mixture of DL-Alanine, Glycine, DL-Lysine and DL-Serine, (called EstG+TRS). Crystals grown in the first condition were soaked in 500 mM Tantalium bromide heavy metal solution for 1 hour (crystals called EstG + TaBr). Crystals were flash-cooled in mother liquor. Data of crystals of EstG +TRS (PDB ID 7UDA) were collected at National Synchrotron Light Source-II at beamline 17-ID-2 (FMX) on a Dectris EIGER X 16M while crystals of EstG in complex with SO_4 and TRS (PDB ID 7UIC, EstG+SO_4+TRS) and of EstG bound to tantalum bromide (PDB ID 7UIB, EstG+TaBr) were collected at 17-ID-1 (AMX) on a Dectris EIGER X 9M detector. Diffraction data were collected on a vector defined along the longest axis of the crystal (Miller et al., 2019). The datasets were indexed, integrated, and scaled using fastdp, XDS, and aimless (Kabsch, 2010). All EstG crystals belong to tetragonal space group and diffracted from 2.09 to 2.62 Å.

Since the N-terminal and C-terminal sequence of EstG differed from available homologous proteins, a model of EstG to use in molecular replacement was generated with the RoseTTAFold package (Baek et al., 2021). RoseTTAFold model weights as of July 16, 2021, UniRef30 clusters as of June 2020, PDB templates as of March 3, 2021, and the BFD (Steinegger & Söding, 2018) were used during model prediction. A C-terminal segment (Pro443-Arg462) that was predicted to extend as a random coil away from the molecular envelope was truncated from the model with the lowest predicted coordinate error to generate the final molecular replacement search model. The structure of EstG was determined by molecular replacement using PHASER (McCoy et al., 2007) with the RoseTTAFold model of EstG as a search model (Baek et al., 2021). The data were refined to a final resolution of 2.47, 2.09 and 2.62 Å using iterative rounds of refinement with REFMAC5 (Evans & Murshudov, 2013) and manual rebuilding in Coot (Emsley & Cowtan, 2004). Structures were validated using Coot (Emsley & Cowtan, 2004) and the PDB deposition tools. Each of the three models have more than 95 % of the residues in the preferred regions according to Ramachandran statistics (Table 2.2). Figures were render in PyMOL (v2.2.3, Schrödinger, LLC).

Comparison with other beta lactamase binding proteins

A search using PDBeFOLD (Krissinel & Henrick, 2004) was conducted using EstG as a search model. Among them carboxyesterases, penicillin binding protein EstY29, and simvastatin synthase (PDBs 4IVK (Cha et al., 2013), 4P87 (Ngo et

al., 2014), 3HLB (Gao et al., 2009)) aligned with root-mean-square deviations of 1.39, 1.62, 1.82 Å over 404, 387 and 400 amino acids, respectively. The structure of EstG was used to analyze and display the primary, secondary and quaternary structure of homologous proteins with ENDscript (Robert & Gouet, 2014).

LCMS Analysis

All analysis was performed on a Dionex UHPLC and Q Exactive quadrupole Orbitrap system (Thermo Fisher, Waltham, Massachusetts). Two micrograms of each reaction and unreacted input was injected directly onto a HyperSil Gold C-18 2.1mm x 150mm reversed phase chromatography column. Analytes were separated using an increasing gradient that consisted of 0.1% formic acid in LCMS grade water as buffer A and 0.1% formic acid in LCMS grade acetonitrile as buffer B. Due to the hydrophilic nature of glucans, the gradient began with a 2-minute acquisition at 100% buffer A with a rapid ramp to 100% buffer B by 15 minutes before returning to baseline conditions for the remainder of the 20 minute experiment. The Q Exactive was operated in positive ionization mode using a data dependent acquisition method. An MS1 scan was acquired at 140,000 resolution with a scan range of 150 to 1500 m/z. The three most abundant ions from each MS1 scan were isolated for fragmentation using a three-step collision energy of 10, 30 and 100 and the fragment scans were obtained using 15,000 resolution. Ions with unassigned charge states or more than 3 charges were excluded from fragmentation. To prevent repeat fragmentation any ion within 5 ppm mass deviation of the selected ion was excluded from additional fragmentation for 30

seconds. The complete LCMS method in vendor .meth format and a text adaptation have been uploaded to LCMSMethods.org under the following DOI (dx.doi.org/10.17504/protocols.io.36wgq7djkvk5/v1). All Thermo .RAW instrument files have been uploaded to the MASSIVE public repository (Vizcaíno et al., 2014) under accession MSV000089142. The vendor .RAW files and processed results can be accessed during the review process using the following link: ftp://MSV000089142@massive.ucsd.eduand reviewer password EstG725.

LCMS Data Analysis

All downstream data analysis was performed with Compound Discoverer 3.1 and Xcalibur QualBrowser 2.2 (Thermo Fisher). Briefly, all MS1 ions with a signal to noise of greater than 10:1 from the vendor .RAW files were considered for downstream analysis. The LCMS files were chromatographically aligned using an adaptive curve on all ions within a maximum mass shift of 2 minutes and with less than a 5 ppm mass discrepancy. The files were also normalized to compensate for concentration and loading differences between samples using a constant mean normalization. Ion identities were assigned using the mzCloud and ChemSpider databases using a maximum mass tolerance of 5ppm against library entries. In addition, a similarity search algorithm and custom compound class scoring module were used to flag ions that exhibited common glucose ions following fragmentation. Compounds of interest were flagged in the resulting output report by use of custom filter that eliminated ions that were of decreased abundance in the EstG reacted

70

periplasm relative to both the unreacted periplast fraction and the periplast fraction treated with the EstG$_{S101A}$.

LCMS results

A total of 1,166 LCMS features were identified in the study. After removal of background signal and ions with an m/z of less than 600, 13 prospective ions were identified that appeared to be downregulated following incubation with the EstG protein. Of these molecules only one possessed a fragmentation pattern consistent with a glucan polymeric structure. This ion demonstrated an exact match by mass and an 83.7% fragment similarity to the cyclic hexasaccharide α-cyclodextrin. Figure 2.6C is a mirror plot that demonstrates the level of fragment sequence match between the fragmentation of this ion and α-cyclodextrin.

Data availability

The final coordinates of EstG bound to TRS, EstG bound to SO$_4$ and TRS, EstG bound to $(Ta_6Br_{12})^2$ have been deposited in the PDB with accession codes (7UDA, 7UIC and 7UIB) respectively.

2.7 Figures and Legends
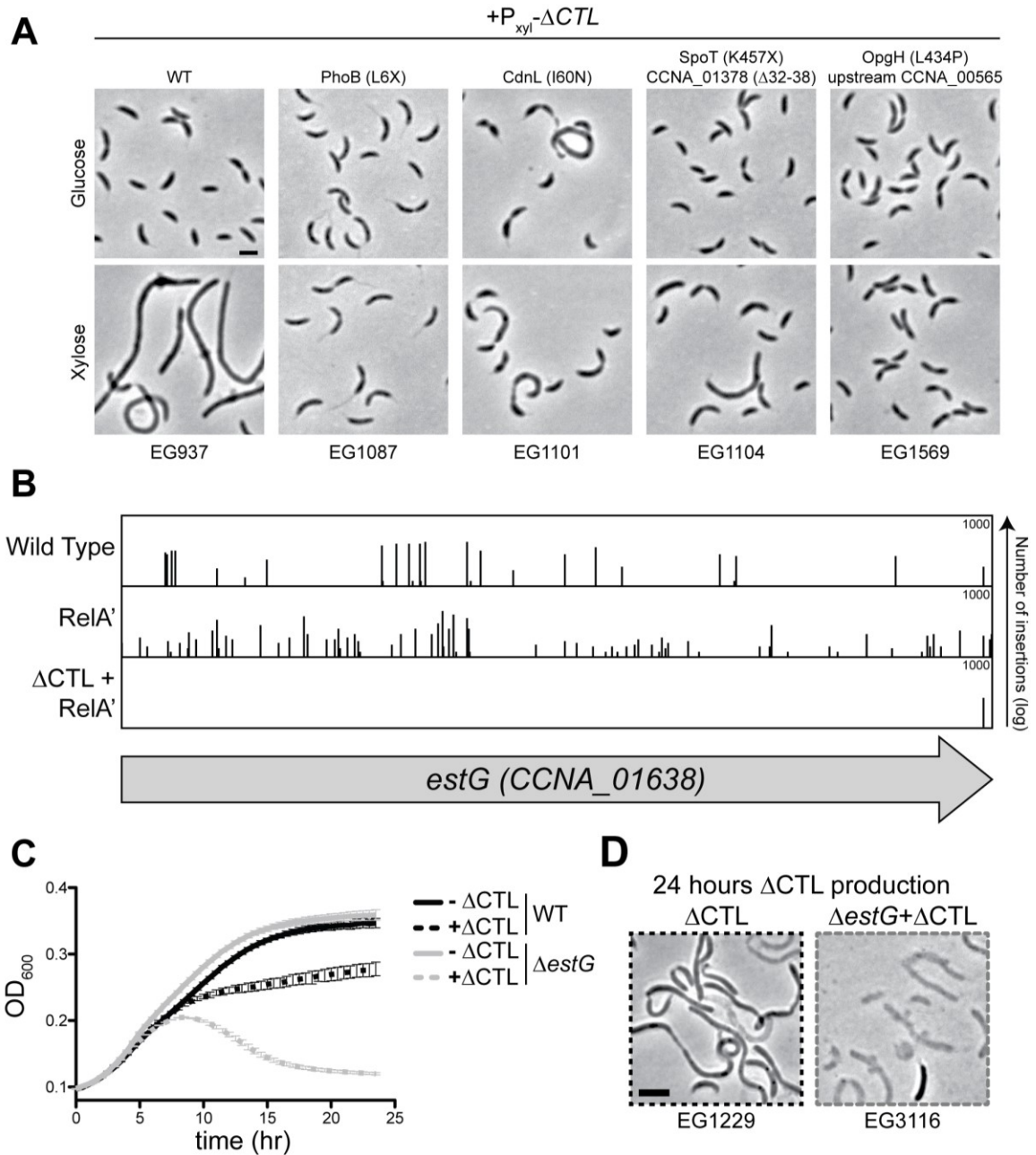
Figure 2.1: EstG is required to suppress ΔCTL-mediated lethality.

A. Phase contrast images of ΔCTL and suppressors +/- ΔCTL production. Indicated strains are grown with 0.3% glucose (-ΔCTL) or 0.3% xylose (+ΔCTL) for 7 hours before imaging. Scale bar, 2 μm. Amino acid X represents a premature stop codon. **B.** Line plot of transposon insertion frequency along the gene locus for *CCNA_01638* (named *estG*) as

determined by transposon sequencing (Tn-Seq) analysis in wild type (WT; EG865), high (p)ppGpp production (RelA', EG1799), and ΔCTL with high (p)ppGpp production (ΔCTL+RelA', EG1616). **C.** Growth curve of strains EG1229 (WT) and EG3116 (Δ*estG)* with and without ΔCTL production (+/- 0.3% xylose) as monitored by OD_{600}. **D.** Phase contrast images of WT and Δ*estG* from the 24-hour timepoint of the growth curve in panel C. Scale bar, 2 μm.
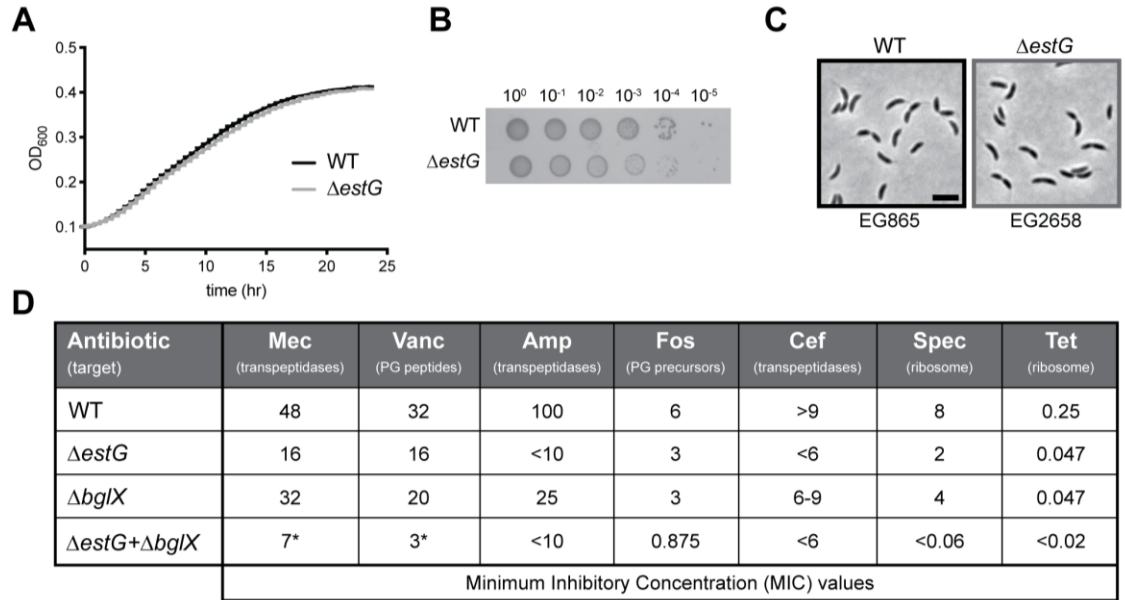
Figure 2.2: ∆*estG* does not impact cell viability or growth in unstressed conditions.

 A. Growth curve, **B.** spot dilutions, and **C.** phase contrast images of wild type (WT, EG865) and ∆*estG* (EG2658). Culture dilutions are as indicated. Scale bar, 2 µm. **D.** Minimum inhibitory concentrations (MIC) of WT (EG865), ∆*estG* (EG2658), ∆*bglX* (EG3279), and ∆*estG*∆*bglX* (EG3282) against peptidoglycan (PG)- and ribosome-targeting antibiotics. Measurements in µg/mL. Mec=mecillinam; Vanc=vancomycin; Amp=ampicillin; Fos=fosfomycin; Cef=cephalexin; Spec=spectinomycin; Tet=tetracycline. Asterisk (*) represents value with a secondary zone of light inhibition.
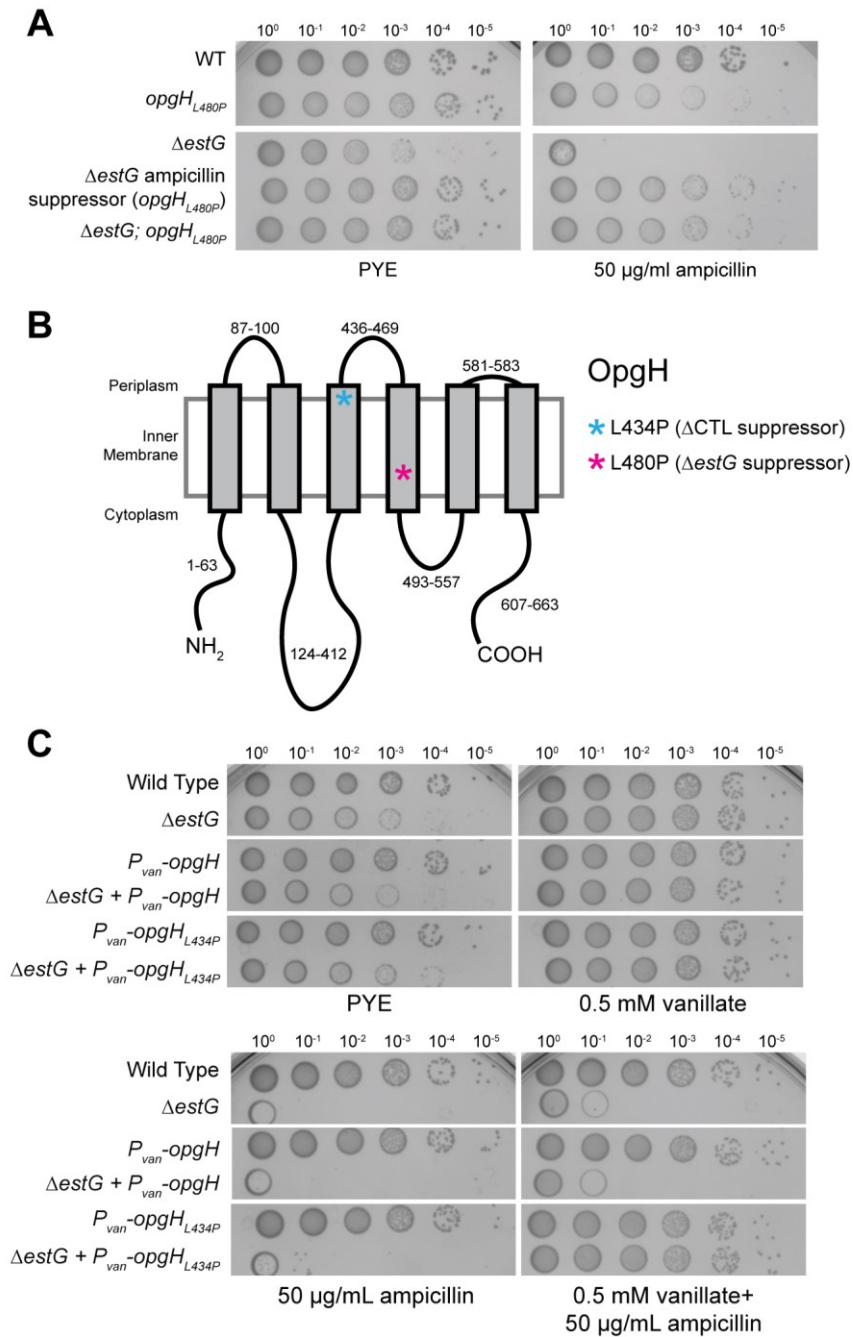
Figure 2.3: *opgH_{L480P}* and *opgH_{L434P}* suppress Δ*estG* sensitivities.

A. Spot dilutions of WT (EG865), *opgH_{L480P}* (EG3369), Δ*estG* (EG2658), Δ*estG* ampicillin

suppressor (EG3105), Δ*estG*; *opgH_{L480P}* (EG3371) grown on PYE agar alone or with 50

µg/mL ampicillin. Culture dilutions are as indicated. **B.** Schematic diagraming predicted topology of OpgH with grey boxes representing transmembrane domains and corresponding amino acids labeled. Asterisks represent approximate location of suppressing point mutations from the ΔCTL (EG1569) and Δ*estG* suppressors (EG3105). **C.** Spot dilutions of indicated strains on PYE agar alone or with added 0.5 mM vanillate and/or 50 µg/mL ampicillin. Strains are WT (EG865), Δ*estG* (EG2658), P_{van}-*opgH* (EG3375) , Δ*estG* + P_{van}-*opgH* (EG3377), P_{van}-*opgH*$_{L434P}$ (EG3577)*,* and Δ*estG* + P_{van}-*opgH*$_{L434P}$ (EG3579).
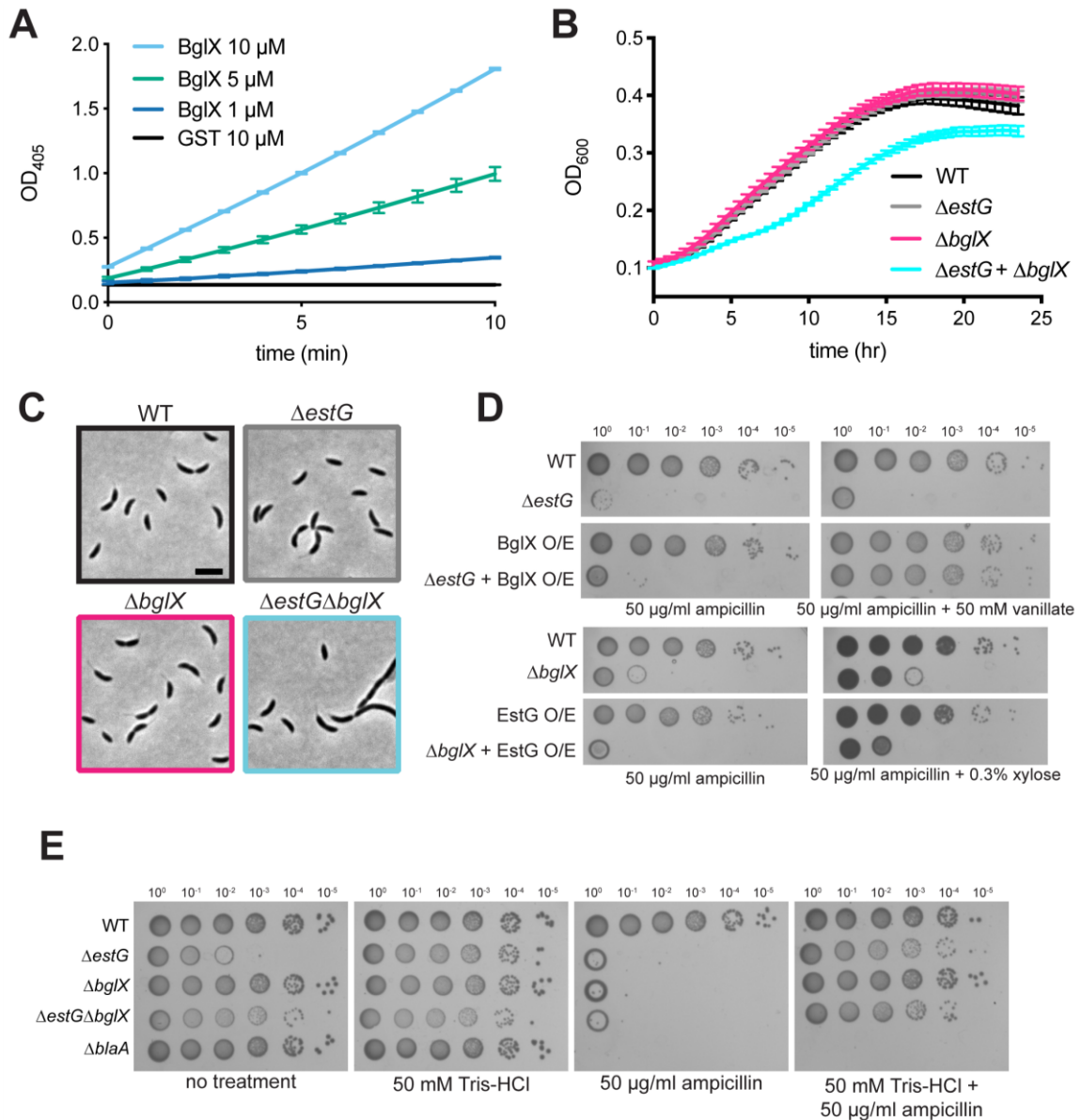
Figure 2.4: BglX is a glucosidase that interacts genetically with *estG*.

A. 4-Nitrophenyl-β-D-glucopyranoside (pNPG) hydrolysis assay with purified BglX or GST at indicated amounts measured at OD_{405}. **B.** Growth curve and **C.** phase contrast images of WT (EG865), Δ*estG* (EG2658), Δ*bglX* (EG3279), and Δ*estG*Δ*bglX* (EG3282). Scale bar, 2 µm. **D.** Spot dilutions on PYE agar with 50 µg/mL ampicillin +/- 50 mM vanillate or 0.3% xylose of WT (EG865), Δ*estG* (EG2658), *P$_{van}$-bglX* (BglX O/E, EG3384), Δ*estG*+ *P$_{van}$-bglX*

(EG3385), Δ*bglX* (EG3279), *P~xyl~-estG* (EG2759), and Δ*bglX+ P~xyl~-estG* (EG3425). **E.** Spot

dilutions on PYE agar alone (no treatment) or with added 50 mM Tris-HCl and/or 50 µg/mL

ampicillin of WT (EG865), Δ*estG* (EG2658), Δ*bglX* (EG3279), Δ*estG*Δ*bglX* (EG3282), and

Δ*blaA* (EG2408). Culture dilutions are as indicated.
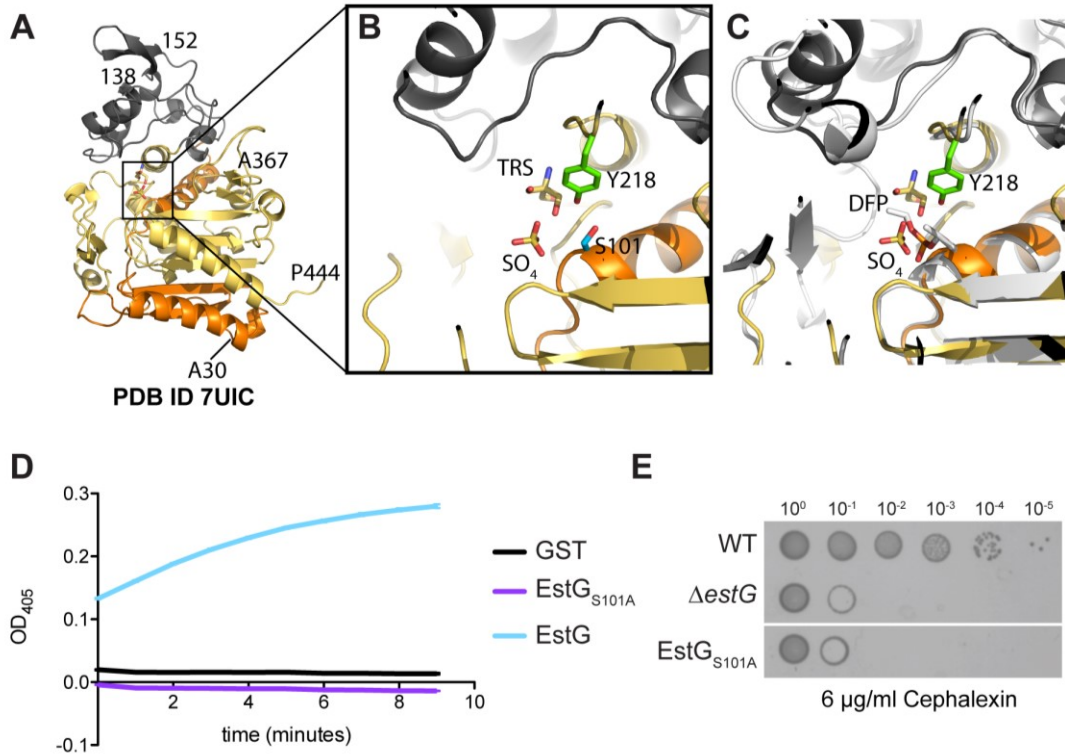
Figure 2.5: EstG is structurally similar to esterases in the β-lactamase family.

A. The structure of EstG displays an α/β hydrolase fold. Ribbon diagram of residues 30-444 with the N-terminal residues 30 to 121 colored in orange, 122-217 colored grey, 218 to 444 in yellow. **B.** Zoom in of putative active site identified by homology to esterases. Ser101 (S101) of motif I is 2.7 Å away from Tyr218 (Y218) of motif II. The active site has a sulfate (SO_4) and a Tris (TRS) molecule bound. **C.** The structural alignment of EstG+ TRS + SO_4 (PDB ID 7UIC) with EstB bound to diisopropyl fluorophosphate (DFP) (PDB ID 1CI8 (Wagner et al., 2009), colored in light grey) displays the partial overlap of the sulfate to the phosphonate of DFP. **D.** p-nitrophenyl butyrate (pNB) hydrolysis of purified EstG, EstG$_{S101A}$, and GST at 10 µM measured at OD_{405}. **E.** Spot dilutions of WT (EG865),

Δ*estG* (EG2658), and EstG$_{S101A}$ (EG2990) on PYE agar plates with 6 μg/mL cephalexin.

Culture dilutions are as indicated.
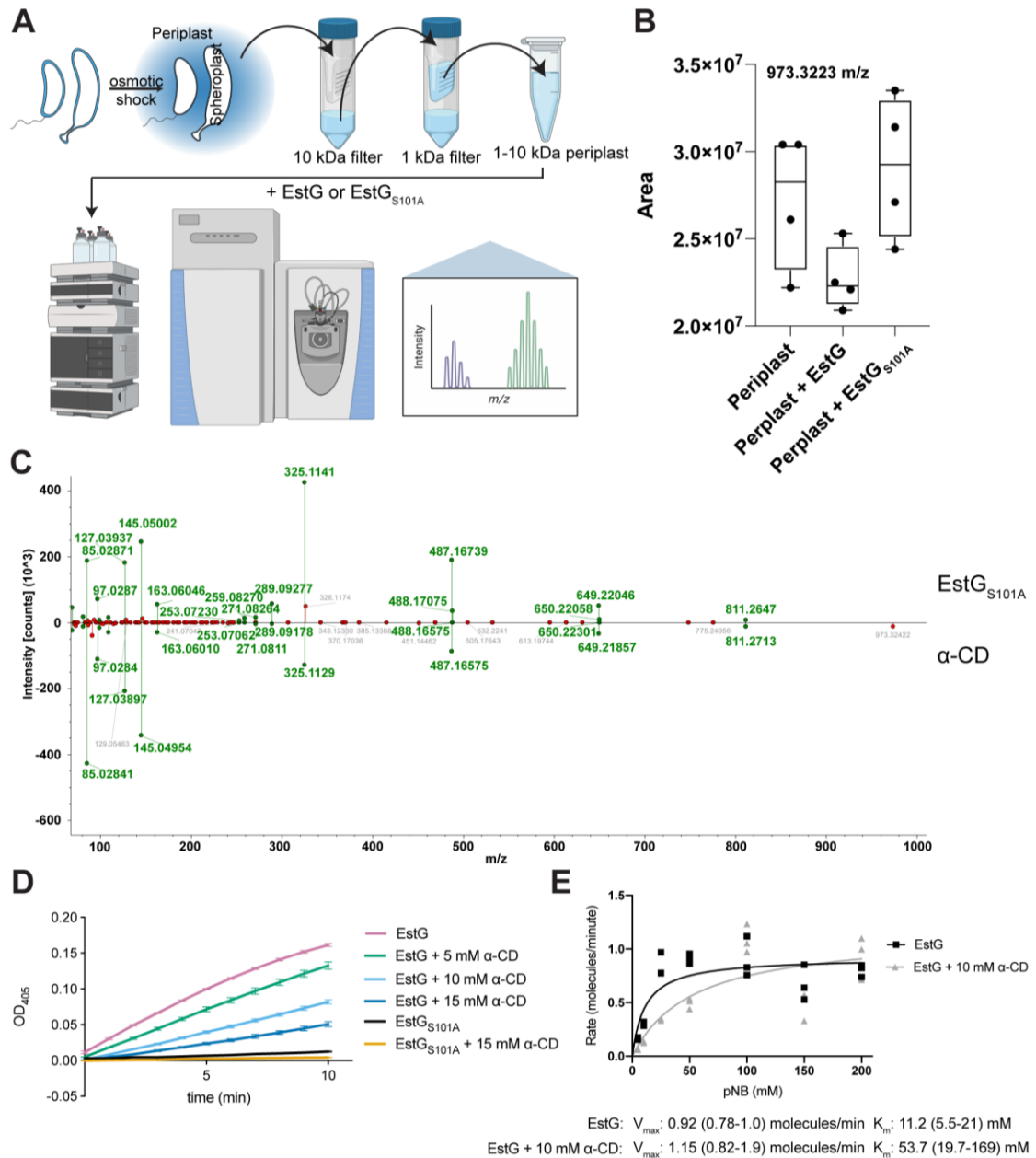
Figure 2.6: A cyclic hexameric glucose is the native substrate of EstG.

A. Schematic outlining the method for isolating periplasmic contents (periplast, blue) and sequential fractionation. Periplast 1-10 kDa was then combined with EstG or EstG$_{S101A}$, and contents were separated and identified with LCMS. **B.** A box-plot displaying the relative abundances of the cyclic hexaglycan with error bars across four technical

replicates in the samples of periplast alone, periplast + EstG, or periplast + EstG$_{S101A}$. Mass of the parental ion is 973.3223 m/z. **C.** MS/MS spectra with the experimental spectra observed in one of the injections of the periplast + EstG$_{S101A}$ as the top of the mirror plot. Bottom half of the mirror plot is the mzCloud reference spectra for α-cyclodextrin (α-CD). **D.** p-nitrophenyl butyrate (pNB) hydrolysis of purified EstG or EstG$_{S101A}$ with increasing amounts of α-CD showing concentration dependent inhibition. **E.** Michaelis–Menten saturation curve of the rates of pNB hydrolysis with EstG or EstG + 10 mM α-CD to show competitive inhibition of the active site. Rate was determined by the slope of the pNB hydrolysis curve at the indicated pNB concentration. Rate is presented as molecules of pNB hydrolyzed per minute. Parenthesis next to values for V$_{max}$ and K$_m$ represent 95% confidence interval.
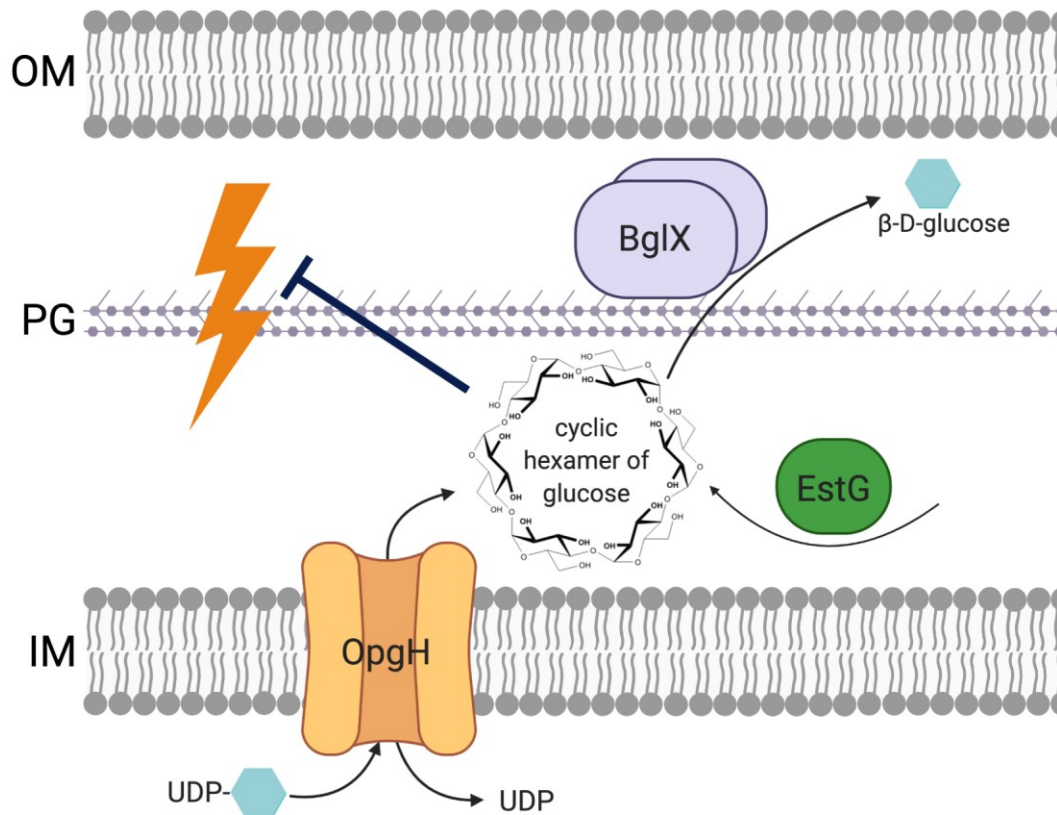
Figure 2.7: EstG protects the cell envelope against stress through its activity on cyclic OPG polymers.

Cell envelope homeostasis during stress is maintained through the actions of EstG and the putative OPG pathway in *Caulobacter*. We propose that OpgH takes cytoplasmic UDP-glucose to synthesize small, cyclic OPG molecules into the periplasm. We believe BglX hydrolyzes these OPGs and EstG modifies it in some way to modulate the osmolarity of the periplasm. Without OPG production or modification, the cell envelope integrity is lost, resulting in hypersensitivity to a variety of environmental changes and antibiotic stresses (represented by yellow lightning bolt). OM=outer membrane, PG=peptidoglycan, IM=inner membrane.

2.8 Supplemental Figures and Legends
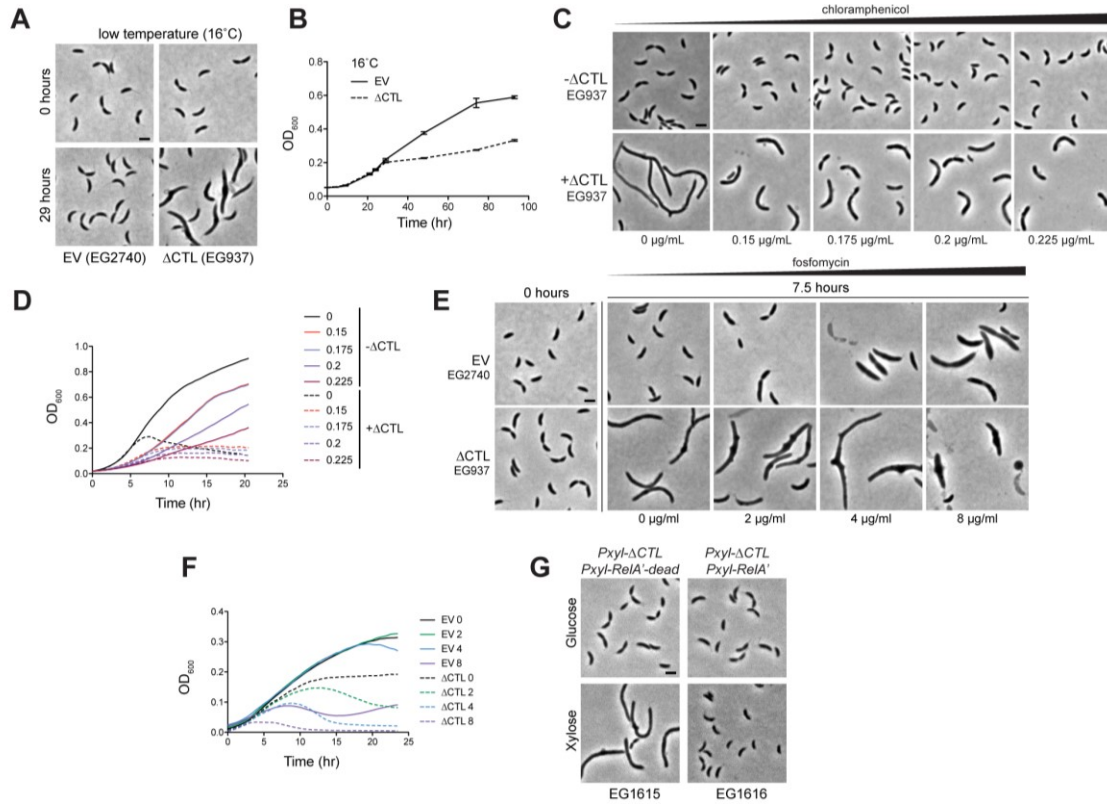
Supplemental Figure 2.1: Slow growth does not suppress ΔCTL.

A. Phase contrast images and **B.** growth curve of empty vector (EV, EG2740) and ΔCTL (EG937) grown with 0.3% xylose at 16°C to slow growth. **C.** Phase contrast images and **D.** growth curve of EG937 in the presence of 0.3% glucose (-ΔCTL) or 0.3% xylose (+ΔCTL) for 7.5 hours with increasing concentrations of chloramphenicol to slow growth. **E**. Phase contrast images and **F.** growth curve of EV and ΔCTL grown with 0.3% xylose with increasing concentrations of fosfomycin to slow growth. **F.** Phase contrast images of ΔCTL producing strains with xylose inducible RelA' (high (p)ppGpp, EG1616) or catalytically dead RelA'dead (WT (p)ppGpp, EG1615) with 7 hours of 0.3% glucose or 0.3% xylose to induce ΔCTL and RelA'/RelA'dead. Scale bar, 2 μm.
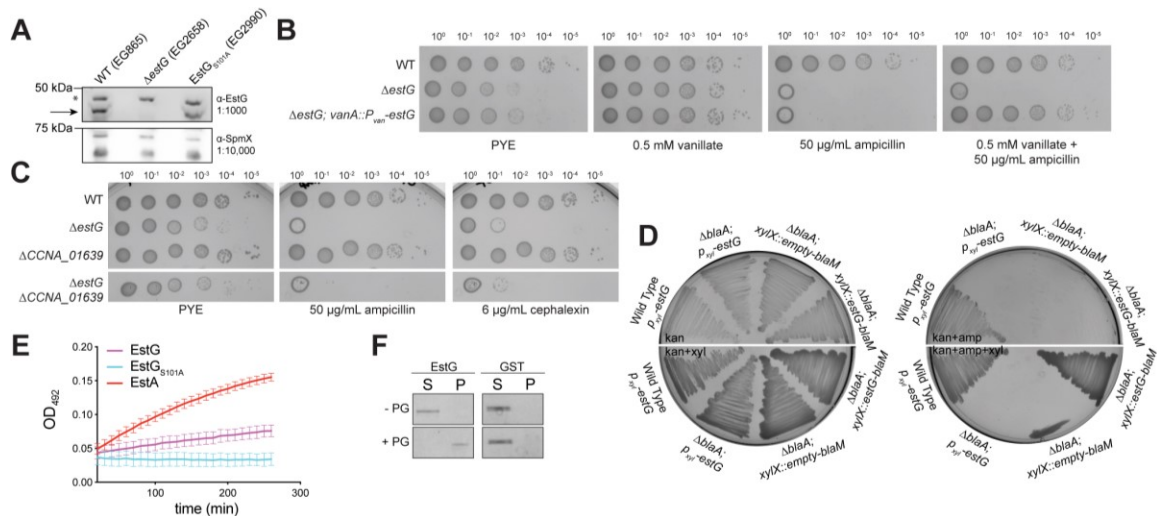
Supplemental Figure 2.2: EstG is a periplasmic protein with broad antibiotic sensitivities.

A. α-EstG (top) and α-SpmX (bottom) immunoblots of indicated strains at indicated dilutions. Arrow indicates band representing EstG. Asterisk denotes non-specific band. **B.** Spot dilutions of WT (EG865), Δ*estG* (EG2658), and Δ*estG* complemented with a vanillate inducible *estG* (EG3075) on PYE agar alone or with 0.5 mM vanillate, 50 µg/mL ampicillin, or both. Culture dilutions are as indicated. **C.** Spot dilutions of WT (EG865), Δ*estG* (EG2658), Δ*CCNA_01639* (EG3044)*,* and Δ*estG*Δ*CCNA_01639* (EG3047) on PYE agar alone or with 50 µg/mL ampicillin or 6 µg/mL cephalexin. Culture dilutions are as indicated. **D**. Periplasmic localization of EstG using indicated strains with fusions to *blaM* in a Δ*blaA* background. Cells are grown on PYE agar plates with indicated additives. Kanamycin 25 µg/mL (kan), 0.3% xylose, and ampicillin 50 µg/mL (amp). **E.** Nitrocefin hydrolysis of indicated proteins over time measured at OD_{492}. **F.** Peptidoglycan (PG) binding ability of purified EstG or GST against wild type (WT) murein/sacculi. Upon ultracentrifugation, proteins unable to bind PG remain in the soluble fraction (S) and proteins that bind PG in the pellet (P).
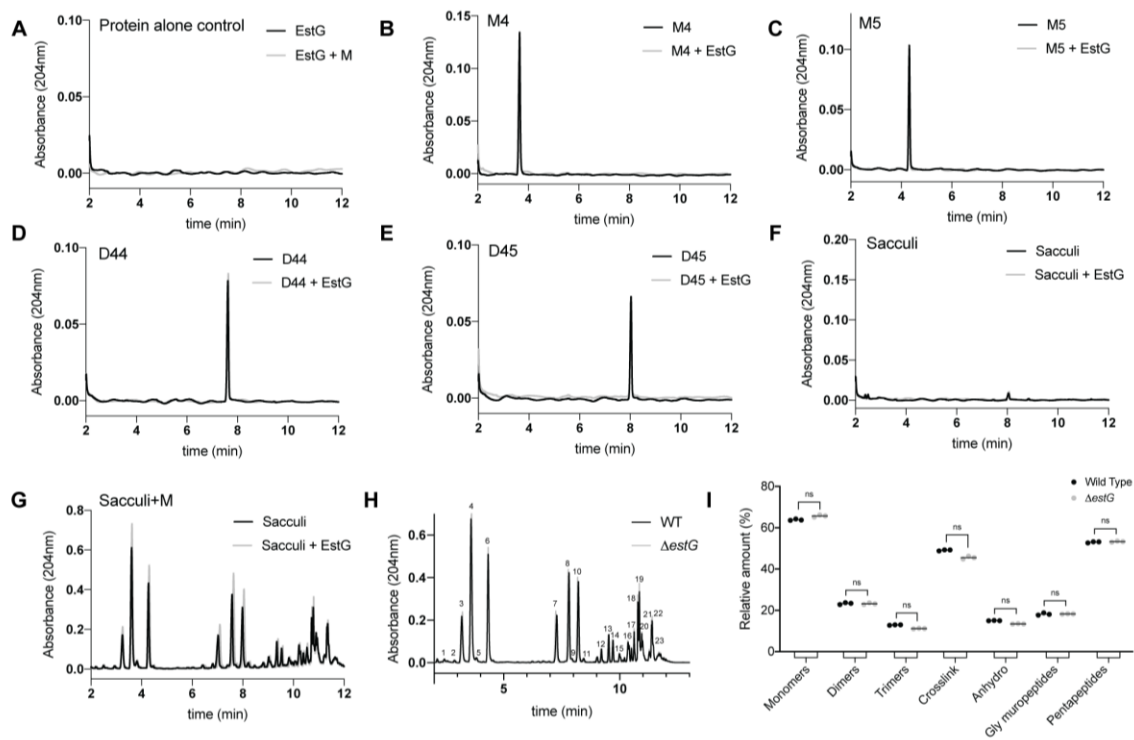
Supplemental Figure 2.3: EstG does not have activity towards the peptidoglycan or its substituent moieties.

In vitro reactions of EstG in the presence of **A.** protein alone, **B.** M4 (monomeric tetrapeptide), **C.** M5 (monomeric pentapeptide), **D.** D44 (dimeric tetrapeptide-tetrapeptide), **E.** D45 (dimeric tetrapeptide-pentapeptide), **F.** WT sacculi, and **G.** sacculi + muramidase treatment. **H.** Representative chromatograms of muropeptides prepared from WT (EG865) and Δ*estG* (EG2658). Relevant muropeptides are identified in Table 2.1. **I.** Relative molar abundance of the indicated muropeptide species from WT (EG865) and Δ*estG* (EG2658): monomers, dimers, trimers, crosslinkage, (1–6 anhydro) N-acetyl muramic acid containing muropeptides (anhydro, glycan chain termini), Gly containing muropeptides (Gly), and pentapeptides (penta).
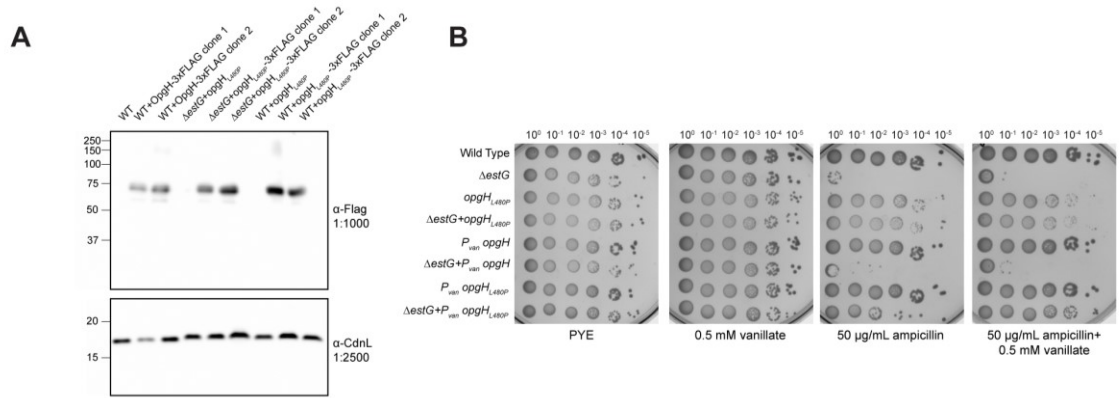
Supplemental Figure 2.4: OpgH$_{L480P}$ is not degraded and can suppress $\Delta estG$ sensitivity in a dominant fashion.

A. α-Flag (top) and α-CdnL (bottom) immunoblots of indicated strains at indicated dilutions demonstrating the stability of a 3x-FLAG tagged variant of OpgH$_{L480P}$. **B.** Spot dilutions on PYE agar alone or with added 0.5 mM vanillate and/or 50 µg/mL ampicillin of WT (EG865), $\Delta estG$ (EG2658), $opgH_{L480P}$ (EG3369), $\Delta estG+opgH_{L480P}$ (EG3371), P_{van}-$opgH$ (EG3375), $\Delta estG + P_{van}$-$opgH$ (EG3377), P_{van}-$opgH_{L480P}$ (EG3440), $\Delta estG+ P_{van}$-$opgH_{L480P}$ (EG3442). Culture dilutions are as indicated.
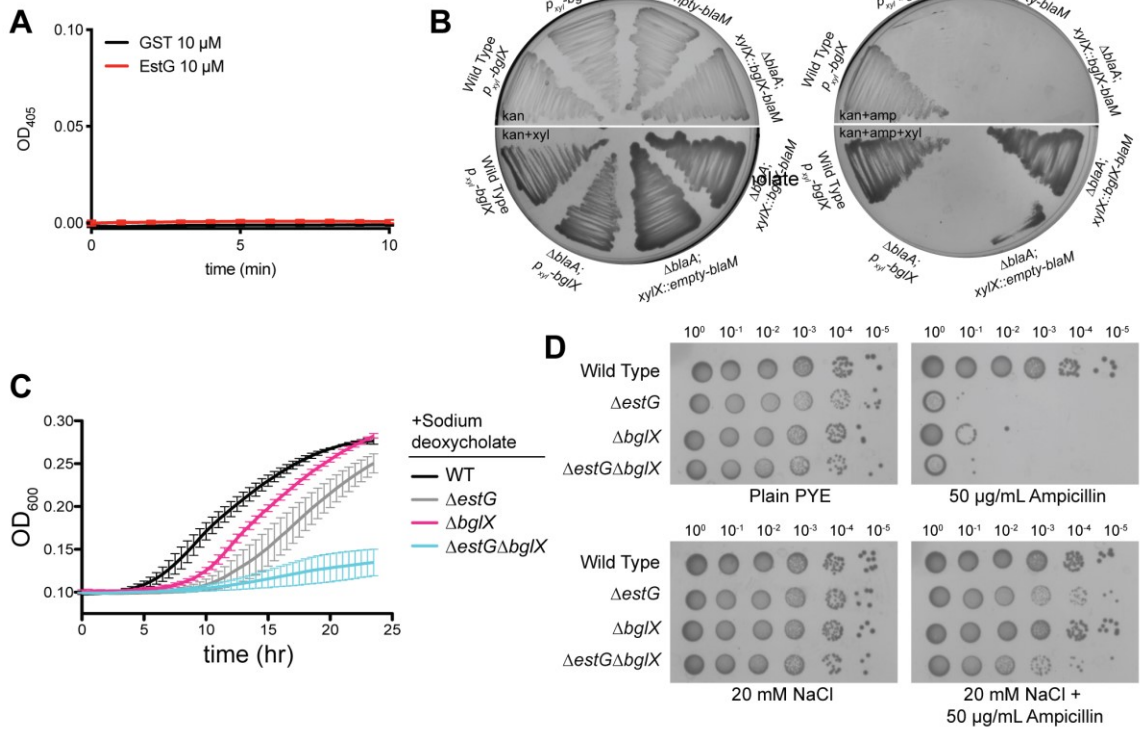
Supplemental Figure 2.5: BglX localization and sensitivities are similar to EstG.

A. 4-Nitrophenyl-β-D-glucopyranoside (pNPG) hydrolysis assay with 10 μM purified EstG or GST measured at OD_{405}. **B.** Periplasmic localization of BglX using indicated strains with fusions to *blaM* in a Δ*blaA* background. Cells are grown on PYE agar plates with indicated additives. Kanamycin 25 μg/mL (kan), 0.3% xylose, ampicillin 50 μg/mL (amp). **C.** Growth curve of WT (EG865), Δ*estG* (EG2658), Δ*bglX* (EG3279), and Δ*estG*Δ*bglX* (EG3282) with 0.6 mg/mL sodium deoxycholate. **D.** Spot dilutions of WT (EG865), Δ*estG* (EG2658), Δ*bglX* (EG3279), and Δ*estG*Δ*bglX* (EG3282) on PYE agar alone or with added 50 μg/mL ampicillin and/or 20 mM NaCl. Culture dilutions are as indicated.
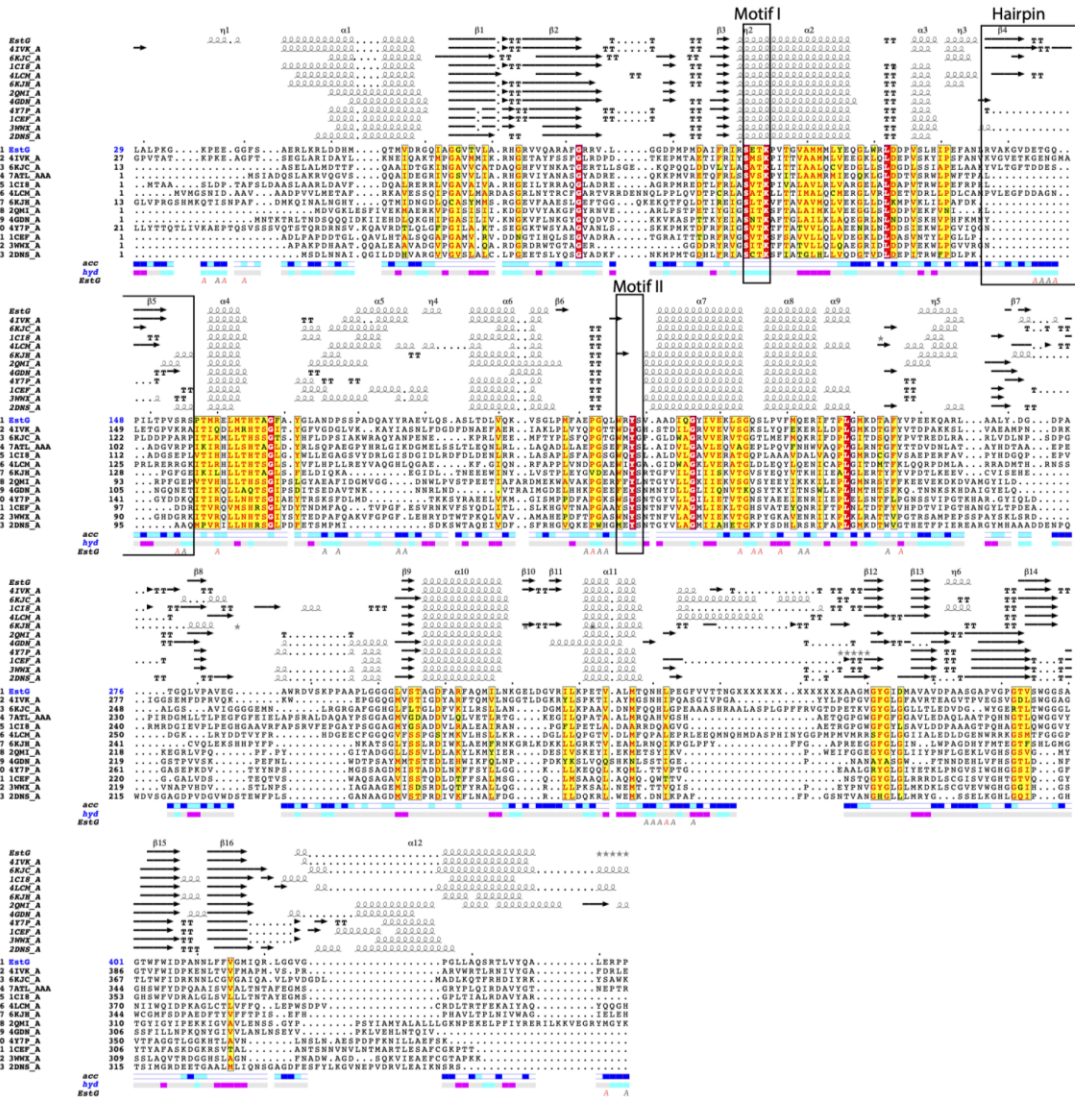
Supplemental Figure 2.6: EstG has structural similarity to related enzymes.

Multiple sequence and structural alignment of EstG and related enzymes displaying primary to quaternary structure information. The secondary structure elements are shown as helices, strands (arrows) and tight turns (TT). The sequence alignment is colored according to residue conservation with red background with white letter for identical, yellow background with red letters for conserved. Solvent accessibility (turquoise and yellow) and hydropathy scales per residue. Letter A indicates protein:protein interaction. The figure was done with ENDscript 2 (Robert & Gouet, 2014).
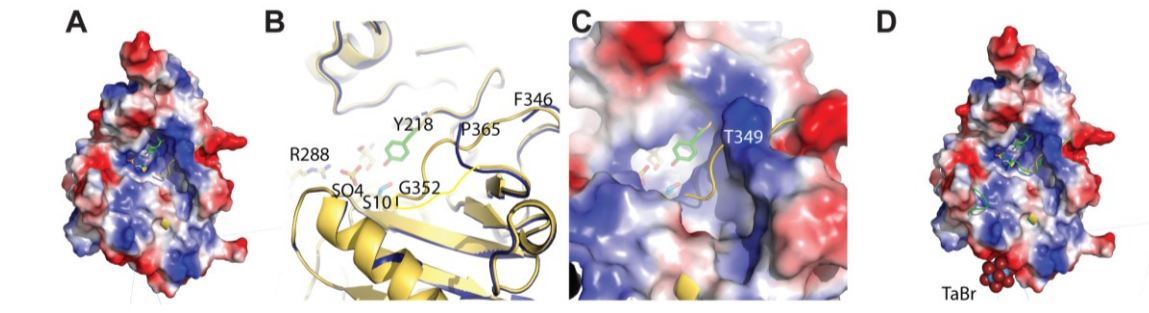
Supplemental Figure 2.7: Loop present in EstG could be involved in catalysis.

A. Electrostatic surface of EstG bound to Tris (TRS) structurally aligned to EstG bound to TRS and sulfate (SO_4) displays the ordered loop F346 to G352 (yellow) and how it might occlude the binding site. Residues Ser101 and Tyr218 are shown in sticks. **B.** Zoom in and **C.** electrostatic surface rendering of the structural differences in loop 346-352. **D.** Structure of EstG bound to TRS structurally aligned to EstG+$(Ta_6Br_{12})^2$ (green cartoon). The tantalum bromide cluster, $(Ta_6Br_{12})^2$ is far from the loop, shown in spheres. EstG+$(Ta_6Br_{12})^2$ structure shows an alternative conformation for loop 272-276 and so protrudes from the surface.
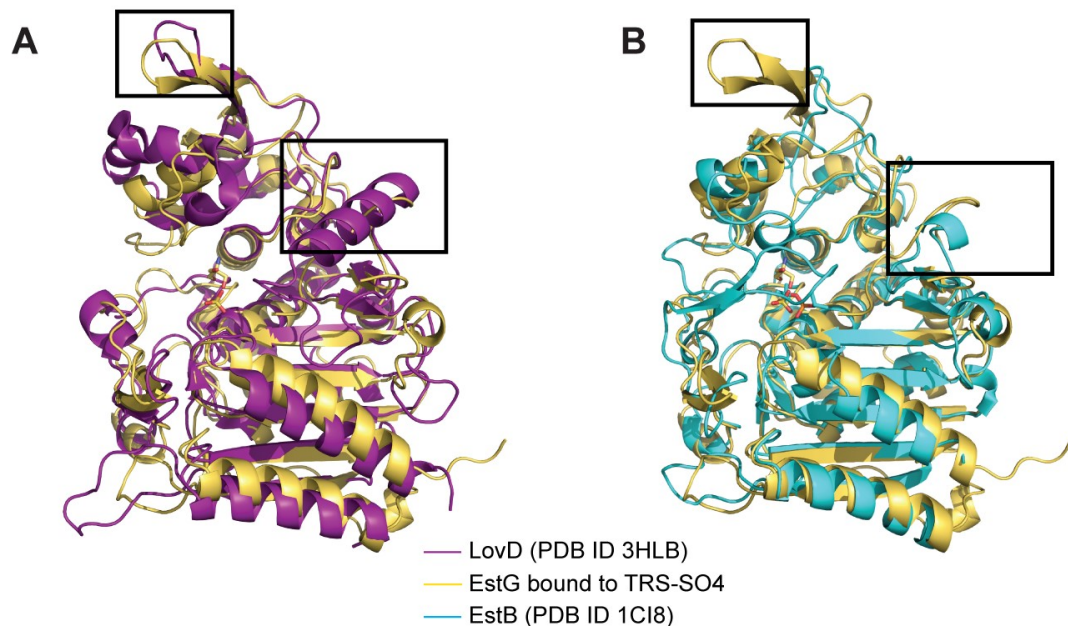
Supplemental Figure 2.8: Structural alignment of EstG with related enzymes.

A. Structural alignment of EstG with LovD (PDB ID 3HLB (Gao et al., 2009), purple) highlighting that EstG lacks the long helix between $\alpha11$ and $\beta12$ (aa 340-350) present in 3HLB (aa 309-321). The hairpin insertion and the top of the hydrolase domain is in a different conformation. **B.** Structural alignment of EstG with EstB (PDB ID 1CI8 (Wagner et al., 2009), cyan) highlighting the insertion of the hairpin formed by $\beta4$ and $\beta5$ in EstG that is absent in EstB and in PDB IDs 4Y7P (Nakano et al., 2015), 1CEF (Kuzin, Liu, Kelly, & Knox, 1995), 3WWX (Arima et al., 2016), 2DNS (Okazaki et al., 2007).
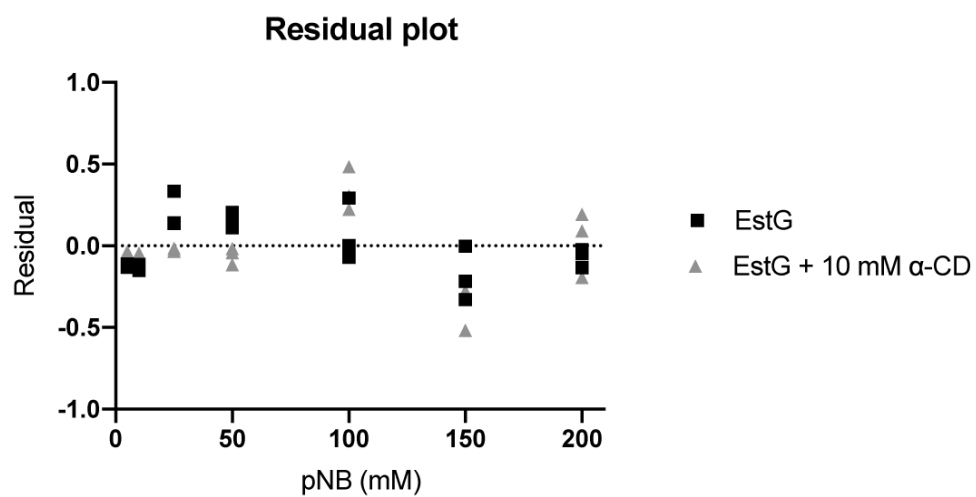
Supplemental Figure 2.9: EstG residual in the presence and absence of α-cyclodextrin.

Residual plot of the rate data from Figure 2.6E, presenting the deviation of the data points from the respective Michaelis-Menten fit.

2.9 Tables

Table 2.1: Deletion of *estG* does not alter the muropeptide profile of

Caulobacter.

Table outlines muropeptide relative molar abundance (%). GlcNAc: N-Acetyl glucosamine. MurNAc: N-Acetyl muramic acid. Ala: Alanine. Glu: Glutamic acid. mDAP: meso-diaminopimelic acid. Gly: Glycine. Statistical analysis performed using t-test analysis. * = $P < 0.05$ and > 10% variation compared to WT.

Peak	Muropeptide	Structure	WT	Δ*estG*
1	M3	GlcNAc-MurNAc-L-Ala-D-Glu-mDAP	0.42	0.3
2	M4^G	GlcNAc-MurNAc-L-Ala-D-Glu-mDAP-Gly	0.37	0.28
3	M5^G	GlcNAc-MurNAc-L-Ala-D-Glu-mDAP-D-Ala-Gly	10.32	10.17
4	M4	GlcNAc-MurNAc-L-Ala-D-Glu-mDAP-D-Ala	30.01	29.48
5	M2	GlcNAc-MurNAc-L-Ala-D-Glu	1.16	0.71
6	M5	GlcNAc-MurNAc-L-Ala-D-Glu-mDAP-D-Ala-D-Ala	19.08	18.26
7	D45^G	M4-M5G (DD-crosslink)	4.69	4.75
8	D44	M4-M4 (DD-crosslink)	7.79	7.78
9	M5$^{G\ Anh}$	GlcNAc-(1-6anhydro)MurNAc-L-Ala-D-Glu-mDAP-D-Ala-Gly	0.71	0.69
10	D45	M4-M5 (DD-crosslink)	7.02	6.98
11	M4^{Anh}	GlcNAc-(1-6anhydro)MurNAc-L-Ala-D-Glu-mDAP-D-Ala	0.75	0.72
12	T445^G	M4-M4-M5^G (DD-crosslink)	0.63	0.79
13	T444	M4-M4-M4 (DD-crosslink)	1.1	1.07
14	T445	M4-M4-M5 (DD-crosslink)	0.87	0.85
15	D45$^{G\ Anh}$	M4-M5$^{G\ Anh}$ (DD-crosslink)	0.73	0.71
16	D44^{Anh}	M4-M4^{Anh} (DD-crosslink)	2.32	2.94
17	D45^{Anh}	M4-M5^{Anh} (DD-crosslink)	2.04	2.69
18	T445$^{G\ Anh}$	M4-M4-M5$^{G\ Anh}$ (DD-crosslink)	1.68	1.81
19	T444^{Anh}	M4-M4-M4^{Anh} (DD-crosslink)	2.72	2.97
20	T445^{Anh}	M4-M4-M5^{Anh} (DD-crosslink)	1.88	2.04
21	T445$^{G\ Anh,Anh}$	M4-M4^{Anh}-M5$^{G\ Anh}$ (DD-crosslink)	0.54	0.69

22	T444^{Anh,Anh}	M4-M4^{Anh}-M4^{Anh} (DD-crosslink)	2.46	2.44
23	T445^{Anh,Anh}	M4-M4^{Anh}-M5^{Anh} (DD-crosslink)	0.73	0.9

Table 2.2: X-ray crystallography data collection and refinement statistics.

	EstG+ TRS (PDB ID 7UDA)	EstG+SO$_4$+TRS (PDB ID 7UIC)	EstG+(Ta$_6$Br$_{12}$)^2 (PDB ID 7UIB)
Data Collection	May 27, 1v	Jul 16 (AMX), Au	Jul 16 (AMX)
Diffraction source	NSLS-II X17-ID-2	NSLS-II X17-ID-1	NSLS-II X17-ID-1
Wavelength (Å)	0.979321	0.920120	0.920120
Temperature (K)	100	100	100
Detector	Dectris EIGER X 16M	Dectris EIGER X 9M	Dectris EIGER X 9M
Space group	P4$_1$	P4$_1$	P4$_1$
a, b, c (Å)	110.3, 110.3, 55.9	111.2, 111.2, 56.8	111.7, 111.7, 57.4
α, β, γ (°)	90.0, 90.0, 90.0	90.0, 90.0, 90.0	90.0, 90.0, 90.0
Resolution range (Å)	29.60–2.47 (2.57-2.47)	28.44-2.09 (2.14-2.09)	28.71-2.62 (2.75-2.62)
Total no. of reflections	162,539 (16,345)	288,425 (19,596)	195,511 (22,742)
No. of unique reflections	24,085 (2,515)	41,361(2,900)	21,379(2,741)
Completeness (%)	99.0 (91.9)	99.0 (91.9)	99.5 (96.9)
Redundancy	6.7 (6.5)	7.0 (6.8)	9.1(8.3)
$\langle I/\sigma(I) \rangle$	10.9 (2.4)	12.4 (2.6)	16.9(3.1)
R$_{merge}$	0.99 (0.71)	0.086 (0.77)	0.10(0.76)
R$_{meas}$	0.11 (0.84)	0.10 (0.90)	0.11(0.81)
R$_{pim}$	0.06 (0.44)	0.05(0.47)	0.03(0.27)
CC$_{1/2}$	0.99 (0.75)	0.99 (86.3)	0.99(0.79)
Refinement			
Resolution range (Å)	29.62-2.47 (2.53-2.47)	27.83-2.09 (2.14-2.09)	27.96-2.70 (2.77-2.70)
No. of reflections, working set	22,895,1171	39,246	18,687
R$_{work}$/R$_{free}$	0.18/0.22 (0.30/0.35)	0.17/0.21 (0.24/0.25)	0.20/0.24 (0.30/0.32)
No. of non-H atoms			
EstG	3,093	3,031	3069
ligand	34	7	39
Total of non-H atoms	3,127	3,253	3,085

R.m.s. deviations			
Bonds (Å)	0.009	0.012	0.012
Angles (°)	1.74	0.001	1.731
Wilson B-factor (Å^2)	52	43	47
Average B factors (Å^2)			
EstG	54	42	52
ligand	58	43	80
Total average B factor	56	42	68
Ramachandran (%)			
Favorable	95.2	96.98	94.36
Allowed	3.8	2.26	3.92
Outlier	1.0	0.76	1.72

*Values in parentheses are for highest-resolution shell. All atoms refer to non-H atoms.

2.10 Supplemental Tables

Supplemental Table 2.1: List of extragenic suppressor mutations in ΔCTL

List of extragenic suppressor mutations				
Suppressors derived from EG937				
Strain name	Gene number	Description	Gene/Protein	Mutation
EG1087	CCNA_00296	phosphate regulon response regulator PhoB	PhoB	L6X
EG1092	CCNA_01855	iron/manganese superoxide dismutase		Q28R
	CCNA_02204	ketol-acid reductoisomerase/2-dehydropantoate 2-reductase		V112A
EG1101	CCNA_00690	CarD-like transcriptional regulator	CdnL	I60N
	CCNA_00659	type I restriction-modification system restriction subunit		I551F
EG1104	CCNA_01622	ppGpp hydrolase-synthetase relA/spoT	SpoT	K457X
	CCNA_01378	protein-L-isoaspartate O-methyltransferase		32_38del
EG1105	CCNA_00013	protein-PII uridylyltransferase	GlnD	K57X
EG1106	CCNA_00013	protein-PII uridylyltransferase	GlnD	K457X
EG1107	CCNA_03824	2-polyprenylphenol 6-hydroxylase accessory protein ubiB		P56fs
	CCNA_02046	nitrogen regulatory protein P-II	GlnB	D88V
Suppressors derived from EG1214				
Strain name	Gene number	Description	Gene/Protein	Mutation
EG1569	CCNA_00565 us; CCNA_R0008 us	upstream of CCNA_00565 gamma-glutamyltranspeptidase, upstream of CCNA_R0008 tRNA-Arg		229 bp upstream of ATG
	CCNA_02097	CCNA_02097 periplasmic glucan glucosyltransferase (MdoH?)		L434P
EG1570	CCNA_00524	CCNA_00524 conserved hypothetical cytosolic protein		fs L369
EG1571	CCNA_00524	CCNA_00524 conserved hypothetical cytosolic protein		fs L369
EG1572	CCNA_02032	CCNA_02032 NADH-quinone oxidoreductase chain B	nuoB	W72L

EG1573		intergenic between cpdR and CCNA_00782 aminobenzoyl-glutamate transport protein - tRNA-Val?		
	CCNA_00524	CCNA_00524 conserved hypothetical cytosolic protein		D46N
EG1574	CCNA_03642	CCNA_03642 succinate dehydrogenase flavoprotein subunit		fs
EG1575	CCNA_03771	upstream of CCNA_03771 dehydrogenase with MaoC-like domain		
EG1576	CCNA_00524	CCNA_00524 conserved hypothetical cytosolic protein		fs L369
EG1577	CCNA_00892	CCNA_00892 phosphoenolpyruvate-protein phosphotransferase	PtsP	R129Q
EG1578	CCNA_03563	CCNA_03563 ATP synthase delta chain		L181P
EG1579	CCNA_03563 us	upstream of CCNA_03563 ATP synthase delta chain		
		CCNA_01037 GntR family transcriptional regulator		
EG1581	CCNA_02032	CCNA_02032 NADH-quinone oxidoreductase chain B	nuoB	
	between CCNA_01563 & CCNA_01566	intergenic between CCNA_01563 and CCNA_01566		
EG1582	between CpdR and CCNA_00782	intergenic between cpdR and CCNA_00782 aminobenzoyl-glutamate transport protein		
	CCNA_00726	CCNA_00726 acyl coA dehydrogenase		
EG1583	CCNA_01995	CCNA_01995 phosphatidate cytidylyltransferase		
EG1585	CCNA_01622	ppGpp hydrolase-synthetase relA/spoT	SpoT	A438V
	CCNA_02252	CCNA_02252 methylcrotonyl-CoA carboxylase carboxyl transferase subunit		
EG1586	CCNA_01305	upstream of CCNA_01305 rspJ SSU ribosomal protein S10P		
EG1587	CCNA_00524	CCNA_00524 conserved hypothetical cytosolic protein		fs L369
EG1588	CCNA_01163	CCNA_01163 ice nucleation protein		
		CCNA_01163 ice nucleation protein		

	CCNA_03632	CCNA_03632 hypothetical protein		

Supplemental Table 2.2: List of extragenic suppressors in ∆estG

List of extragenic suppressor mutations				
Suppressors derived from EG2658				
Strain name	Gene number	Description	Gene/Protein	Mutation
EG3105	CCNA_00639	heme:hemopexin-binding protein		G201A (G**G**C-->G**C**C)
	CCNA_02097	periplasmic glucan glucosyltransferase	OpgH	L480P (C**T**G-->C**C**G)
EG3106	CCNA_R0142/CCNA_01566	small non-coding RNA/hypothetical protein		intergenic (+3/+17)
	CCNA_02066	phytoene/squalene synthase family protein		∆8 bp (403-410)
EG3101	CCNA_R0142/CCNA_01566	small non-coding RNA/hypothetical protein		intergenic (+3/+17)
EG3068	CCNA_02018	NADH-quinone oxidoreductase chain K	NuoK	C (252/306 nt)

2.11 References

Alegun, O., Pandeya, A., Cui, J., Ojo, I., & Wei, Y. (2021). Donnan potential across the outer membrane of gram-negative bacteria and its effect on the permeability of antibiotics. *Antibiotics*, *10*(6). https://doi.org/10.3390/antibiotics10060701

Alvarez, L., Hernandez, S., de Pedro, M. A., & Cava, F. (2016). Ultra-Sensitive, High-Resolution Liquid Chromatography Methods for the High-Throughput Quantitative Analysis of Bacterial Cell Wall Chemistry and Structure. *Bacterial Cell Wall Homeostasis: Methods and Protocols*, 11–27. https://doi.org/https://doi.org/10.1007/978-1-4939-3676-2_2

Arima, J., Shimone, K., Miyatani, K., Tsunehara, Y., Isoda, Y., Hino, T., & Nagano, S. (2016). Crystal structure of d -stereospecific amidohydrolase from Streptomyces sp. 82F2 - Insight into the structural factors for substrate specificity. *FEBS Journal*, *283*(2), 337–349. https://doi.org/10.1111/febs.13579

Baek, M., DiMaio, F., Anishchenko, I., Dauparas, J., Ovchinnikov, S., Lee, G. R., … Baker, D. (2021). Accurate prediction of protein structures and interactions using a three-track neural network. *Science*, *373*(6557), 871–876. https://doi.org/10.1126/science.abj8754

Bohin, J. P. (2000). Osmoregulated periplasmic glucans in Proteobacteria. *FEMS Microbiology Letters*, *186*(1), 11–19. https://doi.org/10.1016/S0378-1097(00)00110-5

Bontemps-Gallo, S., Bohin, J.-P., & Lacroix, J.-M. (2017). Osmoregulated Periplasmic Glucans. *EcoSal Plus*, *7*(2). https://doi.org/10.1128/ecosalplus.esp-0001-2017

Bontemps-Gallo, S., & Lacroix, J. M. (2015). New insights into the biological role of the osmoregulated periplasmic glucans in pathogenic and symbiotic bacteria. *Environmental Microbiology Reports*, *7*(5), 690–697. https://doi.org/10.1111/1758-

2229.12325

Boutte, C. C., & Crosson, S. (2011). The complex logic of stringent response regulation in Caulobacter crescentus: Starvation signalling in an oligotrophic environment. *Molecular Microbiology*, *80*(3), 695–714. https://doi.org/10.1111/j.1365-2958.2011.07602.x

Cha, S. S., An, Y. J., Jeong, C. S., Kim, M. K., Jeon, J. H., Lee, C. M., … Lee, J. H. (2013). Structural basis for the β-lactamase activity of EstU1, a family VIII carboxylesterase. *Proteins: Structure, Function and Bioinformatics*, *81*(11), 2045–2051. https://doi.org/10.1002/prot.24334

Christen, B., Abeliuk, E., Collier, J. M., Kalogeraki, V. S., Passarelli, B., Coller, J. A., … Shapiro, L. (2011). The essential genome of a bacterium. *Molecular Systems Biology*, *7*(528), 1–7. https://doi.org/10.1038/msb.2011.58

Daitch, A. K., & Goley, E. D. (2020). Uncovering Unappreciated Activities and Niche Functions of Bacterial Cell Wall Enzymes. *Current Biology*, *30*(19), R1170–R1175. https://doi.org/10.1016/j.cub.2020.07.004

Desmarais, S. M., De Pedro, M. A., Cava, F., & Huang, K. C. (2013). Peptidoglycan at its peaks: How chromatographic analyses can reveal bacterial cell wall structure and assembly. *Molecular Microbiology*, *89*(1), 1–13. https://doi.org/10.1111/mmi.12266

Emsley, P., & Cowtan, K. (2004). Coot: Model-building tools for molecular graphics. *Acta Crystallographica Section D: Biological Crystallography*, *60*(12 I), 2126–2132. https://doi.org/10.1107/S0907444904019158

Evans, P. R., & Murshudov, G. N. (2013). How good are my data and what is the resolution? *Acta Crystallographica Section D: Biological Crystallography*, *69*(7), 1204–1214. https://doi.org/10.1107/S0907444913000061

Falchi, F. A., Maccagni, E. A., Puccio, S., Peano, C., De Castro, C., Palmigiano, A., …

Sperandeo, P. (2018). Mutation and suppressor analysis of the essential lipopolysaccharide transport protein LptA reveals strategies to overcome severe outer membrane permeability defects in Escherichia coli. *Journal of Bacteriology*, *200*(2). https://doi.org/10.1128/JB.00487-17

Fisher, J. F., & Mobashery, S. (2020). Constructing and deconstructing the bacterial cell wall. *Protein Science*, *29*(3), 629–646. https://doi.org/10.1002/PRO.3737

Gallego-Garcia, A., Iniesta, A. A., Gonzalez, D., Collier, J., Padmanabhan, S., & Eliis-Arnanz, M. (2017). Caulobacter crescentus CdnL is a non-essential RNA polymerase-binding protein whose depletion impairs normal growth and rRNA transcription. *Scientific Reports*, *7*(August 2016), 1–16. https://doi.org/10.1038/srep43240

Gao, X., Xie, X., Pashkov, I., Sawaya, M. R., Laidman, J., Zhang, W., … Tang, Y. (2009). Directed Evolution and Structural Characterization of a Simvastatin Synthase. *Chemistry and Biology*, *16*(10), 1064–1074. https://doi.org/10.1016/j.chembiol.2009.09.017

Girardot, C., Scholtalbers, J., Sauer, S., Su, S.-Y., & Furlong, E. E. M. (2016). Open Access Je, a versatile suite to handle multiplexed NGS libraries with unique molecular identifiers. https://doi.org/10.1186/s12859-016-1284-2

Gonzalez, D., & Collier, J. (2014). Effects of (p)ppGpp on the progression of the cell cycle of caulobacter crescentus. *Journal of Bacteriology*, *196*(14), 2514–2525. https://doi.org/10.1128/JB.01575-14

Hill, N. S., Buske, P. J., Shi, Y., & Levin, P. A. (2013). A Moonlighting Enzyme Links Escherichia coli Cell Size with Central Metabolism. *PLoS Genetics*, *9*(7). https://doi.org/10.1371/journal.pgen.1003663

Holtje, J. V., Fiedler, W., Rotering, H., Walderich, B., & Van Duin, J. (1988). Lysis induction of Escherichia coli by the cloned lysis protein of the phage MS2 depends

on the presence of osmoregulatory membrane-derived oligosaccharides. *Journal of Biological Chemistry*, *263*(8), 3539–3541. https://doi.org/10.1016/s0021-9258(18)68956-2

Huang, K. C., Mukhopadhyay, R., Wen, B., Gitai, Z., Wingreen, N. S., & Fisher, M. E. (2008). Cell shape and cell-wall organization in Gram-negative bacteria. Retrieved from www.pnas.org/cgi/content/full/

Juan, J., Armenteros, A., Tsirigos, K. D., Sønderby, C. K., Petersen, T. N., Winther, O., … Nielsen, H. (2019). Brief CommuniCation SignalP 5.0 improves signal peptide predictions using deep neural networks. *Nature Biotechnology*, *37*. https://doi.org/10.1038/s41587-019-0036-z

Judd, E. M., Comolli, L. R., Chen, J. C., Downing, K. H., Moerner, W. E., & McAdams, H. H. (2005). Distinct constrictive processes, separated in time and space, divide Caulobacter inner and outer membranes. *Journal of Bacteriology*, *187*(20), 6874–6882. https://doi.org/10.1128/JB.187.20.6874-6882.2005

Kabsch, W. (2010). Integration, scaling, space-group assignment and post-refinement. *Acta Crystallographica Section D: Biological Crystallography*, *66*(2), 133–144. https://doi.org/10.1107/S0907444909047374

Kennedy, E. P., Schneider, [, Reinhold, J. E., Rumley, V., Kennedy, M. K. &, & Biol,) J. (1982). Osmotic regulation and the biosynthesis of membrane derived oligosaccharides in Escherichia coli. *Proceedings of the National Academy of Sciences of the United States of America*, *79*(4 I), 1092–1095. https://doi.org/10.1073/PNAS.79.4.1092

Krissinel, E., & Henrick, K. (2004). Secondary-structure matching (SSM), a new tool for fast protein structure alignment in three dimensions. *Acta Crystallographica Section D: Biological Crystallography*, *60*(12 I), 2256–2268. https://doi.org/10.1107/S0907444904026460

Krogh, A., Larsson, B., Von Heijne, G., & Sonnhammer, E. L. L. (2001). Predicting transmembrane protein topology with a hidden Markov model: Application to complete genomes. *Journal of Molecular Biology*, *305*(3), 567–580. https://doi.org/10.1006/jmbi.2000.4315

Kuzin, A. P., Liu, H., Kelly, J. A., & Knox, J. R. (1995). Binding of Cephalothin and Cefotaxime to D-Ala-D-Ala-Peptidase Reveals a Functional Basis of a Natural Mutation in a Low-Affinity Penicillin-Binding Protein and in Extended-Spectrum β-Lactamases. *Biochemistry*, *34*(29), 9532–9540. https://doi.org/10.1021/bi00029a030

Lariviere, P. J., Mahone, C. R., Santiago-Collazo, G., Howell, M., Daitch, A. K., Zeinert, R., … Goley, E. D. (2019). An Essential Regulator of Bacterial Division Links FtsZ to Cell Wall Synthase Activation. *Current Biology*, *29*(9), 1460-1470.e4. https://doi.org/10.1016/j.cub.2019.03.066

Li, H., & Durbin, R. (2010). Fast and accurate long-read alignment with Burrows-Wheeler transform, *26*(5), 589–595. https://doi.org/10.1093/bioinformatics/btp698

Li, H., Handsaker, B., Wysoker, A., Fennell, T., Ruan, J., Homer, N., … Subgroup, D. P. (2009). The Sequence Alignment/Map format and SAMtools. *BIOINFORMATICS APPLICATIONS NOTE*, *25*(16), 2078–2079. https://doi.org/10.1093/bioinformatics/btp352

Lubin, E. A., Henry, J. T., Fiebig, A., Crosson, S., & Laub, M. T. (2016). Identification of the PhoB regulon and role of PhoU in the phosphate starvation response of Caulobacter crescentus. *Journal of Bacteriology*, *198*(1), 187–200. https://doi.org/10.1128/JB.00658-15/FORMAT/EPUB

Mahasenan, K. V., Batuecas, M. T., De Benedetti, S., Kim, C., Rana, N., Lee, M., … Mobashery, S. (2020). Catalytic Cycle of Glycoside Hydrolase BglX from Pseudomonas aeruginosa and Its Implications for Biofilm Formation. *ACS Chemical*

Biology, *15*(1), 189–196. https://doi.org/10.1021/acschembio.9b00754

May, K. L., & Grabowicz, M. (2018). The bacterial outer membrane is an evolving antibiotic barrier. *PNAS*, *115*. https://doi.org/10.1073/pnas.1812779115

Mccarthy, D. J., Chen, Y., & Smyth, G. K. (2012). Differential expression analysis of multifactor RNA-Seq experiments with respect to biological variation. *Nucleic Acids Research*, *40*. https://doi.org/10.1093/nar/gks042

McCoy, A. J., Grosse-Kunstleve, R. W., Adams, P. D., Winn, M. D., Storoni, L. C., & Read, R. J. (2007). Phaser crystallographic software. *Journal of Applied Crystallography*, *40*(4), 658–674. https://doi.org/10.1107/S0021889807021206

Meier, E. L., Daitch, A. K., Yao, Q., Bhargava, A., Jensen, G. J., & Goley, E. D. (2017). FtsEX-mediated regulation of the final stages of cell division reveals morphogenetic plasticity in Caulobacter crescentus. *PLoS Genetics*, *13*(9), 1–25. https://doi.org/10.1371/journal.pgen.1006999

Miller, M. S., Maheshwari, S., Shi, W., Gao, Y., Chu, N., Soares, A. S., … Gabelli, S. B. (2019). Getting the most out of your crystals: Data collection at the new high-flux, Microfocus MX beamlines at NSLS-II. *Molecules*, *24*(3). https://doi.org/10.3390/molecules24030496

Möll, A., Schlimpert, S., Briegel, A., Jensen, G. J., & Thanbichler, M. (2010). DipM, a new factor required for peptidoglycan remodelling during cell division in Caulobacter crescentus. *Molecular Microbiology*, *77*(1), 90–107. https://doi.org/10.1111/J.1365-2958.2010.07224.X

Nakano, S., Okazaki, S., Ishitsubo, E., Kawahara, N., Komeda, H., Tokiwa, H., & Asano, Y. (2015). Structural and computational analysis of peptide recognition mechanism of class-C type penicillin binding protein, alkaline D-peptidase from Bacillus cereus DF4-B. *Scientific Reports*, *5*(April), 1–12. https://doi.org/10.1038/srep13836

Ngo, T. D., Ryu, B. H., Ju, H., Jane, E. J., Kim, K. K., & Kim, T. D. (2014).

Crystallographic analysis and biochemical applications of a novel penicillin-binding protein/β-lactamase homologue from a metagenomic library. *Acta Crystallographica Section D: Structural Biology*, *D70*, 2455–2466.

Okazaki, S., Suzuki, A., Komeda, H., Yamaguchi, S., Asano, Y., & Yamane, T. (2007). Crystal Structure and Functional Characterization of a D-Stereospecific Amino Acid Amidase from Ochrobactrum anthropi SV3, a New Member of the Penicillin-recognizing Proteins. *Journal of Molecular Biology*, *368*(1), 79–91. https://doi.org/10.1016/j.jmb.2006.10.070

Price, M. N., Wetmore, K. M., Waters, R. J., Callaghan, M., Ray, J., Liu, H., … Deutschbauer, A. M. (2018). Mutant phenotypes for thousands of bacterial genes of unknown function. *Nature*, *557*(7706), 503–509. https://doi.org/10.1038/s41586-018-0124-0

Radhakrishnan, S. K., Thanbichler, M., & Viollier, P. H. (2008). The dynamic interplay between a cell fate determinant and a lysozyme homolog drives the asymmetric division cycle of Caulobacter crescentus. *Genes and Development*, *22*(2), 212–225. https://doi.org/10.1101/gad.1601808

Rajagopal, S., Eis, N., Bhattacharya, M., & Nickerson, K. W. (2003). Membrane-derived oligosaccharides (MDOs) are essential for sodium dodecyl sulfate resistance in Escherichia coli. *FEMS Microbiology Letters*, *223*(1), 25–31. https://doi.org/10.1016/S0378-1097(03)00323-9

Robert, X., & Gouet, P. (2014). Deciphering key features in protein structures with the new ENDscript server. *Nucleic Acids Research*, *42*(W1), 320–324. https://doi.org/10.1093/nar/gku316

Robinson, J. T., Thorvaldsdóttir, H., Winckler, W., Guttman, M., Lander, E. S., Getz, G., & Mesirov, J. P. (2011). Integrative genomics viewer. *Nature Publishing Group*. https://doi.org/10.1038/nbt0111-24

Robinson, M. D., Mccarthy, D. J., & Smyth, G. K. (2010). edgeR: a Bioconductor

package for differential expression analysis of digital gene expression data.

BIOINFORMATICS APPLICATIONS NOTE, *26*(1), 139–140.

https://doi.org/10.1093/bioinformatics/btp616

Ryu, B. H., Ngo, T. D., Yoo, W., Lee, S., Kim, B. Y., Lee, E., … Kim, T. D. (2016).

Biochemical and Structural Analysis of a Novel Esterase from Caulobacter

crescentus related to Penicillin-Binding Protein (PBP). *Scientific Reports*, *6*(July),

1–15. https://doi.org/10.1038/srep37978

Silhavy, T. J., Kahne, D., & Walker, S. (2010). The bacterial cell envelope. *Cold Spring

Harbor Perspectives in Biology*, *370*(1679), 1–17.

https://doi.org/10.1098/rstb.2015.0019

Sonnhammer, E. L. L., & Krogh, A. (2008). A hidden Markov model for predicting

transmembrane helices in protein sequence. *Sixth Int. Conf. on Intelligent Systems

for Molecular Biology*, 8. Retrieved from papers://4b986d00-906f-493f-a74b-

71e29d82b719/Paper/p6291

Steinegger, M., & Söding, J. (2018). Clustering huge protein sequence sets in linear

time. *Nature Communications*, *9*(1). https://doi.org/10.1038/s41467-018-04964-5

Stock, J. B., Rauch, B., & Roseman, S. (1977). Periplasmic space in Salmonella

typhimurium and Escherichia coli. *Journal of Biological Chemistry*, *252*(21), 7850–

7861. https://doi.org/10.1016/S0021-9258(17)41044-1

Sundararajan, K., Miguel, A., Desmarais, S. M., Meier, E. L., Casey Huang, K., & Goley,

E. D. (2015). The bacterial tubulin FtsZ requires its intrinsically disordered linker to

direct robust cell wall construction. *Nature Communications*, *6*, 1–14.

https://doi.org/10.1038/ncomms8281

Sutterlin, H. A., Shi, H., May, K. L., Miguel, A., Khare, S., Huang, K. C., & Silhavy, T. J.

(2016). Disruption of lipid homeostasis in the Gram-negative cell envelope activates

a novel cell death pathway. *Proceedings of the National Academy of Sciences*, *113*(11), E1565–E1574. https://doi.org/10.1073/PNAS.1601375113

Thorvaldsdottir, H., Robinson, J. T., & Mesirov, J. P. (2012). Integrative Genomics Viewer (IGV): high-performance genomics data visualization and exploration. *BRIEFINGS IN BIOINFORMATICS, 14*. https://doi.org/10.1093/bib/bbs017

Vizcaíno, J. A., Deutsch, E. W., Wang, R., Csordas, A., Reisinger, F., Ríos, D., … Hermjakob, H. (2014). ProteomeXchange provides globally coordinated proteomics data submission and dissemination. *Nature Biotechnology*, *32*(3), 223–226. https://doi.org/10.1038/nbt.2839

Wagner, U. G., Petersen, E. I., Schwab, H., & Kratky, C. (2009). EstB from Burkholderia gladioli: A novel esterase with a β-lactamase fold reveals steric factors to discriminate between esterolytic and β-lactam cleaving activity. *Protein Science*, *11*(3), 467–478. https://doi.org/10.1110/ps.33002

Weaver, A., Alvarez, L., Rosch, K., Ahmed, A., Wang, G., Van Nieuwenhze, M., … Dörr, T. (2022). Lytic transglycosylases mitigate periplasmic crowding by degrading soluble cell wall turnover products. *ELife*, *11*, 1–23. https://doi.org/10.7554/eLife.73178

West, L., Yang, D., & Stephens, C. (2002). Use of the Caulobacter crescentus genome sequence to develop a method for systematic genetic mapping. *Journal of Bacteriology*, *184*(8), 2155–2166. https://doi.org/10.1128/JB.184.8.2155-2166.2002

Wetmore, K. M., Price, M. N., Waters, R. J., Lamson, J. S., He, J., Hoover, C. A., … Deutschbauer, A. (2015). Rapid quantification of mutant fitness in diverse bacteria by sequencing randomly bar-coded transposons. *MBio*, *6*(3), 1–15. https://doi.org/10.1128/mBio.00306-15

Woldemeskel, S. A., & Goley, E. D. (2017). Shapeshifting to Survive : Shape Determination and Regulation in Caulobacter crescentus. *Trends in Microbiology*,

xx, 1–15. https://doi.org/10.1016/j.tim.2017.03.006

Woldemeskel, S., Daitch, A. K., Alvarez, L., Panis, G., Zeinert, R., Gonzalez, D., …

Goley, E. D. (2020). The conserved transcriptional regulator CdnL is required for

metabolic homeostasis and morphogenesis in Caulobacter.

https://doi.org/10.1371/journal.pgen.1008591

Chapter 3. OpgH is an essential regulator of

Caulobacter morphology

3.1 Abstract

Bacterial growth and division rely on intricate regulation of morphogenetic complexes to remodel the cell envelope without compromising envelope integrity. The focus in recent years has been on the regulation of cell wall synthetic and metabolic enzymes, though other cell envelope components likely play a role in morphogenesis as well. Components required to maintain osmotic homeostasis are among these understudied envelope enzymes that contribute to cell morphology. A primary factor required to protect envelope integrity in low osmolarity environments is OpgH, the synthase of osmoregulated periplasmic glucans (OPGs). Here, we describe the essentiality of OpgH in the α-proteobacterium, *Caulobacter crescentus*, and characterize the cell morphology defects associated with loss of OpgH. Depletion of OpgH results in striking asymmetric bulging and lysis, along with misregulation of the cell wall and associated morphogenetic complexes. Furthermore, the enzymatic activity of OpgH is responsible for preventing morphological defects as expression of an OpgH mutant that disrupts a conserved glycosyltransferase motif within OpgH phenocopies the depletion. Our data establish a surprising function for an OpgH

homolog in morphogenesis and reveal an essential role of OpgH in maintaining proper cell morphology during normal growth and division.

3.2 Introduction

Bacteria inhabit an impressive range of environments and can adapt to sudden changes in environmental conditions. One parameter that can vary significantly in different niches is osmolarity, ranging from dilute freshwater habitats to highly concentrated soil. The α-proteobacterium, *Caulobacter crescentus* (hereafter *Caulobacter*), is well-established as a model for physiological adaptation in the face of changing environments. Originally classified as an aquatic oligotroph, there is now evidence for the ability of *Caulobacter* to also inhabit more complex soil environments (Wilhelm, 2018). Within these diverse habitats, *Caulobacter* is capable of exquisitely tuning its physiology as needed to propagate through growth and division.

The surrounding environment and available nutrients dictate the *Caulobacter* cell cycle progression (Curtis and Brun, 2010). *Caulobacter* undergoes distinct morphological changes as it proceeds through its cell cycle. A newborn, flagellated swarmer cell has the ability to move and search for nutrients before differentiating into a sessile stalked cell (Curtis and Brun, 2010). This transition involves a stereotyped set of physiological changes including shedding its flagellum and growing a thin extension of the cell envelope called the stalk (Curtis and Brun, 2010). This stalked cell can then undergo a cycle of cell division, as characterized by replication and segregation of the chromosome, elongation of the cell body, growth of a flagellum opposite the stalked pole, and cytokinesis (Curtis and Brun, 2010). This asymmetric life cycle enables swarmer cells the

ability to find a new environment while requiring stalked cells to adapt within a given environment and any changes they experience there.

Caulobacter has distinct cellular structures and processes that enable its survival in changing environments. Notably, the bacterial cell envelope serves as the physical barrier between the cell and its environment (Silhavy et al., 2010). The Gram-negative cell envelope comprises the inner and outer cell membranes and the periplasmic space (periplasm) formed between them. Within the periplasm is the peptidoglycan (PG) cell wall which provides structure and shape to the cell and protects the cell from lysis due to turgor pressure (Huang et al., 2008). PG biosynthesis is coordinated by the localization and activity of two conserved morphogenetic complexes: the elongasome/Rod complex and the divisome, responsible for elongation and division, respectively (Daitch and Goley, 2020). Without the cell wall, any changes in osmolarity would quickly alter cell shape and result in lysis.

In addition to the cell wall, some bacteria also produce glucose polymers in the periplasm, called osmoregulated periplasmic glucans (OPGs, previously referred to as membrane-derived oligosaccharides). OPGs are described as the only periplasmic component that is regulated in changing osmotic environments and are thought to function as an osmoprotectant (Bontemps-Gallo et al., 2017). Theoretically, OPGs modulate the osmolarity of the periplasm to protect the cytoplasmic osmolarity from environmental changes. OPGs are produced across proteobacteria, though their structure can vary drastically, ranging from 5 to 24 glucose units and sometimes bearing modifications from phospholipids or

intermediary metabolism (Bontemps-Gallo et al., 2017). We recently identified the first OPG in Caulobacter, as a cyclic, hexamer of glucose (Daitch et al., 2022). The synthase of OPGs has been well-characterized in other organisms as the inner membrane protein, OpgH. In *Escherichia coli*, *opgH* is necessary for OPG production (Kennedy et al., 1982). Some organisms, including *E. coli*, encode additional *opg* genes, such as *opgG and opgD*, which are postulated to modify OPGs (Bontemps-Gallo et al., 2017). Surprisingly, however, the only *opg* homolog encoded in *Caulobacter* is *opgH* (*CCNA_02097)*. Also notably, *Caulobacter opgH* is annotated as essential (Christen et al., 2011), unlike characterized *opgH* homologs in other organisms. We were especially intrigued by the essentiality of *opgH* given the unique influence of osmolarity in *Caulobacter*'s growth environments and decided to investigate OpgH further.

In this work, we explore the role of OpgH in *Caulobacter* morphogenesis. The role of OpgH and consequences of its loss have not been characterized in an organism that required OpgH for viability, as *opgH* is non-essential in other well-studied organisms. Here, we confirm the essentiality of *opgH* in *Caulobacter* and discover striking morphological defects associated with OpgH depletion or loss of enzymatic activity. Our data reveal a novel role of an essential OpgH enzyme in maintaining cell morphology.

3.3 Results

3.3.1 OpgH is essential in *Caulobacter*

This study was initiated through our interest in identifying essential components of the cell envelope that contribute to morphogenesis. Transposon sequencing indicated that *opgH* (*CCNA_02097),* encoding an inner membrane bound, periplasmic glucan glycosyltransferase, was essential in *Caulobacter* (Christen et al., 2011). This was surprising because in *E. coli*, *opgH* is non-essential and deletion of *opgH* yields minimal morphological defects (Hill et al., 2013). We therefore sought to validate the reported essentiality of *opgH* in *Caulobacter*. Indeed, we were unable to generate a clean deletion of *opgH*. We were, however, able to make an OpgH depletion strain. This strain has a clean deletion of *opgH* at the native locus with a vanillate-inducible copy of *opgH* at the *vanA* locus (strain number EG3421). When grown with vanillate to induce OpgH (+ OpgH), cells looked morphologically wild type (WT) in both the complex media peptone yeast extract (PYE) and in defined minimal media (M2G) (Figure 3.1A t=0). With OpgH, cells grew comparably to WT *Caulobacter* in both liquid (measured by optical density) (Figure 3.1B) and solid media (measured by spot dilution) (Figure 3.1C). When OpgH was depleted for three hours in PYE without vanillate (- OpgH), the cells exhibited a slight elongation and widening of the cell body. This phenotype was exacerbated over the course of the depletion, with five and seven hours showing prominent morphological defects, including asymmetrical bulging and cell lysis (Figure 3.1A). The bulging and lysis phenotype was also present in M2G, but was slightly less severe and began later in the course of depletion (Figure 3.1A).

In addition to morphological defects, prolonged depletion of OpgH quickly became lethal in PYE or M2G, as seen by growth curve (Figure 3.1B) and spot dilution (Figure 3.1C). Slight overexpression of *opgH* from the vanillate-inducible promoter in the presence of native *opgH* did not impact cell growth, indicating that lethality observed is a result of the depleting the OpgH protein (Figure 3.1B,C *vanA::P_{van}-opgH*).

We were surprised by the speed at which we began to see morphological defects from depleting OpgH. Notably, we see morphological changes by three hours of depletion, which is approximately two cell cycles in PYE. Typically, depletion of a protein requires growth to reduce the available pool of protein, and morphological changes require enzymatic remodeling of PG during growth and division. Since the morphological defects we observed occurred fairly quickly, we wondered whether the morphology change resulting from OpgH depletion required active cell growth. To test this, we depleted OpgH in the presence of sub-lethal concentrations of chloramphenicol to inhibit cell growth. Depleting OpgH in the absence of chloramphenicol yielded the expected asymmetrical bulging and lysis. However, these phenotypes were suppressed in the presence of chloramphenicol (Supplemental Figure 3.1). This suggested that active growth and division is needed to deplete OpgH and/or enable morphological phenotypes and ultimate lethality.

3.3.2 OpgH depletion has prominent morphological defects and asymmetric bulging

The unique bulging phenotype of the depletion observed by eye motivated us to quantify the shape changes resulting from loss of OpgH. Using CellTool (Pincus and Theriot, 2007) to perform principal component analysis of cell morphology, we analyzed the OpgH depletion strain in the presence and absence of 0.5 mM vanillate after five hours in PYE. Using this analysis, we saw a statistically significant difference between the cells with OpgH present (+ van) compared to cells without OpgH (- van) in the top four shape modes (Figure 3.2A). The shape modes approximately reflected the following features: shape mode 1-length, shape mode 2-curvature, shape mode 3-width, shape mode 4-asymmetrical bulging. From this quantification, cells depleted of OpgH for five hours were typically longer, less curved, and wider than cells with OpgH (Figure 3.2A). For shape mode 4, which roughly corresponds to asymmetrical bulging, we have reported the absolute values, since the bulging can appear on either side of a cell outline. Our analysis indicates that cells producing OpgH rarely, if ever, exhibit asymmetric bulging while this is frequently observed in the OpgH-depleted condition (Figure 3.2A). Since shape mode 4 captures the unique asymmetrical bulging, we plotted it against shape mode 1 to visualize the variety of shapes, notably asymmetric bulging, present in the OpgH-depleted cells (Figure 3.2B). Additionally, we measured the shape variance of the four shape modes when OpgH was depleted in M2G. The OpgH-depleted cells in M2G (M2G - van) all have a statistically significant

differences in shape modes 1 through 4 compared to cells with OpgH present (M2G + van) (Supplemental Figure 3.2).

We were especially interested in the unique asymmetrical bulging phenotype of the OpgH depleted cells. To investigate this asymmetry, we leveraged the inherent cell polarity of *Caulobacter* to determine if the bulging consistently occurred at the same pole or was random. Every *Caulobacter* cell has a defined orientation, bearing a stalked pole and a swarmer pole, that can be visually tracked over the course of a few cell cycles. We performed timelapse microscopy of the OpgH-depleted cells in the absence of vanillate to observe depletion over the course of five hours. The most notable phenotypes are summarized in Figure 3.3, including asymmetrical bulging, elongation, multiple constriction events, and lysis. From our timelapse analysis, we were able to follow single cells through their life cycles, which allowed us to orient the cells and identify the stalked (old) or swarmer (new) pole of a given cell. As illustrated in the final panel of Figure 3.3 (Figure 3.3, old pole asymmetric bulging), we determined that bulging exclusively occurs in the stalked half of the cell (nearest to the old pole). As the localization of OpgH is diffuse along the entire body of the cell in both PYE and M2G media (Supplemental Figure 3.3), this suggested that the bulging is not related to OpgH localization, but to differential sensitivity of one or more factors unique to the stalked pole during OpgH depletion.

3.3.3 Cell wall synthesis is disrupted during OpgH depletion

The primary determinant of cell shape is the PG cell wall, so we hypothesized that bulging is a result of misregulated PG synthesis. We therefore sought to visualize

active PG synthesis in the OpgH-depleted cells. Using the fluorescent D-amino acid, HADA (Kuru et al., 2015), we captured a snapshot of active PG synthesis over the course of OpgH depletion. The HADA patterning of the OpgH depletion strain grown with vanillate corresponded with the expected localization of PG synthesis in WT *Caulobacter*. HADA incorporated broadly along the cell body in swarmer cells and then localized to mid-cell in stalked and pre-divisional cells (Figure 3.4A). We also determined the localization pattern via demographs to illustrate HADA localization on a population level of 300 cells. The smallest cells, representative of newborn swarmer cells, have diffuse HADA incorporation, and as the cell length increased, representative of stalked and pre-divisional cells, the HADA localization became more focused to mid-cell at the division plane (Figure 3.4A). This was consistent over the course of seven hours of growth in the cells with OpgH. When vanillate was removed and OpgH was depleted, we began to observe atypical HADA incorporation starting at five hours (Figure 3.4B). At five hours of depletion, HADA incorporation was more diffuse, but still yielded a thick band near mid-cell which was typically at the thinnest part of the asymmetric bulges (Figure 3.4B). By seven hours of depletion, the HADA incorporation was almost entirely diffuse and, in some cases, we observed minimal incorporation (Figure 3.4B). From these data we conclude that PG synthesis is spatially misregulated in the absence of OpgH.

3.3.4 Divisome and elongasome machinery are mislocalized in OpgH-depleted cells

The spatial misregulation of PG synthesis we observed during OpgH depletion aligns with the profound morphological defects that occur without OpgH. We hypothesized that misregulation of PG synthesis could be attributed to a mislocalization of the PG synthetic machinery associated with the divisome or elongasome. We began with the elongasome and characterized the localization of an mNeonGreen tagged RodZ (mNG-RodZ) under the control of its native promoter. RodZ is an essential part of the elongasome complex and its localization corresponds to sites of PG synthesis, as coordinated by the Rod complex (Alyahya et al., 2009). RodZ localization is dependent on the localization of MreB, the actin homolog that directs localization of elongasome proteins. In WT cells, RodZ and MreB exhibit a patchy localization that focuses at midcell in stalked and predivisional cells. This WT localization pattern of RodZ was consistent in cells with OpgH present (Figure 3.5A). In contrast, when OpgH was depleted, RodZ became diffuse and created puncta along the cell by five hours of depletion, which was exacerbated by seven hours (Figure 3.5A). Additionally, we noticed an increase in mNG-RodZ signal over the course of depletion. Since mNG-RodZ was under the control of the native RodZ promoter, this could be attributed to an inability to turn over RodZ or a mechanism to increase production of RodZ as OpgH is depleted.

As we depleted OpgH, we observed a loss of midcell RodZ localization. Since RodZ's midcell localization is also dependent on FtsZ, we next assessed

FtsZ localization. FtsZ, the master regulator of the divisome, is an essential protein. FtsZ forms a dynamic scaffold, called the Z-ring, that directs assembly of the divisome to the future division site (Erickson et al., 2010). When OpgH was present, mNG-FtsZ consistently formed tight midcell bands (Figure 3.5B). We note that the demographs of mNG-FtsZ localization with OpgH have more unipolar FtsZ than typically observed with other FtsZ fluorescent fusions (Barrows et al., 2020; Meier et al., 2017; Woldemeskel et al., 2017). We attribute this difference to the slight overexpression of OpgH in this background that may slightly alter the temporal dynamics of FtsZ localization. In contrast, when OpgH was depleted, mNG-FtsZ created wider bands by three hours of depletion that were often shifted away from midcell (Figure 3.5B, white arrows). This off-center FtsZ localization potentially aligns with the asymmetric HADA incorporation (Figure 3.4B) and bulging. By five hours of depletion, FtsZ was almost entirely diffuse (Figure 3.5B). This aberrant Z-ring placement explains the inability of RodZ to properly localize, and suggests that by five hours of depletion, both the divisome and elongasome are unable to properly localize and direct PG synthesis.

We next turned our attention to the Z-ring positioning protein, MipZ, which is a negative regulator of FtsZ assembly (Thanbichler and Shapiro, 2006). MipZ follows the *Caulobacter* chromosome segregation machinery, forming a unipolar focus in swarmer cells, and then becoming bipolar as the origin of replication splits into two. Bipolar MipZ inhibits FtsZ polymerization at the poles, and directs Z-ring formation at midcell. MipZ-YFP localization in cells with OpgH was consistent with WT MipZ localization over the *Caulobacter* cell cycle (Figure 3.5C). Over the

course of OpgH depletion for five hours, however, MipZ-YFP formed distinct puncta along the cell, with some cells exhibiting more than three MipZ-YFP foci (Figure 3.5C). After seven hours of OpgH depletion, MipZ-YFP was almost entirely diffuse, while only sometimes forming puncta (Figure 3.5C). Notably, after seven hours, the demograph of MipZ-YFP localization showed a slight exclusion of MipZ-YFP from the poles (Figure 3.5C). We propose that mislocalization of MipZ in cells lacking OpgH is a key factor that leads to mislocalization of the divisome and elongasome, yielding the pleiotropic morphological defects we have observed. OpgH

3.3.5 Glycosyltransferase activity of OpgH is required to maintain proper morphology

Given that OpgH is an OPG synthase, we wondered if its enzymatic activity is required to maintain cell morphology. OpgH has auxiliary roles in other bacteria in addition to its function as an OPG synthase; for instance, *E. coli* OpgH synthesizes OPGs and also acts as an inhibitor of FtsZ to modulate cell size with nutrient availability (Hill et al., 2013). This moonlighting activity of *E. coli* OpgH is likely not conserved in *Caulobacter* since its OpgH lacks much of the N-terminal FtsZ interacting domain and also does not localize to the divisome (Supplemental Figure 3.3). Moreover, the enzymatic activity of *E. coli* OpgH is not required to regulate FtsZ. To directly probe the role of the enzymatic activity for *Caulobacter* OpgH, we sought to characterize the D-X-D motif, consisting of amino acids 245-247 (D-A-D). Enzymes in the GT-A family of glycosyltransferases all contain a conserved D-X-D motif, responsible for binding the phosphate group on a

nucleotide donor and coordinating a divalent cation required for activity (Breton et al., 2006). Mutation of either aspartate residue in the D-X-D motif eliminates the glycosyltransferase activity *in vitro* of other enzymes within this family, while not disrupting the fold of the enzyme (Wiggins and Munro, 1998).

We initially attempted to convert the latter aspartate to an alanine (OpgH$_{D247A}$) at the native OpgH locus, but were unsuccessful. This was not entirely surprising since we hypothesized that this mutation may yield a non-functional enzyme. Instead, we investigated the phenotype of cells producing this mutant by creating a strain harboring a native deletion of *opgH*, along with a vanillate-inducible WT copy of OpgH and a xylose-inducible copy of either WT OpgH or the OpgH$_{D247A}$ mutant. Depletion of both copies of OpgH resulted in the expected elongation and bulging phenotype, and expression of WT *opgH* yielded normal growth and morphology. However, production of OpgH$_{D247A}$ with xylose phenocopied depletion of OpgH (Figure 3.6A). We additionally verified the lethality of the OpgH$_{D247A}$ mutant with spot dilutions, where production of the OpgH$_{D247A}$ mutant yielded only a few colonies likely due to leaky expression of WT OpgH (Figure 3.6B). We also note the appearance of mucoid colonies when WT *opgH* and *opgH$_{D247A}$* are co-expressed, which appears consistent among two biological clones, perhaps due to overexpression of the impaired mutant (Figure 3.6B). Ultimately, the identification of this catalytically dead mutant of OpgH that phenocopies its depletion implicates OpgH's glycosyltransferase activity in maintaining cellular morphology.

3.4 Discussion

In this work, we have highlighted the essential and previously undiscovered role of OpgH in *Caulobacter* morphogenesis. We have confirmed that *opgH* is essential (Figure 3.1) and characterized the unique morphological defects associated with loss of OpgH. Without OpgH, *Caulobacter* cells become elongated and develop asymmetric bulges (Figure 3.2). These observed bulges always occur at the stalked pole, and typically result in lysis (Figure 3.3). Through the use of PG labeling probes, we have shown that these phenotypes likely result from misregulation of PG insertion (Figure 3.4), resulting from mislocalization of the divisome and elongasome (Figure 3.5). Interestingly, we can attribute the morphological defects of OpgH depletion to the glycosyltransferase activity of OpgH, as a catalytically dead OpgH mutant phenocopied the depletion (Figure 3.6).

The essentiality of *Caulobacter* OpgH and morphological defects associated with its loss provide a pivotal opportunity to elucidate the mechanism of action of OpgH and the OPG biosynthesis pathway. The previously studied OpgH homologs have all been nonessential, which limits the questions that we can ask. For instance, it is more challenging to study functional mutants *in vivo* or conduct genetic screens in an organism where OpgH is nonessential. Thus, this provides an appealing possibility for future work on *Caulobacter* OpgH, potentially including avenues such as a mutagenesis screen to isolate novel mutants or a larger scale functional domain analysis study. We have begun to probe this through the identification of functional OpgH mutants that suppressed the lethality

of cell envelope stresses in a hypersensitive mutant (Daitch et al., 2022). These mutants, as well as extragenic mutations isolated from suppressor screens, will be valuable in elucidating the mechanistic role of OpgH and OPGs in cell envelope homeostasis.

Though our data have implicated the glycosyltransferase activity of OpgH with the resulting morphological defects, we do not have direct evidence that the *Caulobacter* OpgH can synthesize OPGs. However, we have previously identified a genetic interaction between OpgH and the novel OPG metabolic enzymes, EstG and BglX (Daitch et al., 2022). In this study, we determined the substrate of EstG as a cyclic hexameric sugar, which is the first OPG identified in *Caulobacter* (Daitch et al., 2022). Further biochemical studies are necessary to determine if this cyclic OPG is in fact the product of OpgH.

Our results indicate the importance of OPG synthesis for localizing a variety of morphogenetic complexes. Since MipZ is delocalized in OpgH depleted cells, this suggests that MipZ might be responsible for the mislocalized morphogenetic proteins, since MipZ influences FtsZ and divisome placement, which consequently influences elongasome localization (Goley et al., 2011; Thanbichler and Shapiro, 2006). Alternatively, OPG synthesis might disrupt cellular energetics through glucose or carbon metabolism, which could consequently impact the morphogenetic complexes. This is plausible since both MipZ and FtsZ require energy-rich nucleotides (ATP and GTP respectively) to fuel their localization and dynamics (Erickson et al., 2010; Thanbichler and Shapiro, 2006). Despite the important role of the primary morphogenetic complexes, we were most surprised

by the prominent asymmetric bulging resulting from OpgH depletion. Typically, cell bulging is a consequence of misregulation either the elongasome/Rod complex or the divisome. The bulging that results from misregulation of the elongasome in *Caulobacter* (e.g. depleting MreB) (Figge et al., 2004), results in cell rounding and produces lemon shaped cells. Bulging from a divisome mutant (i.e. a ΔCTL mutant of FtsZ) (Barrows et al., 2020; Sundararajan et al., 2015), results in envelope bulges only where ΔCTL is localized. Though cell bulging results from a variety of elongasome and divisome mutants, the OpgH depletion phenotype was unique in its asymmetry, with bulging primarily on the stalked side of the cell. Because of this, it is possible that the asymmetrical bulging is not due to the primary morphogenetic complexes, but instead en unexplored cellular factor that directs PG synthesis asymmetrically. For instance, loss of OpgH might misregulate other PG synthetic enzymes, such as the L,D-transpeptidases, which primarily crosslink PG in the stalk resulting in the observed asymmetry.

We have established that OpgH, and likely OPG production, play a crucial role in *Caulobacter* cell morphogenesis and our results suggest an unexplored connection between osmoregulation and the cellular morphogenetic complexes. As discussed above, *E. coli* OpgH has a direct connection with the divisome as an inhibitor of FtsZ. Though *Caulobacter* OpgH lacks this interaction domain and does not have a distinct localization pattern, we cannot rule out the existence an interaction between OpgH and components of the divisome, elongasome, or other internal organization factor. However, given the importance of OpgH catalytic activity, our data suggests an effect of OPGs on morphogenetic complexes. This

genetic or biochemical connection between OpgH and its interacting partners as well as cellular changes from OPG production remains an avenue for future work. Overall, our findings have established a fundamental homeostatic role for an essential OpgH homolog and we have uncovered a novel connection between the OPG pathway and cellular morphology.

3.5 Materials and Methods

Caulobacter crescentus growth media and conditions

C. crescentus NA1000 cells were grown at 30˚C in peptone-yeast extract (PYE) medium. Xylose was used at a concentration of 0.3% (w/v) and vanillate at 0.5 mM for induction experiments. Antibiotics used in liquid (solid) medium as are follows: gentamycin, 1 (5) µg/mL; kanamycin, 5 (25) µg/mL; spectinomycin, 25 (100) µg/mL. Streptomycin was used at 5 µg/mL in solid medium. For growth curves, a Tecan Infinite M200 Pro plate reader measured absorbance every 30 minutes at OD_{600} of a 100 µL culture volume in a 96 well plate in biological triplicate with intermittent shaking. For spot dilutions, cells were grown up to mid-log phase and diluted to an OD_{600} of 0.05. Cells were then serially diluted up to 10^{-6} and 5 µL of each dilution was spotted onto a PYE plate with indicated inducer and/or antibiotic. Plates were incubated at 30˚C for 48 hours.

Atypical strain construction

We could not make the following strains in low osmolarity PYE media, so they were constructed in M2G minimal media: EG3421 (*opgH::ΔopgH; vanA::P$_{van}$-opgH*), EG3770 (*opgH::ΔopgH; vanA::P$_{van}$-opgH, xylX::P$_{xyl}$-mNG-FtsZ*), EG3790 (*opgH::ΔopgH; vanA::P$_{van}$-opgH, xylX::P$_{rodZ}$-mNG-rodZ*), EG3808 (*opgH::ΔopgH; vanA::P$_{van}$-opgH, xylX::P$_{xyl}$-mipZ-YFP*), EG3828 (*opgH::ΔopgH; vanA::P$_{van}$-opgH; xylX::P$_{xyl}$-opgH*), EG3787 (*opgH::ΔopgH; vanA::P$_{van}$-opgH; xylX::P$_{xyl}$-opgH$_{D247A}$*). For a 500 mL batch of M2G plates, autoclave 465 mL of water and 7.5 g agar (1.5%). Once cooled, add 25 mL of 5x M2 salts, 500 µL of 500 mM $MgSO_4$, 500

µL of 10 mM FeSO$_4$ 10 mM EDTA (Sigma F-0518), and 0.3% glucose. Additional antibiotics or media supplements for selection were added at this time.

Microscopy

Cells in exponential phase were immobilized on 1% agarose pads and imaged using a Nikon Eclipse Ti inverted microscope equipped with a Nikon Plan Fluor 100X (NA1.30) oil Ph3 objective and Photometrics CoolSNAP HQ^2 cooled CCD camera. Images were processed using Adobe Photoshop. Levels were adjusted to the same level across samples in a given experiment. Cell shape analysis was performed using CellTool and demographs were generated using Oufti. Inducible fluorescent fusion proteins were induced for 1 hour with 0.3% xylose before indicated imaging timepoint.
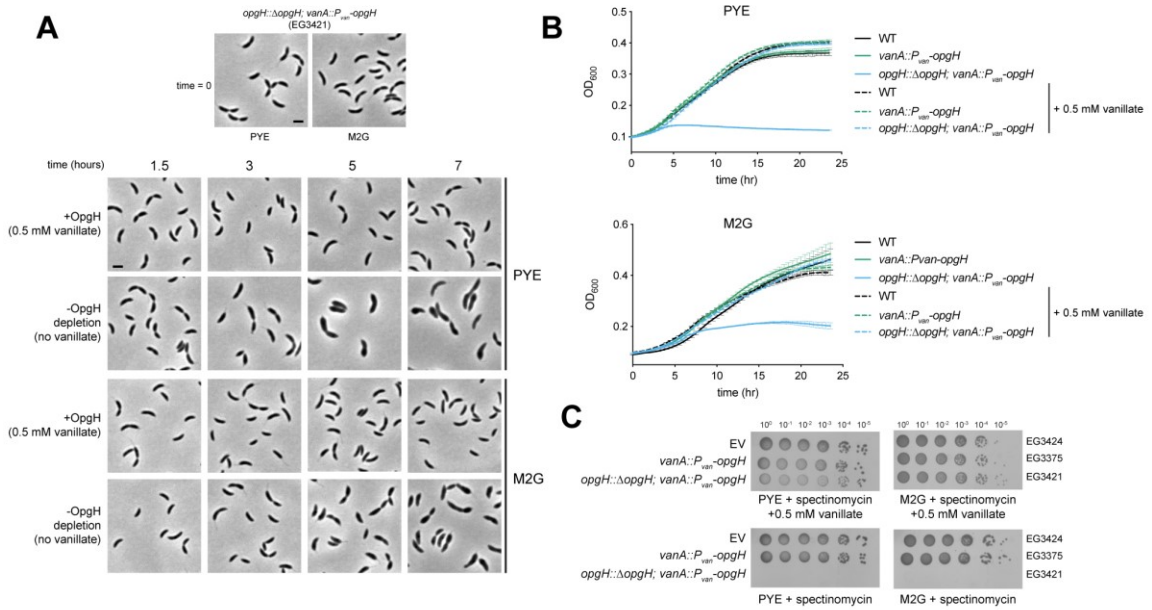
3.6 Figures and Legends

Figure 3.1: OpgH is essential for viability.

A. Phase contrast images of OpgH depletion strain (EG3421) in the presence and absence of 0.5 mM vanillate over the course of seven hours. Cells were either grown in complex media (PYE, peptone yeast extract) or minimal media (M2G) as indicated. Scale bar, 2 μm. **B.** Growth curve of WT (EG865), *opgH*-producing (EG3375), and OpgH depletion (EG3421) in PYE or M2G. **C.** Spot dilutions of an empty vector (EV, EG3424), *opgH*-producing (EG3375), and OpgH depletion (EG3421) on PYE or M2G plates with indicated antibiotics and inducer.
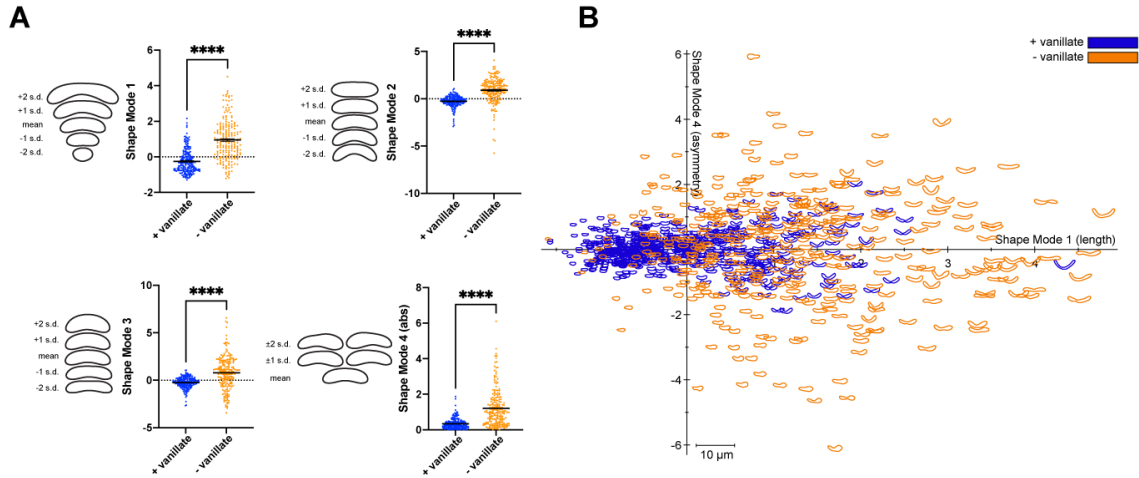
Figure 3.2: Cells lacking OpgH have atypical morphological defects.

A. Principal component analysis (PCA) of the OpgH depletion strain (EG3421) after 5 hours with 0.5 mM vanillate (blue) or without vanillate (orange). Scatter plots of 200 cells are shown for shape modes 1, 2, 3, and 4 which correspond to length, curvature, width, and asymmetrical bulging. Contours are shown on the left to indicate the mean shape and 1 or 2 standard deviations from the mean. Shape mode 4 is showing the absolute value. Statistical analysis uses a Mann-Whitney unpaired t-test. **** = $P < 0.0001$. **B.** Plot of shape mode 4 (asymmetrical bulging) versus shape mode 1 (length) values for the OpgH depletion strain with vanillate (blue) or without vanillate for 5 hours (orange).
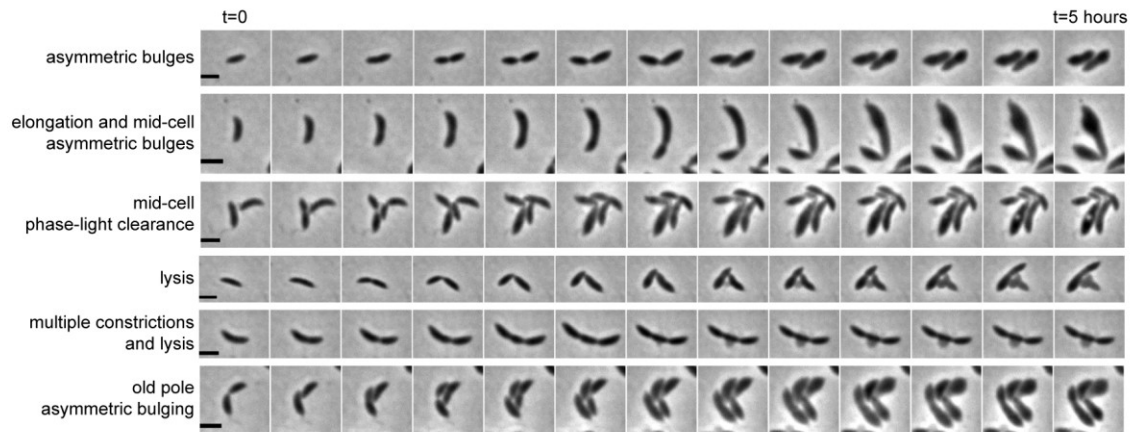
Figure 3.3: Loss of OpgH has pleotropic shape defects and lysis.

Time-lapse micrographs of prominent phenotypes of OpgH depletion over the course of 5 hours (EG3421). Scale bar, 2 μm.
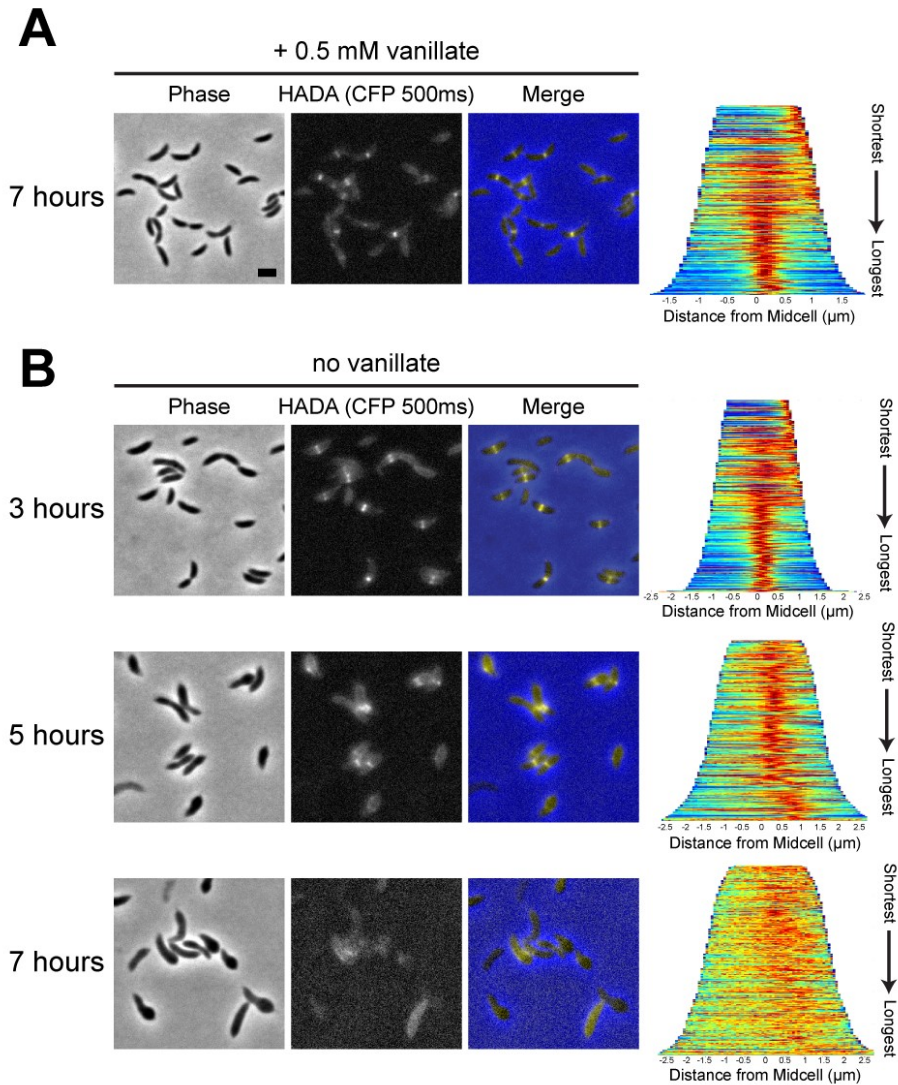
Figure 3.4: OpgH depletion results in misincorporation of cell wall material.

Phase contrast, epifluorescence, and merged images showing HADA incorporation **(A)** with vanillate at 7 hours and **(B)** without vanillate over the course of 7 hours in the OpgH depletion strain (EG3421). Corresponding demographs show the normalized HADA intensity arranged from shortest to longest for 300 cells. Scale bar, 2 μm.
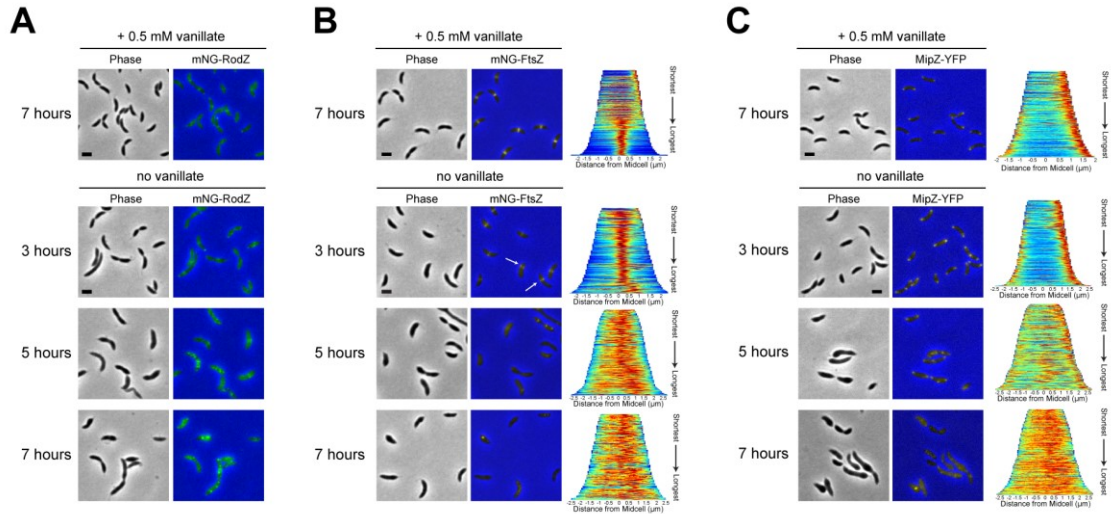
Figure 3.5: Divisome and elongasome proteins are mislocalized in OpgH depleted cells.

Phase contrast and epifluorescence merged images of **(A)** mNG-RodZ (EG3790), **(B)** mNG-FtsZ (EG3770), and **(C)** MipZ-YFP (EG3808) localization of OpgH depletion cells with (7 hours) and without 0.5 mM vanillate (at 3, 5, and 7 hours). White arrows indicate examples of asymmetric mNG-FtsZ localization. Scale bar, 2 µm.
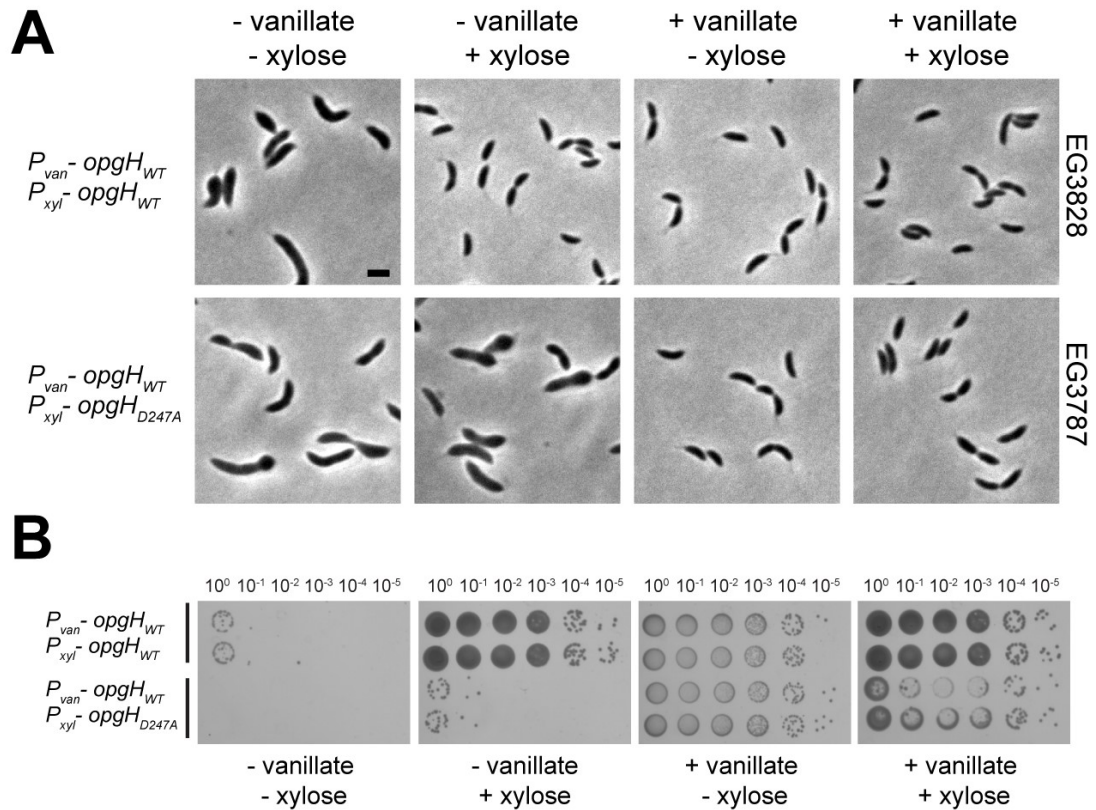
Figure 3.6: OpgH_{D247A} mutant cannot complement loss of OpgH.

**A.** Phase contrast images of the OpgH depletion strain (Δ*opgH* + P_van-*opgH*) with xylose inducible WT *opgH* (EG3828) or *opgH*_{D247A} (EG3787). Cells have been depleted or induced with indicated additive for five hours. Scale bar, 2 μm. **B.** Spot dilutions of the same strains grown on PYE with indicated inducer for two days. Two biological clones of each are presented.

## 3.7 Supplemental Figures and Legends
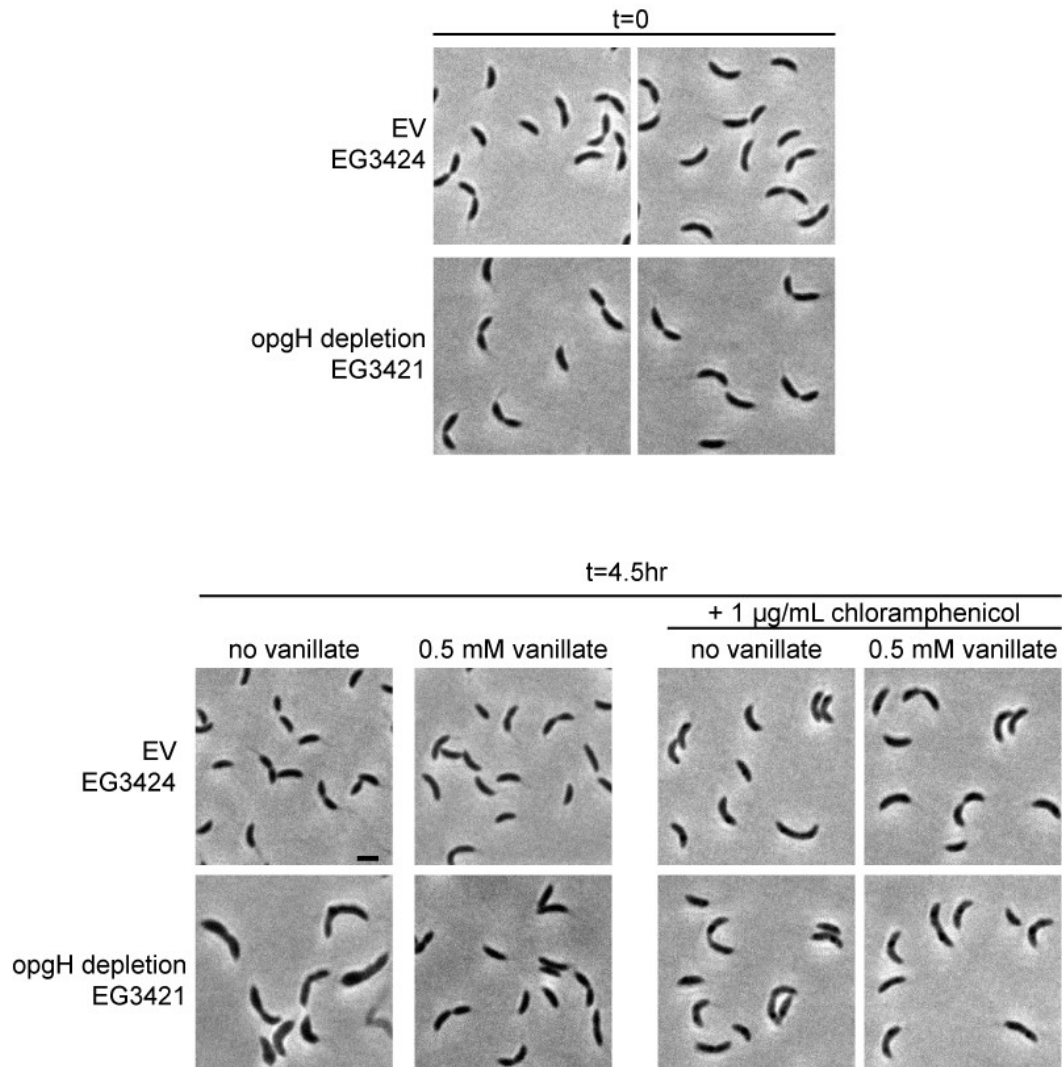
Supplemental Figure 3.1: OpgH depletion phenotype is reliant on cell growth.

Phase contrast images of and empty vector (EV, EG3424) and OpgH depletion strain (EG3421) at the start (t=0) and end (t=4.5 hours) of treatment with sub-lethal chloramphenicol (1 μg/mL) in the presence and absence of vanillate. Scale bar, 2 μm.
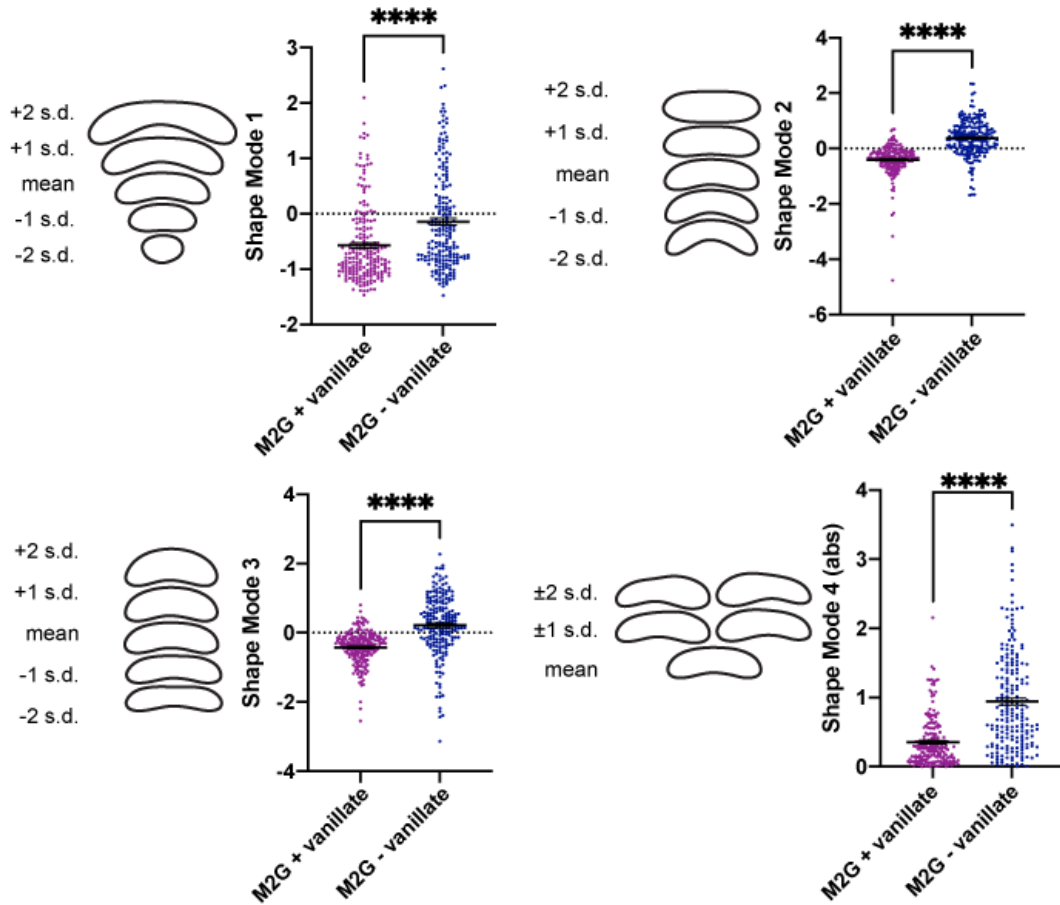
Supplemental Figure 3.2: OpgH depletion has morphological defects in minimal media

Principal component analysis (PCA) of the OpgH depletion strain (EG3421) after 5 hours grown in M2G with 0.5 mM vanillate (purple) or without vanillate (blue). Scatter plots of 200 cells are presented. Shape modes 1, 2, 3, and 4 correspond to length, curvature, width, and asymmetrical bulging. Contours indicate the mean shape and 1 or 2 standard deviations from the mean. Shape mode 4 shows the absolute value. Statistical analysis uses a Mann-Whitney unpaired t-test. **** = $P < 0.0001$.
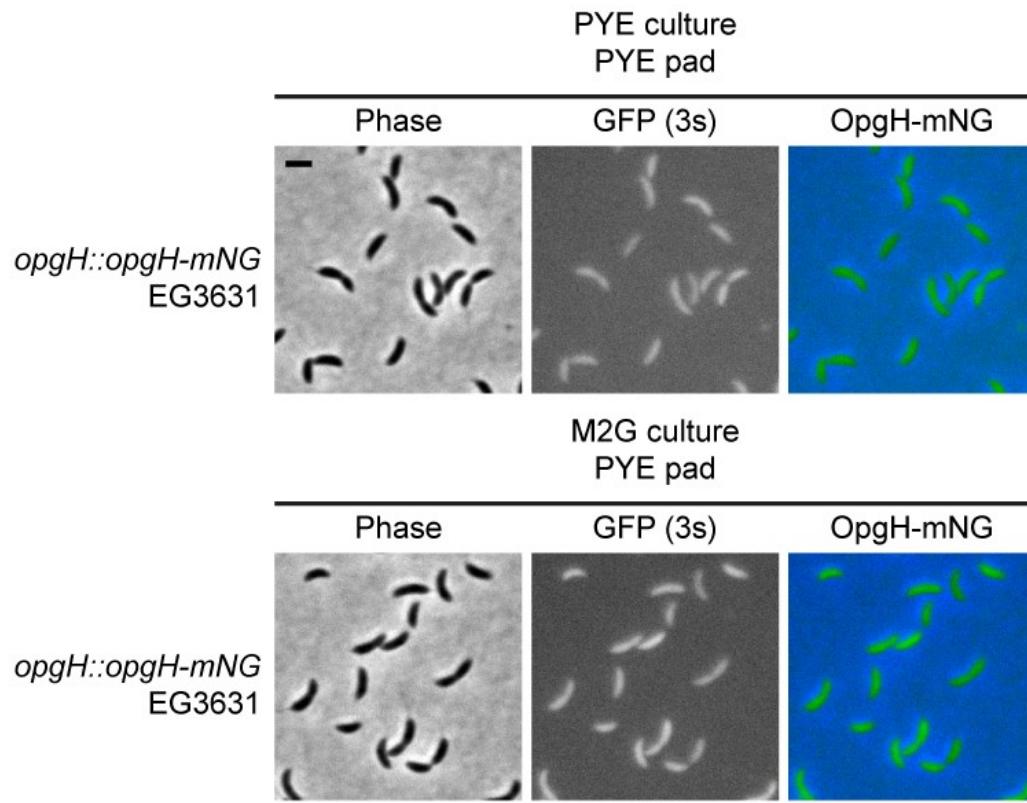
Supplemental Figure 3.3: OpgH is diffuse within the cell.

Phase contrast, epifluorescence, and merged images showing localization of OpgH with

a C-terminal mNeonGreen (mNG) tag (EG3631) grown in PYE or M2G. Scale bar, 2 µm.

3.8 References

Alyahya SA, Alexander R, Costa T, Henriques AO, Emonet T, Jacobs-Wagner C. 2009. RodZ, a component of the bacterial core morphogenic apparatus. *Proc Natl Acad Sci U S A* **106**:1239–1244. doi:10.1073/pnas.0810794106

Barrows JM, Sundararajan K, Bhargava A, Goley ED. 2020. FtsA Regulates Z-Ring Morphology and Cell Wall Metabolism **202**:1–20.

Bontemps-Gallo S, Bohin J-P, Lacroix J-M. 2017. Osmoregulated Periplasmic Glucans. *EcoSal Plus* **7**. doi:10.1128/ecosalplus.esp-0001-2017

Breton C, Šnajdrová L, Jeanneau C, Koča J, Imberty A. 2006. Structures and mechanisms of glycosyltransferases. *Glycobiology* **16**:29–37. doi:10.1093/glycob/cwj016

Christen B, Abeliuk E, Collier JM, Kalogeraki VS, Passarelli B, Coller JA, Fero MJ, McAdams HH, Shapiro L. 2011. The essential genome of a bacterium. *Mol Syst Biol* **7**. doi:10.1038/MSB.2011.58

Curtis PD, Brun Y V. 2010. Getting in the Loop: Regulation of Development in Caulobacter crescentus . *Microbiol Mol Biol Rev* **74**:13–41. doi:10.1128/mmbr.00040-09

Daitch AK, Goley ED. 2020. Uncovering Unappreciated Activities and Niche Functions of Bacterial Cell Wall Enzymes. *Curr Biol* **30**:R1170–R1175. doi:10.1016/j.cub.2020.07.004

Daitch AK, Orsburn BC, Chen Z, Alvarez L, Eberhard CD, Sundararajan K, Zeinert R, Kreitler DF, Jakoncic J, Chien P, Cava F, Gabelli SB, Bumpus NN, Goley ED. 2022. EstG is a novel esterase required for cell envelope

integrity. *bioRxiv* 2022.04.12.488081. doi:10.1101/2022.04.12.488081

Erickson HP, Anderson DE, Osawa M. 2010. FtsZ in Bacterial Cytokinesis: Cytoskeleton and Force Generator All in One. *Microbiol Mol Biol Rev* **74**:504–528. doi:10.1128/mmbr.00021-10

Figge RM, Divakaruni A V., Gober JW. 2004. MreB, the cell shape-determining bacterial actin homologue, co-ordinates cell wall morphogenesis in Caulobacter crescentus. *Mol Microbiol* **51**:1321–1332. doi:10.1111/j.1365-2958.2003.03936.x

Goley ED, Yeh YC, Hong SH, Fero MJ, Abeliuk E, Mcadams HH, Shapiro L. 2011. Assembly of the Caulobacter cell division machine. *Mol Microbiol* **80**:1680–1698. doi:10.1111/j.1365-2958.2011.07677.x

Hill NS, Buske PJ, Shi Y, Levin PA. 2013. A Moonlighting Enzyme Links Escherichia coli Cell Size with Central Metabolism. *PLoS Genet* **9**. doi:10.1371/journal.pgen.1003663

Huang KC, Mukhopadhyay R, Wen B, Gitai Z, Wingreen NS, Fisher ME. 2008. Cell shape and cell-wall organization in Gram-negative bacteria.

Kennedy EP, Schneider [, Reinhold JE, Rumley V, Kennedy MK&, Biol) J. 1982. Osmotic regulation and the biosynthesis of membrane derived oligosaccharides in Escherichia coli. *Proc Natl Acad Sci U S A* **79**:1092–1095. doi:10.1073/PNAS.79.4.1092

Kuru E, Tekkam S, Hall E, Brun Y V., Van Nieuwenhze MS. 2015. Synthesis of fluorescent D-amino acids and their use for probing peptidoglycan synthesis and bacterial growth in situ. *Nat Protoc* **10**:33–52.

doi:10.1038/nprot.2014.197

Meier EL, Daitch AK, Yao Q, Bhargava A, Jensen GJ, Goley ED. 2017. FtsEX-mediated regulation of the final stages of cell division reveals morphogenetic plasticity in Caulobacter crescentus. *PLoS Genet* **13**:1–25. doi:10.1371/journal.pgen.1006999

Pincus Z, Theriot JA. 2007. Comparison of quantitative methods for cell-shape analysis. *J Microsc* **227**:140–156. doi:10.1111/j.1365-2818.2007.01799.x

Silhavy TJ, Kahne D, Walker S. 2010. The bacterial cell envelope. *Cold Spring Harb Perspect Biol* **370**:1–17. doi:10.1098/rstb.2015.0019

Sundararajan K, Miguel A, Desmarais SM, Meier EL, Casey Huang K, Goley ED. 2015. The bacterial tubulin FtsZ requires its intrinsically disordered linker to direct robust cell wall construction. *Nat Commun* **6**:1–14. doi:10.1038/ncomms8281

Thanbichler M, Shapiro L. 2006. MipZ, a Spatial Regulator Coordinating Chromosome Segregation with Cell Division in Caulobacter. *Cell* **126**:147–162. doi:10.1016/j.cell.2006.05.038

Wiggins CAR, Munro S. 1998. Activity of the yeast MNN1 α-1,3-mannosyltransferase requires a motif conserved in many other families of glycosyltransferases. *Proc Natl Acad Sci U S A* **95**:7945–7950. doi:10.1073/pnas.95.14.7945

Wilhelm RC. 2018. Following the terrestrial tracks of Caulobacter - redefining the ecology of a reputed aquatic oligotroph. *ISME J* **12**:3025–3037. doi:10.1038/s41396-018-0257-z

Woldemeskel SA, McQuillen R, Hessel AM, Xiao J, Goley ED. 2017. A
conserved coiled-coil protein pair focuses the cytokinetic Z-ring in
Caulobacter crescentus. *Mol Microbiol* **105**:721–740.
doi:10.1111/mmi.13731

CURRICULUM VITAE

Allison Katharine Daitch   May 2022

Educational History:

Ph.D.   2022   Program in Biochemistry, Cellular and Molecular Biology

Johns Hopkins University School of Medicine

Mentor: Erin Goley, PhD

B.S.   2016   Biology, Concentration Cell Biology and Molecular

Genetics

University of Maryland, College Park

Other Professional Experiences

Intern   2021   Defense Intelligence Agency,

Department of Defense

Student researcher   2014-2016   Daniel Dwyer, PhD, University of Maryland

Summer intern   2013-2014   Sarven Sabunciyan, PhD, Johns Hopkins

University School of Medicine

Intern   2011-2014   Molecular Diagnostics, Akonni Biosystems

Research Travel Awards

Turock Travel Award	2020	$750
		Financial support for conference travel
GSA Travel Award	2019	$500
		Financial support for conference travel

Academic Honors

2016	Cum Laude	University of Maryland, College Park

Publications; Peer-reviewed

Daitch AK, Goley ED. (2020). Uncovering Unappreciated Activities and Niche Functions of Bacterial Cell Wall Enzymes. *Current Biology*. DOI: 10.1016/j.cub.2020.07.004. PMID: 33022262.

Woldemeskel SA, **Daitch AK**, Alvarez L, Panis G, Zeinert R, Gonzalez D, Smith E, Collier J, Chien P, Cava F, Viollier PH, Goley ED. (2020). The conserved transcriptional regulator CdnL is required for metabolic homeostasis and morphogenesis in *Caulobacter*. *PLOS Genetics*. DOI: 10.1371/journal.pgen.1008591

Lariviere PJ, Mahone CR, Santiago-Collazo G, Howell M, **Daitch AK**, Zeinert R, Chien P, Brown PJB, Goley ED. (2019). Activation of SEDS-PBP cell wall synthases by an essential regulator of bacterial division. *Current Biology*. DOI: 10.1016/j.cub.2019.03.066

Meier EL, **Daitch AK**, Yao Q, Bhargava A, Jensen GJ, Goley ED. (2017). FtsEX-mediated regulation of the final stages of cell division reveals morphogenetic

plasticity in *Caulobacter crescentus*. *PLOS Genetics*. DOI:

10.1371/journal.pgen.1006999

Publications; Pre-print

Daitch AK, Orsburn BC, Chen Z, Alvarez L, Eberhard CD, Sundararajan K,

Zeinert R, Kreitler DF, Jakoncic J, Chien P, Cava F, Gabelli SB, Bumpus NN,

Goley ED. (2022). EstG is a novel esterase required for cell envelope integrity.

bioRxiv. 10.1101/2022.04.12.488081

Posters and Abstracts

Daitch AK, Sundararajan K, Zeinert R, Alvarez L, Chien P, Cava F, Goley ED.

(August 2019) A novel cell wall enzyme contributes to bacterial survival during

cell wall stress. *Molecular Genetics of Bacteria and Phages Conference*,

Madison, WI (*Poster*)

Daitch AK, Sundararajan K, Zeinert R, Chien P, Goley ED. (August 2019) A

novel cell wall enzyme contributes to bacterial survival during cell wall stress.

Biological Chemistry Retreat, Baltimore, MD (*Poster*)

Daitch AK, Sundararajan K, Zeinert R, Chien P, Goley ED. (May 2019) A novel

cell wall enzyme contributes to bacterial survival during cell wall stress. *Johns

Hopkins Alumni Weekend Student Research Rounds Poster Session,* Baltimore,

MD (*Poster*)

Daitch AK, Sundararajan K, Zeinert R, Chien P, Goley ED. (May 2019) A novel cell wall enzyme contributes to bacterial survival during cell wall stress. *Graduate Student Association Poster Session*, Baltimore, MD (*Poster*)

Daitch AK, Sundararajan K, Zeinert R, Chien P, Goley ED. (May 2018) A novel cell wall enzyme contributes to bacterial survival during cell wall stress. *BCMB program retreat*, Cambridge, MD (*Poster*)

Daitch AK, Sundararajan K, Zeinert R, Chien P, Goley ED. (May 2017) A novel cell wall enzyme contributes to bacterial survival during cell wall stress. *BCMB program retreat*, Cambridge, MD (*Poster*)

Service and Leadership

2017-2022	Thread Head of Family	Mentor Baltimore Youth
2019-2021	Program Representative	JHSOM Graduate Student Association
2020	Conference Organizer	CauloCon Virtual Conference
2019-2020	Cat Socializer	Baltimore Animal Rescue and Care Shelter
2018-2020	Teaching Assistant	Fundamentals of Genetics
2017-2019	Student Representative	BCMB Policy Committee